SU-SEL-64-053

Band Structure and Electron-Electron Interactions in Copper and Silver—Photoemission Studies

by
C. N. Berglund

June 1964

Technical Report No. 5205-1

Prepared under
Center for Materials Research
Contract SD 87-4850-47

SOLID-STATE ELECTRONICS LABORATORY

STANFORD ELECTRONICS LABORATORIES

STANFORD UNIVERSITY • STANFORD, CALIFORNIA

SEL-64-053

BAND STRUCTURE AND ELECTRON-ELECTRON INTERACTIONS IN COPPER AND SILVER--PHOTOEMISSION STUDIES

by

C. N. Berglund

June 1964

Technical Report No. 5205-1

Prepared under
Center for Materials Research
Contract SD 87-4850-47

Solid-State Electronics Laboratory
Stanford Electronics Laboratories
Stanford University Stanford, California

ABSTRACT

Photoemission studies are used to determine in detail many of the electronic properties of the metals copper and silver over an energy range from the bottom of the d-band (approximately 6 ev below the Fermi level, to 12.5 ev above the Fermi level. Measurements of the spectral distribution of the quantum yield and of the energy distribution of photoemitted electrons from copper and silver under monochromatic radiation are described and interpreted in terms of the energy-band structure of the metals and the inelastic-scattering mechanisms for energetic electrons.

The effects on the photoemission measurements of direct and indirect optical transitions, electron-electron scattering, lifetime broadening, and the Auger process are described. These processes are identified in the experimental data, and used to obtain information on the density of states, the effect of matrix elements, the optical selection rules, the mean free paths for scattering of energetic electrons, and the energy loss per scattering event in both copper and silver. In addition, information is gained on the effect of the plasma frequency in silver at $\hbar\omega = 3.85$ ev.

CONTENTS

CONTENTS (Continued)

ILLUSTRATIONS

ILLUSTRATIONS (Continued)

ILLUSTRATIONS (Continued)

ILLUSTRATIONS (Continued)

LIST OF SYMBOLS

A	constant
B	constant
B(E)	threshold function
c	velocity of light in free space
C_0	constant
C(E)	threshold function
e	electronic charge
E	electron energy
E_F	Fermi energy
E_V	electron energy with respect to vacuum level

E_W	work function
$\mathcal{E}_k$	unit vector in the k direction
$\mathcal{E}_o$	amplitude of electric vector of electromagnetic field
f	oscillator strength
F(E)	Fermi function
g	scattering function
G	electron generation rate
G_{opt}	optical electron generation rate
G_{sc}	scattering electron generation rate
$\hbar$	reduced Planck's constant = $h/2\pi$
H	Hamiltonian
H_I	interaction Hamiltonian
H_{osc}	plasma-oscillation Hamiltonian
H_{sr}	short-range Hamiltonian
k	extinction coefficient
$\bar{k}$	momentum vector
k_c	cutoff wave vector
K	correction factor
K_e	relative dielectric constant
ℓ	mean free path for electron-electron scattering
L	attenuation length for energetic electrons
m	free electron mass
m^*	electron effective mass
n	index of refraction
n_p	photon flux
N	number of electrons photoemitted per photon per unit energy
N_A	number of electrons excited by Auger process
N_ω	number of electrons photoemitted per photon per unit energy at frequency ω
N_T	transition rate
$\bar{p}$	electron momentum
p_c	critical momentum for electron escape in photoemission

p_{esc}	electron escape probability
p_{10}	momentum matrix element
p_k	conjugate momentum
p_s	electron-electron scattering probability
$P(E_1,k_1;E_0,k_0)$	transition probability--initial state to final state
P_s	integrated electron-electron scattering probability
q_k	collective coordinate
$\underline{r}$	position vector
R	electron escape rate
R_e	reflectivity
T	absolute temperature in degrees Kelvin
v_g	electron group velocity
Y	quantum yield per absorbed photon
Y'	quantum yield per incident photon
α	absorption coefficient
δ	delta function
∇_k	differential vector operator with respect to k
ϵ_0	permittivity of free space
ϵ_1	real part of dielectric constant
ϵ_2	imaginary part of dielectric constant
Λ	frequency associated with lifetime for scattering
ρ	density of states
τ	lifetime of carrier in electronic state
ω	angular frequency of electromagnetic radiation
μ	mobility
σ	conductivity

ACKNOWLEDGMENT

The author wishes to express his deep appreciation to Professor W. E. Spicer for his excellent guidance, suggestions, and encouragement throughout the course of this work. He also wishes to thank N. B. Kindig for his help in setting up the vacuum ultraviolet monochromator and for many valuable discussions of the work, and Phillip McKernan for providing the experimental phototubes and for solving many of the problems associated with their construction.

I. INTRODUCTION

The electronic properties of metals have been subjects of both experimental and theoretical study for many years. Copper in particular has been of considerable interest because of its close relation to the magnetic metals, and more recently because of its possible application in novel amplifiers [Ref. 1].

There has been considerable progress in the theoretical treatment of electrons in metals. Two independent energy-band calculations for copper have recently been made using different methods and assuming slightly different potentials [Refs. 2, 3]. The agreement of these calculations with each other and with experiment is relatively good. It had previously been widely believed that the band structure of metals having high-lying d levels similar to copper was very sensitive to details of the crystal potential employed. The band calculations indicate that such is not the case. Electron-scattering processes in metals have been treated quantum-mechanically by Bohm and Pines [Ref. 4], and electron-electron scattering in particular has been considered by Motizuki and Sparks [Ref. 5] and Quinn [Ref. 6].

Many experimental techniques are available for studying the electronic properties of metals. Methods such as de Haas-van Alphen, cyclotron resonance, magnetoacoustic, high-field magnetoresistance, and anomalous skin-effect measurements [Refs. 7-11] give a great deal of information on states near the Fermi surface. Studies of thin metal films on semiconductors give information on the range and mean free path for scattering of hot electrons in metals [Ref. 12]. Soft X-ray emission and absorption measurements give some information on some of the important features of the band structure [Ref. 13], and optical absorption and reflectivity measurements can be interpreted in detail if the band structure and selection rules are well known [Ref. 14]. However, all of these techniques are restricted either in the energy range over which they can be used or in the detail with which the measurements can be interpreted.

As a technique for studying electronic properties of solids, photoemission has several advantages over other experimental methods [Ref. 15]. In contrast to other optical measurements, the energy of

the electrons can be measured after excitation in photoemission studies, and information gained on the initial and final states involved in optically excited transitions. In addition, since photoemission is a two-step process involving optical excitation of electrons in the solid followed by electron transport to the surface of the solid and escape into vacuum (with or without electron scattering), information can be obtained both on the optical transition probabilities including selection rules, matrix elements, and densities of states, and on the scattering mechanisms including mean free paths and energy loss per collision. This information is available over a very wide energy range centered about the Fermi level.

The purpose of this work was to use photoemission to study in detail the optical and electronic processes in the metals copper and silver over a range of photon energy from 1.5 ev to 11.5 ev. Copper was chosen because of the wide general interest in its properties as illustrated by the extensive theoretical investigations and recent range measurements, and because of the ease with which it can be worked and obtained in high purity. Silver was the logical second metal to study because its strong similarity to copper allows comparison and checks of the interpretation and analysis of the data. In Chapters II and III, the experimental techniques used and the applicable theory of photoemission are described; in Chapters IV and V, the experimental results for copper and silver including descriptions and analyses of the data are given; and in Chapter VI, the results are discussed and a comparison of the band structure and electronic properties of silver and copper is made.

II. THEORY OF PHOTOEMISSION

A. OPTICAL EXCITATION

Optical absorption in solids can be divided into three types according to the mechanism [Ref. 16]: 1) lattice absorption, 2) absorption involving localized states such as impurities and lattice defects, and 3) fundamental absorption involving electronic interband or intraband transitions. Lattice absorption occurs in the infrared region of the spectrum and results in the creation of phonons. This process does not result in energetic electrons which can escape from the solid, and is not important in photoemission. Absorption involving impurities or lattice defects may be important in semiconductors at photon energies less than band-gap energy; however, in metals this absorption process can usually be neglected. Absorption due to electronic transitions can be divided into that due to intraband transitions and that due to interband transitions. Intraband absorption, commonly referred to as free carrier absorption, has been treated quantum-mechanically by Kronig [Ref. 17], and considered more rigorously by Fan and Becker [Ref. 18] and others. Ehrenreich and Philipp [Ref. 19] have shown that the effect of intraband transitions can be separated from other effects in most metals, and in the case of copper and silver has negligible effect on the optical properties at photon energies above 2.1 ev and 3.5 ev respectively. Absorption due to optically excited interband transitions is most important in photoemission studies and will be considered in detail.

1. Direct Transitions

The probability per second of an electron in state (E_0, k_0) in a solid absorbing a photon can be determined from first-order time-dependent perturbation theory if the wave functions of the initial and final states are known. If this calculation is carried out, the probability per second of an electron being excited to state (E_1, k_1) is given by [Ref. 20]

$$P(E_1,k_1;E_0,k_0) = \frac{Af_{10}\mathcal{E}_o^2\Lambda}{\pi\hbar\omega\left[\left(\frac{E_1 - E_0}{\hbar} - \omega\right)^2 + \Lambda^2\right]} \qquad (1)$$

where $\mathcal{E}_o$ is the magnitude of the electric vector of the monochromatic incident radiation at frequency ω, A is a constant for any given material, Λ is the frequency associated with the lifetime for scattering of an electron in the excited state, τ, and f_{10} is the oscillator strength for the transition as given by Smith in terms of the momentum matrix element p_{10} [Ref. 21]

$$f_{10} = \frac{2|p_{10}|^2}{m\hbar\omega} \tag{2}$$

If the frequency Λ is much smaller than the bandwidth of the exciting radiation, and if f_{10} is a slowly varying function of the energy of the final state, Eq. (1) may be integrated over the continuum of final states, giving

$$P(E_1,k_1;E_0,k_0) = \frac{Af_{10}\mathcal{E}_o^2\delta(E_1 - E_0 - \hbar\omega)}{\hbar\omega} \tag{3}$$

where the delta function assures conservation of energy in the optically excited transition. When Λ is not small compared to the bandwidth of the radiation, a "lifetime broadening" occurs. This phenomenon is observed in photoemission studies of both copper and silver, and will be described in later chapters.

If the two states involved in the transition can be represented by Bloch functions, it is found that the momentum matrix element in Eq. (3) is large only when the initial- and final-state k-vectors are equal [Ref. 21]. Applying this condition to Eq. (3), the first-order probability of a transition between the two states is significant only when energy and k-vector are conserved. Transitions of this kind are usually referred to as vertical or direct transitions.

In a real solid, the total number of transitions per second per unit volume is given by Eq. (3) multiplied by the density of states available for the transitions under the restrictions of energy and k-vector conservation. Since the number of states per unit volume between energy E and (E + dE) is

$$\rho(E)dE = \frac{2}{8\pi^3}\int \frac{dE\ ds}{|\nabla_k E(k)|} \tag{4}$$

where the integration is performed over the constant energy surface E_1, the joint density of states required in Eq. (3) for direct transitions is

$$\rho(E_1,E_0)\ dE_1 = \int \frac{2dE_1\delta(E_1 - E_0 - \hbar\omega)\ ds}{8\pi^3|\nabla_k[E_1(k) - E_0(k)]|} \tag{5}$$

giving for the number of transitions per second per unit volume

$$N_T(E_1,E_0)\ dE_1 = \frac{Af_{10}\mathcal{E}_o^2}{\hbar\omega}\ \rho(E_1,E_0)F(E_0)[1 - F(E_1)]\ dE_1 \tag{6}$$

where $F(E)$ is the Fermi function.

2. Indirect Transitions

It has been suggested by several authors that conservation of k-vector may not be an important selection rule for transitions involving some electronic states in solids. Herring [Ref. 22] has shown that if the following condition is not satisfied, detailed application of band theory (which requires conservation of k) to the electronic states of the carriers may not be valid:

$$\mu >> 134\ \frac{m^*}{m}\ \frac{100^\circ}{T}\ \text{cm}^2/\text{v sec}, \tag{7}$$

where μ is the carrier mobility, m^* is the effective carrier mass, and T is the absolute temperature in degrees Kelvin. Experimental results have indicated that conservation of k is not important in optically excited transitions in Cs_3Sb, CdS, and other semiconductors [Refs. 23, 24]. These results are consistent with Eq. (7). In this work, transitions in which conservation of k-vector is unimportant will be considered as indirect transitions.

If conservation of k-vector is not necessary for the matrix element in Eq. (2) to be finite, the transition rate will no longer be given by Eq. (6). The transition rate will be proportional to the density of filled states at E_0, the density of empty states at E_1, and the transition probability given by Eq. (3). Therefore, within a constant factor

$$N_T(E_1,E_0)\,dE_1 = \frac{Af_{10}\mathcal{E}_o^2}{\hbar\omega}\,\rho(E_0)F(E_0)\rho(E_1)[1 - F(E_1)]\delta(E_1 - E_0 - \hbar\omega)\,dE_1 \quad (8)$$

When conservation of k-vector is a strong selection rule, indirect transitions may occur if some additional process accompanies the transition which conserves k-vector. In real solids, scattering by defects or emission or absorption of phonons may accomplish conservation of k-vector.

Hall, Bardeen, and Blatt [Ref. 25] have calculated the relative indirect-transition probability for an electron using second-order perturbation theory and assuming that momentum is conserved by emission or absorption of a phonon. If the phonon energy is neglected and the scattering frequency is small compared to the bandwidth of the exciting radiation, the process may be considered as either (1) absorption of a photon and transition to a virtual state i (k-vector and energy being conserved) with subsequent absorption or emission of a phonon and transition to the final state, or (2) absorption or emission of a phonon and transition to the virtual state j with subsequent absorption of a photon and transition to the final state (k-vector and energy being conserved). These mechanisms are illustrated in Fig. 1. The resulting transition rate in this process may be written

$$N_T(E_1,E_0)\,dE_1$$

$$= \frac{B\mathcal{E}_o^2}{\hbar\omega}\,(f'_{i0}f_{Pli} + f'_{1j}f_{Pj0})\rho(E_1)\rho(E_0)F(E_0)[1 - F(E_1)]\delta(E_1 - E_0 - \hbar\omega)\,dE_1$$

$$= \frac{B\mathcal{E}_o^2}{\hbar\omega}\,(f'_{10}f_P)\rho(E_1)\rho(E_0)F(E_0)[1 - F(E_1)]\delta(E_1 - E_0 - \hbar\omega)\,dE_1 \quad (9)$$

where $\rho(E)$ is the density of states at E, B is a combination of fundamental constants, f'_{10} is the oscillator strength associated with transitions to or from the virtual states involving photon absorption shown in Fig. 1, and f_P is the term representing the probability of momentum conservation by absorption or emission of a phonon. In general, f_P will depend on the equilibrium phonon densities, the phonon energy,

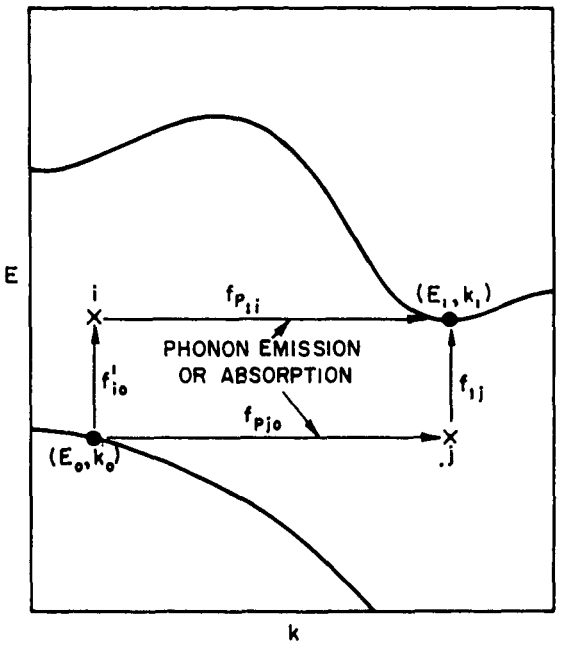

FIG. 1. INDIRECT TRANSITIONS INVOLVING PHONONS.

and the deformation potential in the solid being considered. As a result, it may be temperature dependent.

3. Relation of Transition Probability to the Optical Constants

At photon energies where excitation of electronic interband transitions is the predominant absorption process in a solid, the transition probabilities derived above can be related to the optical constants. The power absorbed per unit volume by the excitation of transitions is given by

$$\text{Power} = \hbar\omega \int_0^\infty N_T(E_1, E_0)\, dE_1 \qquad (10)$$

where $N_T(E_1, E_0)$ is the transition rate per unit volume due to radiation at frequency ω. Remembering that the conductivity σ is defined classically in terms of the absorption of power $\sigma \mathcal{E}_o^2/2$ per unit volume,

$$\sigma = \frac{2h\omega}{\mathcal{E}_o^2} \int_0^\infty N_T(E_1, E_0)\, dE_1 \qquad (11)$$

Since copper and silver are nonmagnetic, $\mu \approx \mu_0$ and σ and K_e are related to the index of refraction n and the extinction coefficient k by [Ref. 20]

$$n^2 - k^2 = K_e \quad \text{and} \quad 2nk = \frac{\sigma}{\omega \epsilon_0} \qquad (12)$$

One can consider Maxwell's equations in terms of a real and an imaginary dielectric constant, ϵ_1 and ϵ_2 respectively, where

$$\epsilon_1 = K_e \quad \text{and} \quad \epsilon_2 = \frac{\sigma}{\omega \epsilon_0} \qquad (13)$$

The absorption coefficient α is defined as $4\pi k/\lambda$, and may be written, using Eq. (12), as

$$\alpha = \frac{\sigma}{nc\epsilon_0} \qquad (14)$$

where c is the velocity of light in free space.

Much of the information obtained from photoemission measurements involves the absorption coefficient. In order to relate these data through Eqs. (14) and (11) to the transition probabilities and the densities of states, it is often necessary to know the index of refraction n as a function of ω. Although n may be determined from K_e and σ through Eq. (12), and theoretical expressions for K_e and σ are available, the wave functions and selection rules in a solid are not generally known well enough to permit accurate calculation of n. For both copper and silver, n has been measured for photon energies from 1 to 25 ev, and where it is required their data will be used in reduction of the experimental results [Ref. 19].

B. INELASTIC SCATTERING

Inelastic scattering of energetic electrons in a solid can have a pronounced effect on experimental results obtained from photoemission studies. In addition to the lifetime broadening effect described previously, strong scattering reduces the probability of electrons escaping from the solid without scattering and increases the probability of

electrons escaping from the solid after having scattered one or more times. As a result of this scattering process, information on the energy of the electron, after optical excitation, is destroyed to some extent, since it is sometimes difficult to determine which of the escaping electrons have not been scattered before escaping. It will be shown that one of the most important electron-scattering mechanisms in a metal is electron-electron scattering. In order to interpret photoemission data, as quantitative a knowledge as possible of the effect of this scattering process is necessary.

Consider a gas of electrons imbedded in a background of uniform positive charges whose density is equal to that of the electrons. The Hamiltonian of the system is

$$H = \sum_i \frac{\bar{p}_i^{\,2}}{2m} + \frac{1}{2} e^2 \sum_{i \neq j} \left| \frac{1}{\bar{r}_i - \bar{r}_j} \right| \tag{15}$$

where the first term is the sum of the electron kinetic energies and the second term corresponds to their coulomb interaction. The coulomb interaction between the i^{th} and j^{th} electrons may be expanded in a Fourier series in a box of unit volume

$$\frac{1}{2} e^2 \frac{1}{|\bar{r}_i - \bar{r}_j|} = 2\pi e^2 \sum_k \frac{1}{k^2} \exp[i\bar{k} \cdot (\bar{r}_i - \bar{r}_j)] \tag{16}$$

Placing Eq. (16) in Eq. (15) gives

$$H = \sum_i \frac{\bar{p}_i^{\,2}}{2m} + 2\pi e^2 \sum_{i \neq j} \sum_k \frac{\exp[i\bar{k} \cdot (\bar{r}_i - \bar{r}_j)]}{k^2} \tag{17}$$

By introducing collective coordinates q_k and conjugate momenta p_k, the Hamiltonian in Eq. (17) has been expressed by Bohm and Pines [Ref. 4] in terms of a long-range organized collective oscillation, H_{osc}; short-range screened coulomb interaction, H_{sr}; and the interaction between collective fields and individual electrons, H_I.

$$H = \sum_i \frac{\bar{p}_i^{\,2}}{2m} + H_{osc} + H_{sr} + H_I \tag{18}$$

$$H_{osc} = -\frac{1}{2} \sum_{k<k_c} (p_k p_{-k} + \omega_p^{\,2} q_k q_{-k}) \tag{19}$$

$$H_{sr} = 2\pi e^2 \sum_{i \neq j} \sum_{k>k_c} \frac{\exp[i\bar{k} \cdot (\bar{r}_i - \bar{r}_j)]}{k^2} \tag{20}$$

$$H_I = (4\pi)^{1/2} \frac{e}{m} \sum_{ik<k_c} \mathcal{E}_k \cdot \left(\bar{p}_i - \frac{\hbar\bar{k}}{2}\right) q_k \exp(i\bar{k} \cdot \bar{r}_i) \tag{21}$$

where k_c is the cutoff wave vector, or screening parameter, beyond which organized oscillation is not possible, ω_p is the plasma frequency, and $\mathcal{E}_k$ denotes a unit vector in the $\bar{k}$ direction. Bohm and Pines showed that the H_I term is almost always negligible compared to H_{sr}, and Quinn (using a self-energy or quasi-particle approach) showed that the mean free path for plasmon creation in aluminum, for electrons with energies less than twice the Fermi energy, is much larger than the mean free path for electron-electron scattering [Ref. 6]. Assuming the same is true in copper and silver, the dominant interaction term in Eq. (18) is that associated with electron-electron scattering, H_{sr}, over the range of electron energy considered (0 to 11.5 ev above Fermi energy) in the photoemission work to be described.

The free-electron-gas model assumed above is not a good approximation to metals such as copper and silver because of the d-bands which are located only a few electron volts below the Fermi level. However, from the experimental results, it seems most reasonable that the Hamiltonian of these metals can be separated into components similar to those of the free electron gas, and that H_{sr} will again be the dominant interaction term.

If H_{sr} is considered as a small perturbation, the probability per second of an electron in state (E',k') being scattered to state

(E,k) and exciting an electron in state (E_0,k_0) to state (E_1,k_1) is [Ref. 12]

$$P_s = \frac{2\pi}{\hbar} \left| < k', k_0 \left| H_{sr} \right| k, k_1 > \right|^2 \delta(E' - E - E_1 + E_0) \qquad (22)$$

To find the total probability of an electron with energy E' being scattered to some other energy, Eq. (22) must be summed over all possible states corresponding to k_0, k_i', k, k_1, E, E_1, and E_0. This summation may be carried out if the squared matrix element in Eq. (22) is known. However, many features of the scattering process can be determined without knowing the matrix element. The summation can be changed to an integral by including the appropriate densities of states and Fermi functions in the standard way. Using this approach, the probability per second of an electron with energy E' being scattered to an energy between E and $(E + dE)$ is

$$p_s(E',E)\, dE = \int_0^\infty \left\{ \frac{2\pi}{\hbar} \left| M \right|^2 \rho(E)\rho(E_0)\rho(E_0 + E' - E)F(E_0)[1 - F(E_0 + E' - E)] \right.$$

$$\left. [1 - F(E)]\, dE \right\} dE_0 \qquad (23)$$

where $\left| M \right|^2$ is the squared matrix element in Eq. (22). Defining

$$g(E',E) = \int_0^\infty \frac{2\pi}{\hbar} \left| M \right|^2 \rho(E_0)\rho(E_0 + E' - E)F(E_0)[1 - F(E_0 + E' - E)]\, dE_0 \qquad (24)$$

Eq. (23) becomes

$$p_s(E',E)\, dE = \rho(E)[1 - F(E)]g(E',E)\, dE \qquad (25)$$

and the probability of an electron with energy E' being scattered to any energy is

$$P_s(E') = \int_0^{E'} \rho(E)[1 - F(E)]g(E',E)\, dE \qquad (26)$$

Motizuki and Sparks [Ref. 5] have calculated $P_s(E')$ exactly for a free electron gas, assuming the Fermi function at absolute zero and H_{sr} given by the Yukawa potential [Ref. 26]. They obtained for the scattering probability for electrons with energy near the Fermi energy

$$P_s(E') \propto \frac{(E' - E_F)2}{\sqrt{E'}} \tag{27}$$

where E_F is the Fermi energy. For comparison, Eq. (26) calculated assuming M to be a constant and assuming constant density of states is

$$P_s(E') \propto (E' - E_F)^2 \tag{28}$$

The close agreement between Eqs. (27) and (28) indicates that the strong energy dependence of the scattering probability is due to a large extent to the summation over the states available to take part in the scattering, rather than to the matrix element.

The reciprocal of the transition probability given by Eq. (26) is defined as the lifetime for scattering, τ. Assigning an average group velocity $v_g(E')$ to electrons with energy E', the mean free path for electron-electron scattering is

$$\ell(E') = v_g(E')\tau(E') = \frac{v_g(E')}{P_s(E')} \tag{29}$$

C. PROBABILITY OF ELECTRON ESCAPE

1. Effect of Inelastic Scattering

Consider an electron excited to some energy E and momentum p at a distance x from the surface of a semi-infinite solid as shown in Fig. 2. This electron may have been either directly excited to this state by absorption of a photon, or scattered to it by some scattering process. In order for the electron to escape from the solid without any loss of energy, it must 1) reach the surface without suffering an inelastic collision, and 2) have a momentum component perpendicular to the surface

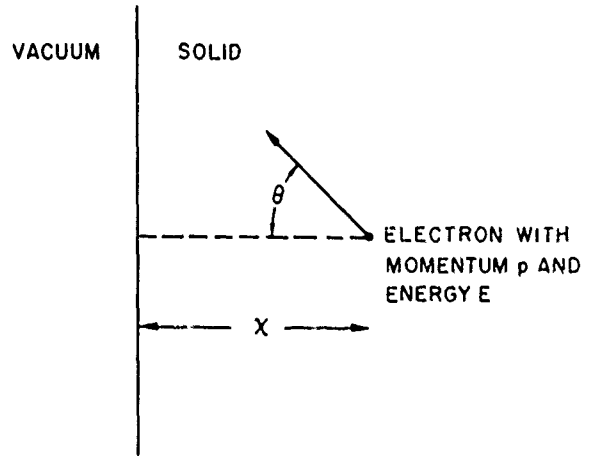

FIG. 2. EXCITATION AND ESCAPE OF ELECTRON IN SEMI-INFINITE PHOTOEMITTER.

greater than some critical momentum p_c, where p_c depends on the work function of the solid and may also be a function of the state of the electron [Ref. 27]. In general, the probability of the electron escaping under these conditions is a function of the mean free paths for inelastic and elastic scattering. However, when the mean free path for inelastic scattering, ℓ, ordinarily a function of electron energy, is much shorter than that for elastic scattering, the two conditions described above can be combined in the following way: If θ is the angle between the direction of electron momentum and the normal to the photoemitting surface, the electron must move $x/\cos\theta$ to reach the surface. Referring to Fig. 2, since the momentum of the electron has a random direction, the probability of the electron escaping without loss in energy is

$$p_{esc}(E,x) = \frac{1}{2}\int_0^{\cos^{-1} p_c/p} \exp\left(-\frac{x}{\ell\cos\theta}\right) \sin\theta\, d\theta \qquad \cos^{-1}\frac{p_c}{p} \quad p \geq p_c \qquad (30)$$

$$= 0 \qquad\qquad\qquad\qquad\qquad\qquad\qquad\qquad\qquad\qquad\qquad\qquad p < p_c$$

Changing variables so that $z = \cos\theta$,

$$p_{esc}(E,x) = \frac{1}{2} \int_{p_c/p}^{1} \exp\left(-\frac{x}{\ell z}\right) dz \qquad p \geq p_c$$

$$= 0 \qquad p < p_c \qquad (31)$$

In optical absorption, the rate at which electrons are excited to energies between E and $(E + dE)$, in a slab of width dx located a distance x from the photoemitting surface of a semi-infinite solid, is of the form

$$G(E,x)\, dE\, dx = G_o(E) e^{-\alpha x}\, dE\, dx \qquad (32)$$

where α is the absorption coefficient. From Eqs. (3) and (32), the rate of escape of electrons with energy between E and $(E + dE)$ is

$$R(E)\, dE = G_o(E)\, dE \int_0^{\infty} e^{-\alpha x}\, p_{esc}(E,x)\, dx \qquad (33)$$

Carrying out the integrations in Eq. (33) with respect to x and z

$$R(E)\, dE = \frac{G_o(E)\, dE}{2\alpha} \left[1 - \frac{p_c}{p} - \frac{1}{\alpha\ell} \ln \frac{1 + \alpha\ell}{1 + (p_c/p)\,\alpha\ell} \right] \qquad (34)$$

Defining as a threshold function $C(E) = (1/2)[1 - (p_c/p)]$, Eq. (34) can be simplified to

$$R(E)\, dE = \frac{KC(E)G_o(E)\, dE}{\alpha + (1/\ell)} \qquad (35)$$

where K, a correction factor, varies from 1/2 to 1 and is the function of $C(E)$ and $\alpha\ell$ plotted in Fig. 3. The function $C(E)$ is zero for electron energies less than the work function above the Fermi level, and has a maximum value of 0.5. The measurements on both silver and

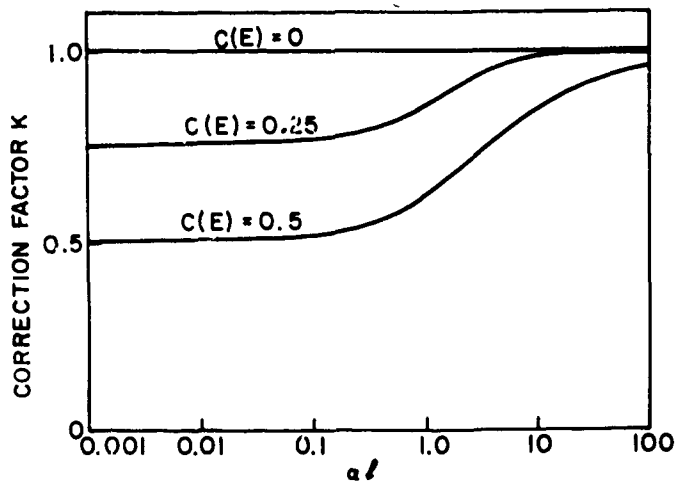

FIG. 3. CORRECTION FACTOR K.

copper indicate that this function is essentially constant for energies greater than 1 ev above the vacuum level.

2. Effect of Elastic Scattering

It has been shown in the previous section that the predominant inelastic-scattering mechanism in the energy range from 1.5 to 11.5 ev above the Fermi level in copper and silver is electron-electron scattering. Another strong scattering mechanism is electron-phonon interaction. However, the energy loss involved in phonon collisions in copper and silver, although finite, is small enough compared to the resolution of the photoemission measurements that the process may be considered as pseudo-elastic. An estimate of the energy loss per collision can be obtained in the following way: In a phonon collision, a phonon is either absorbed or emitted with probability proportional to n and $(n + 1)$ respectively, where n is the equilibrium density of phonons in the metal [Ref. 20]. Assuming the phonon energy corresponds to the Debye temperature (≈ 0.03 ev in Cu, and ≈ 0.02 ev in Ag) [Ref. 28], the energy loss per collision can be averaged over emission and absorption according to the probabilities involved, phonon emission corresponding to an electron-energy decrease equal to the phonon energy, and phonon absorption corresponding to an electron-energy increase of the same magnitude. In copper and silver at $300^{\circ}K$, the average energy

loss per collision is ≈ 0.016 ev and ≈ 0.0075 ev respectively. These values justify the assumption that phonon collisions are lossless.

The process of electron escape from a photoemitter when the mean free path for elastic scattering is comparable to that for inelastic scattering is difficult to describe exactly in closed mathematical form. However, it has been found that the probability of escape of an electron with energy E a distance x from the surface of a photoemitter can be approximated in this case by

$$p_{esc}(E,x) = B(E)e^{-x/L} \tag{36}$$

where $B(E)$ is a function which takes into account the threshold, and L is an attenuation length which depends on the mean free paths for inelastic and elastic collisions [Ref. 29]. Using Eq. (36), calculations similar to those resulting in Eq. (35) give

$$R(E)\ dE = \frac{B(E)G_o(E)\ dE}{\alpha + (1/L)} \tag{37}$$

Stuart, Wooten, and Spicer [Ref. 30] have used the Monte Carlo method to determine L for various values of the mean free paths. Some of their results are shown in Fig. 4. In copper and silver, the absorption coefficient is of the order of 5×10^5 cm^{-1} in the visible and ultraviolet, and the mean free paths for phonon scattering are approximately 500 Å at the Fermi energy [Ref. 31]. Even allowing for the fact that the mean free path for elastic scattering at high electron energies may be somewhat lower than the mean free path for phonon scattering at the Fermi energy, Fig. 4 indicates that $1/L$ will be small compared to α in copper and silver for inelastic-collision mean free paths longer than approximately 500 Å. When the mean free path for inelastic collision is less than 500 Å, L approaches the value of the inelastic-collision mean free path. For these reasons, in copper and silver Eq. (35) may be used over the entire range of electron energies to be studied in this work, the small effect of inelastic collisions being included in the threshold function $C(E)$.

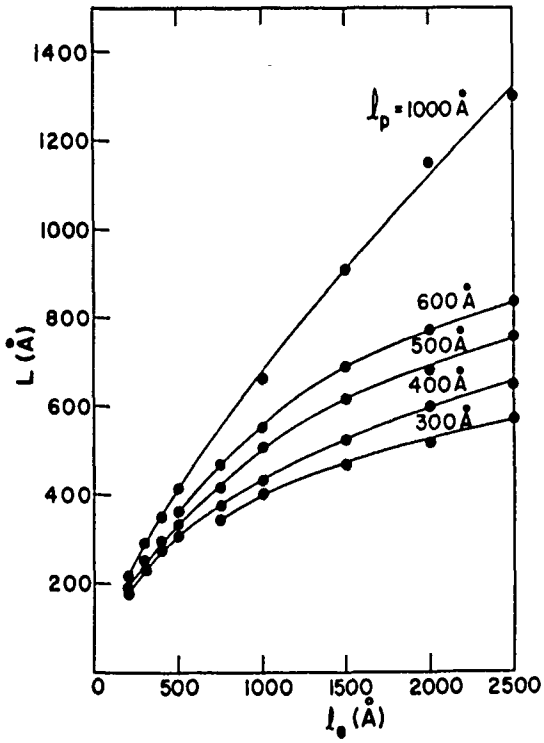

FIG. 4. ATTENUATION LENGTH L CALCULATED USING MONTE CARLO METHOD AS A FUNCTION OF ELECTRON-ELECTRON MEAN FREE PATH ℓ_e AND ELECTRON-PHONON MEAN FREE PATH ℓ_p.

D. ENERGY DISTRIBUTION OF THE PHOTOEMITTED ELECTRONS

Consider electrons in a solid with energy between E and (E + dE) several electron volts above the Fermi level. Electrons may result in this energy range due to either scattering from other energies or photon excitation from states below the Fermi level. Defining $G_{opt}(E,x)\ dE\ dx$ and $G_{sc}(E,x)\ dE\ dx$ as the rate of generation per unit area due to optical excitation and to scattering respectively in a slab of material of width dx a distance x from the photoemitting surface, the contribution of each to the photoemission may be determined.

The absorption coefficient of a solid, α, at frequency ω may be defined as

$$\alpha(\omega) = \int_{E_F}^{E_F+\hbar\omega} \alpha'(\omega,E)\ dE \qquad (38)$$

where $\alpha'(\omega,E)\ dE$ is that part of $\alpha(\omega)$ due to electronic transitions to energy states between E and $(E + dE)$ (the Fermi function at $0^{\circ}K$ has been assumed). If n_p is the flux of photons that is absorbed by the photoemitting material per unit area at frequency ω, then

$$G_{opt}(E,x)\ dE\ dx = n_p \alpha'(\omega,E)\ dE\ e^{-\alpha x}\ dx \qquad (39)$$

In both copper and silver, the effect of scattering is small enough over the electron energy range studied that only those electrons which escape without scattering and those which scatter once before escaping need be considered. The probability of an electron scattering once before escaping is derived exactly in Appendix A. However, the following simple model of the process gives results which agree closely to the detailed calculations, and illustrates the important features.

Suppose that the mean free path for scattering at energy E' is small compared to the absorption depth so that a negligible fraction of electrons excited optically to that energy escapes without scattering. From Eqs. (25) and (26), a fraction $[p_s(E',E)\ dE]/P_s(E')$ of the electrons optically excited to E' are scattered once to an energy between E and $(E + dE)$. If this scattering takes place in a distance small compared to the absorption depth so that the spatial distribution of the electrons after scattering is essentially the same as after optical excitation, then the generation rate at E due to once-scattering of electrons optically excited to E' is

$$G_{sc}(E,x)\ dE\ dx = \frac{p_s(E,E')\ dE\ G_{opt}(E',x)\ dx}{P_s(E')} \qquad (40)$$

The total generation rate at E due to scattering is given by (40) integrated over all E'.

$$G_{sc}(E,x)\ dE\ dx = dx\ dE \int_{E}^{E_F+\hbar\omega} \frac{p_s(E,E')G_{opt}(E',x)\ dE'}{P_s(E')} \qquad (41)$$

Electrons with energy E' can produce electrons at energy E either by themselves being scattered to E or by scattering electrons from states below the Fermi level to E. The probability for these two events can easily be shown to be equal, so the generation rate at E due to scattering is twice that given by Eq. (41).

Combining Eqs. (39) and (41), and substituting in Eq. (35), the number of electrons per absorbed photon that escape from a photoemitter with energy between E and $(E + dE)$ at frequency ω is

$$N_\omega(E)\ dE = \frac{KC(E)\alpha'(\omega,E)\ dE}{\alpha(\omega) + \frac{1}{\ell(E)}} \left[1 + 2 \int_E^{E_F+\hbar\omega} \frac{p_s(E',E)}{P_s(E')} \frac{\alpha'(\omega,E')}{\alpha'(\omega,E)}\ dE' \right] \tag{42}$$

The energy distribution of photoemitted electrons may be related to densities of states and transition probabilities by noting, from Eqs. (11) and (14), that

$$\alpha(\omega) = \frac{2\ \hbar\omega}{nc\epsilon_0 \mathcal{E}_o^2} \int_0^\infty N_T(E',E_0)\ dE' \tag{43}$$

Comparing Eq. (43) to Eq. (38)

$$\alpha'(\omega,E_1) = \frac{2\hbar\omega N_T(E_1,E_0)}{nc\epsilon_0 \mathcal{E}_o^2}. \tag{44}$$

An interesting special case occurs when $\ell(E)$ is long compared to $1/[\alpha(\omega)]$ and the fraction of electrons that escape after scattering is negligible. This occurs in copper and silver for $\hbar\omega$ up to a few electron volts larger than the work function. From Fig. 3, K is unity for $\alpha\ell \gg 1$, so Eq. (42) reduces to

$$N_\omega(E)\ dE = \frac{C(E)\alpha'(\omega,E)\ dE}{\alpha(\omega)} \tag{45}$$

Using Eqs. (43) and (44)

$$N_\omega(E)\,dE = \frac{C(E)N_T(E,E_0)\,dE}{\int_0^\infty N_T(E',E_0)\,dE'} \tag{46}$$

If conservation of k-vector is not important for the optically excited transitions, the expression for $N_T(E,E_0)$ given in Eq. (8) can be used in Eq. (46). Assuming the Fermi function at absolute zero, this becomes

$$N_\omega(E)\,dE = \frac{C(E)f_{10}\rho(E)\rho(E - \hbar\omega)\,dE}{\int_{E_F}^{E_F+\hbar\omega} f_{10}\rho(E')\rho(E' - \hbar\omega)\,dE'} \tag{47}$$

and if f_{10} is energy independent,

$$N_\omega(E)\,dE = \frac{C(E)\rho(E)\rho(E - \hbar\omega)\,dE}{\int_{E_F}^{E_F+\hbar\omega} \rho(E')\rho(E' - \hbar\omega)\,dE'} \tag{48}$$

where E_F is the Fermi energy. It is the expression for the energy distribution given in Eq. (48) that is used to determine the density of states in copper and silver over the energy range for which the assumptions are valid.

The E used in Eq. (42) is the electron energy measured inside the photoemitting material. This energy is related to the electron energy in vacuum, E_v, which is determined from photoemission studies by

$$E_v = E - E_F - E_W \tag{49}$$

where E_W is the work function of the photoemitting metal.

E. QUANTUM YIELD

The quantum yield is defined as the total number of electrons that escape into vacuum from a photoemitting material per absorbed photon. From this definition, and since $C(E)$ in Eq. (42) is zero for E less than $(E_F + E_W)$, the quantum yield is

$$Y(\hbar\omega) = \int_{E_F+E_W}^{\infty} N_\omega(E)\, dE \tag{50}$$

where $N_\omega(E)\, dE$ is given by Eq. (42). From quantum-yield measurements, the value of E_W may be determined and a comparison between the strengths of transitions to states above the vacuum level to those between the vacuum level and the Fermi level may be made.

The yield per absorbed photon Y is related to the yield per incident photon Y' through the reflectivity R_e.

$$Y'(\hbar\omega) = [1 - R_e(\hbar\omega)]Y(\hbar\omega) \tag{51}$$

III. EXPERIMENTAL PROCEDURE

A. THE PHOTOTUBE

A picture of a phototube used in the photoemission studies is shown in Fig. 5, and a diagram showing typical dimensions is shown in Fig. 6. The stem presses, made of uranium glass, have eight 0.050-in. tungsten pins, and the envelope of the tube is pyrex. Nonex glass was originally used in the tubes, but it was found that in tubes using this glass it was difficult to deposit and maintain a monolayer of cesium on the surface of the photocathodes, apparently due to reaction between Cs and envelope. This difficulty disappeared when uranium or pyrex glass was used.

The collector can is formed from 0.005-in. sheet nichrome and cleaned in trichlorethylene, acetone, distilled water, and alcohol. After drying, it is fired in dry hydrogen for 10 min at 1000°C, then mounted on a stem as shown in Fig. 7. There is a metal shield inside the can to prevent copper or silver from depositing on the window of the tube during evaporation. Two cesium channels, obtained from Radio Corporation of America, Princeton, N.J., are shown in the figure. These channels consist of approximately four parts of pure Si or Zr powder and one part of Cs_2CrO_4 powder rolled in thin nickel sheet and crimped. Cesium is given off when a channel is heated to

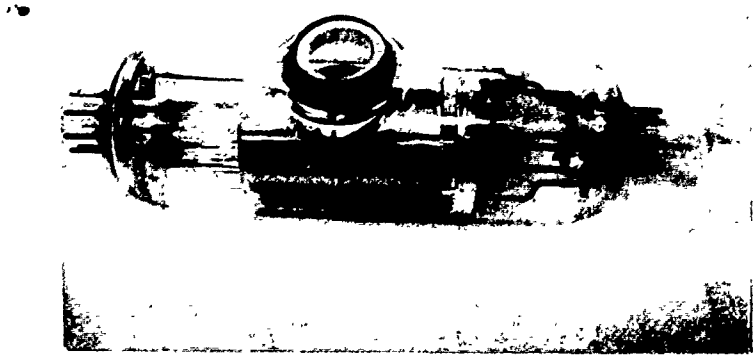

FIG. 5. PHOTOGRAPH OF EXPERIMENTAL PHOTOTUBE.

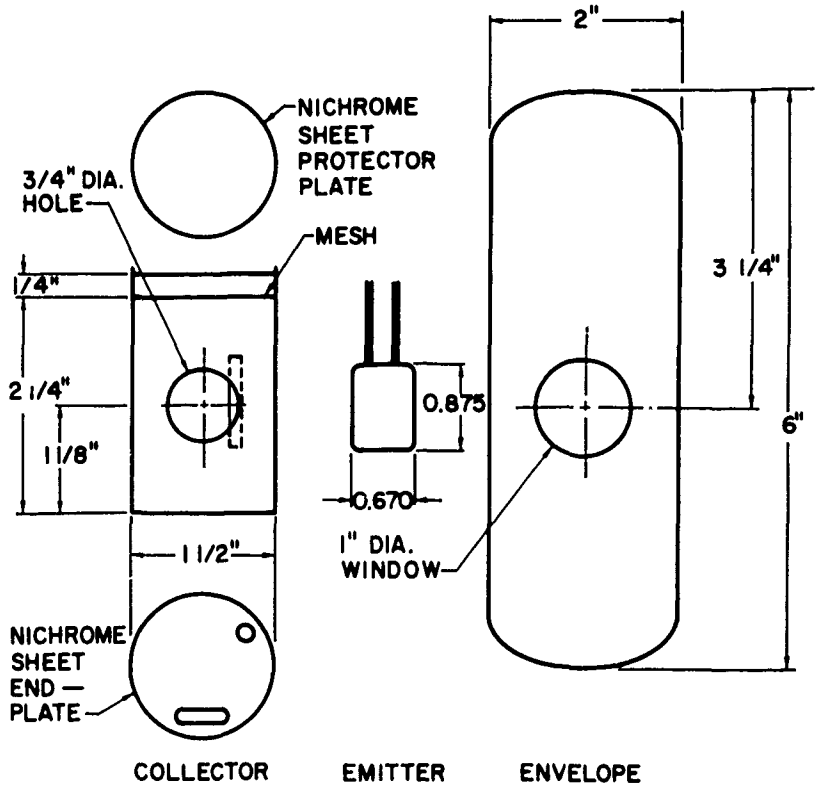

FIG. 6. DIAGRAM OF PHOTOTUBE SHOWING TYPICAL DIMENSIONS.

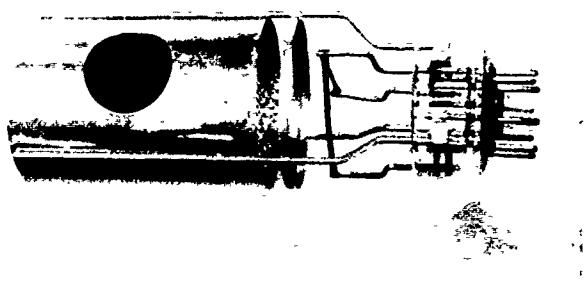

FIG. 7. PHOTOGRAPH OF COLLECTOR CAN IN PHOTOTUBE.

approximately 700°C. The plate between the cesium channels and the collector can prevents impurities in the channels from getting directly onto the photocathode.

The photocathode is cut from 0.050-in. grade A nickel, and polished on progressively finer emery paper ending with 4/0. The plate is polished to a mirror finish with diamond paste and mounted on a stem approximately 1 in. from an evaporator filament as shown in Fig. 8. This filament, of 0.009-in. tantalum wire, has a bead of high-purity silver or copper on it sufficient to produce an evaporated layer on the emitter several times thicker than the maximum optical absorption depth of the metal being studied (layer thickness 2000 Å to 5000 Å). The filaments are prepared by forming the metal bead in a Varian VacIon system at a pressure less than 10^{-7} mm.

The windows used on the tubes are either quartz or lithium fluoride, 1 in. in diameter and 1/16 to 1/8 in. thick. Typical transmission characteristics for both are shown in Fig. 9. In practice, the transmission of each LiF window used was measured before sealing in order that corrections to the experimental results could be made. Tests

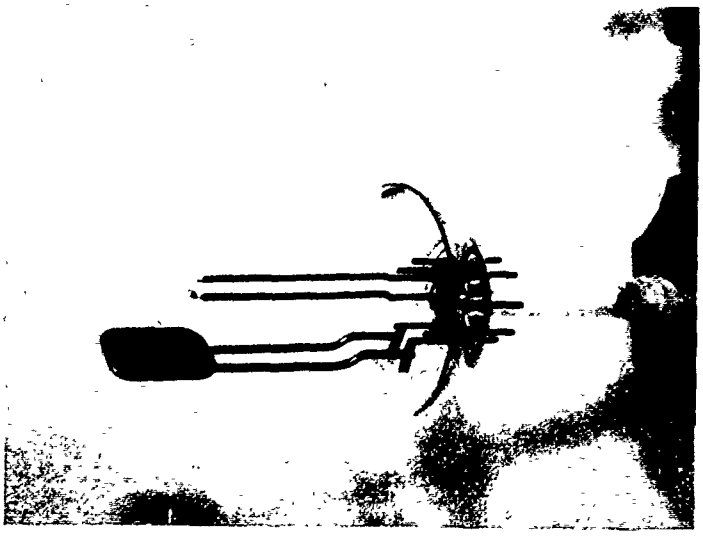

FIG. 8. PHOTOGRAPH OF EMITTER PLATE AND EVAPORATOR FILAMENT IN PHOTOTUBE.

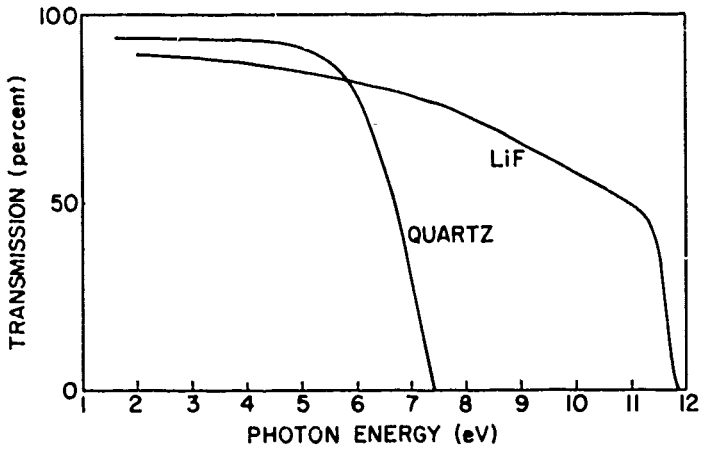

FIG. 9. TYPICAL WINDOW TRANSMISSION CHARACTERISTICS.

indicated that no measurable change in window transmission characteristics occurs in the sealing process. The quartz windows can be sealed directly to the pyrex envelopes using AgCl but, due to the large expansion coefficient of LiF, the LiF windows must be sealed first to a thin (0.010-in.) high-purity silver ring which is then sealed to the envelopes.

Prior to sealing, the windows are prepared by sandblasting a 1/8-in. ring on the edge of one surface with fine alumina powder. The surfaces to be sealed are painted with a thin coat of Hanovia 0.05 liquid bright platinum paint which is fired on at 500°C. While hot, the painted areas of the window and envelope are "tinned" with silver chloride, which melts at approximately 500°C. The silver ring is prepared by annealing in a hydrogen furnace for 10 min at 750°C.

To seal the quartz windows, the window is placed on the envelope in the correct position, and the temperature raised until the silver chloride just melts. Additional silver chloride is "painted" around the seal, and the oven is allowed to cool overnight. A similar procedure is followed for the LiF windows, except that the silver rings are included in the sealing process.

The stem carrying the emitter plate is mounted in a vacuum bell jar and covered by a molybdenum cylinder. The cylinder is heated with radio frequency to approximately 850°C for 15 min to clean the plate, then

removed. The two stems and the envelope are sealed together under a constant flush of 90/10 forming gas to retard oxidation of the metal parts, and the tube sealed on a pump station for processing.

Processing of the tubes is done in the following manner. After evacuation and baking at 250°C for several hours (pressure $\approx 10^{-8}$ mm), the cesium channels are outgassed by slowly increasing the current passed through them. When a current is reached where cesium is beginning to be given off, as determined by the onset of measurable photoemission from the photocathode, the current through the cesium channels is shut off. The metal to be studied is then evaporated onto the photocathode. After evaporation, the cesium channels are fired again, the photocurrent as a function of time being measured. Since the work function of silver or copper is reduced to a minimum when approximately a uniform monatomic layer of cesium is on the surface of the sample, the photocurrent should reach a peak, then begin to decrease as a function of time. When the peak in photocurrent is reached, the cesium channels are shut off and the tube is baked at 100°C. This baking process allows the cesium to spread uniformly throughout the tube. In addition, the last atomic layer of cesium on a surface is generally much more difficult to remove than additional layers due to the strong attraction between cesium and most other substances. For these reasons, essentially all but the last layer of cesium atoms are pumped away during this baking process. This is verified by measuring the photoemission as a function of time during the bake. It is found that the emission current gradually increases to approximately the same maximum value as measured during the depositing of the cesium. The tube is then cooled to room temperature and sealed off, generally at a pressure of about 10^{-8} mm or better.

The way in which the tubes are processed assures that a reasonably uniform layer of cesium is deposited on the cathode and collector, and that the work function of the collector is approximately the same as that of the cathode. By using a microscope lamp focused to a small area on the photocathode or collector, and by measuring the photocurrent, this variation of the work function with position can be determined. In all tubes used for these studies, the variation was small.

B. ENERGY-DISTRIBUTION MEASUREMENTS

Suppose $N_\omega(E)\,dE$ electrons are emitted per second in the energy range between E and $(E + dE)$ by a photoemitter due to radiation at a frequency ω, the energy being measured in vacuum. The photocurrent that flows when a voltage V is applied to a collecting electrode is

$$I_\omega(V) = e \int_{-eV}^{\infty} N_\omega(E)\,dE \tag{52}$$

where the voltage V includes the difference in contact potential between the collector and cathode. In this expression, the effect of space charge in the region between the collector and the photoemitter has been neglected. (The errors involved in this assumption will be described later.) The small-signal conductance of the tube at voltage V_o is

$$g_\omega(V_o) = \left.\frac{dI_\omega(V)}{dV}\right|_{V_o} = e^2 N_\omega(-eV_o) \tag{53}$$

indicating that the energy distribution of photoemitted electrons can be determined by simply measuring the phototube small-signal conductance as a function of retarding potential.

Measurements of the energy distribution of photoemitted electrons have been made by carefully measuring the I-V curve of a phototube illuminated with light at the desired frequency, and graphically differentiating the curve with respect to voltage [Ref. 32]. This technique requires extremely accurate determination of the I-V curve, and any small noises in the measurements generally lead to significant errors. Spicer has used an ac method to perform the differentiation electronically, thus directing measuring the energy distribution of the photoemitted electrons and obtaining more accurate results with less sensitive equipment [Ref. 33]. A new system based on the one described by Spicer, but including some modifications and improvements, was used in this work and will be described in detail.

The circuit used for measuring electron energy distributions for photoemitters exposed to visible and near ultraviolet light is shown in Fig. 10. Light from the monochromator with the desired photon energy is directed normally onto the photocathode in such a way that a negligible amount of light strikes the collector either directly or after reflection from the photoemitter. This assures that negligible photoemission occurs from the collector and that only electrons emitted from the photocathode contribute to the results. The dc voltage is swept at a speed of about 1 v/min from a small positive collector voltage to a negative voltage corresponding to an energy greater than the maximum energy of the photoemitted electrons.

The operation of the circuit is as follows. A small ac voltage from the PAR (Princeton Applied Research) amplifier is superimposed on the dc sweep voltage. This voltage is generally between 10 and 200 mv rms depending on the resolution needed to detect any structure in the energy-distribution curves and the noise present in the measurement. The resulting ac current in the circuit is sampled by the 1-megohm resistor, amplified by the Keithley electrometer, and applied to the input of the PAR amplifier. This amplifier acts as a phase-sensitive detector, and is adjusted to detect the component of current which is

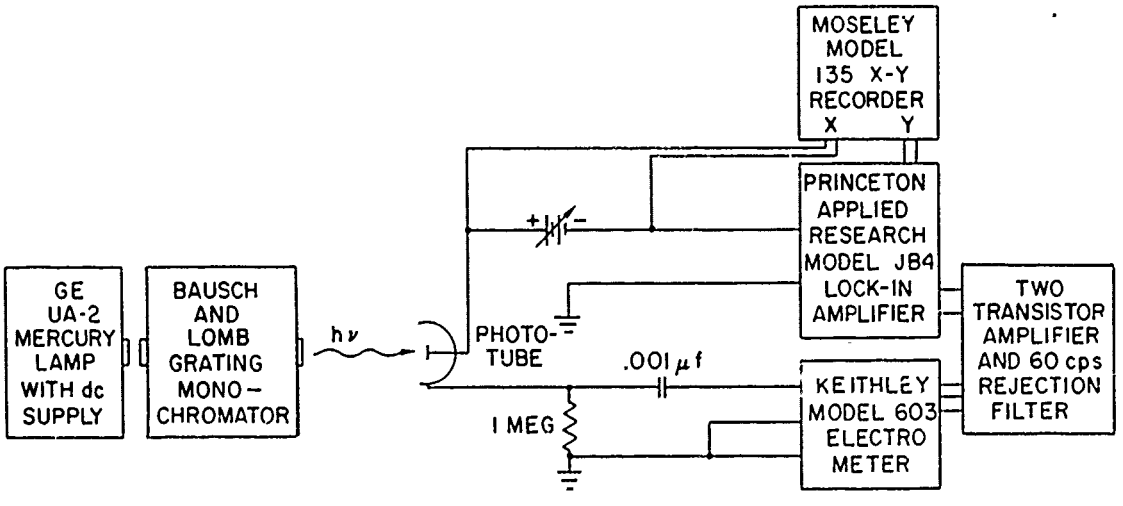

FIG. 10. CIRCUIT FOR MEASURING ELECTRON ENERGY DISTRIBUTIONS--$\hbar\omega < 6$ eV.

proportional to the small-signal conductance of the phototube. The phase of the PAR amplifier is adjusted by turning off the light to the phototube and setting the phase control of the instrument for zero output. Since the ac dark current of the tube is essentially all capacitive, this adjustment assures that only the conductive component of current is detected.

For measurements in the vacuum ultraviolet, a McPherson vacuum ultraviolet monochromator with a hydrogen-discharge Hinteregger-type light source was used. However, due to the lower intensity of this source as compared to those used in the visible and near ultraviolet, the capacitive signal component from the photocube was much greater than the conductive component, and the simple circuit shown in Fig. 10 was not sensitive enough to provide satisfactory results. A circuit which compensates for the tube capacitance and reduces the effect of noise and stray pickup in the sweep-voltage section of the circuit is shown in Fig. 11. When the variable capacitance is adjusted to be equal to the tube capacitance, the capacitive and noise components of the signal cancel out due to the differential amplifying property of the Keithley Model 603 amplifier. This circuit allows measurements at much lower light intensities than the circuit shown in Fig. 10, with fewer noise problems.

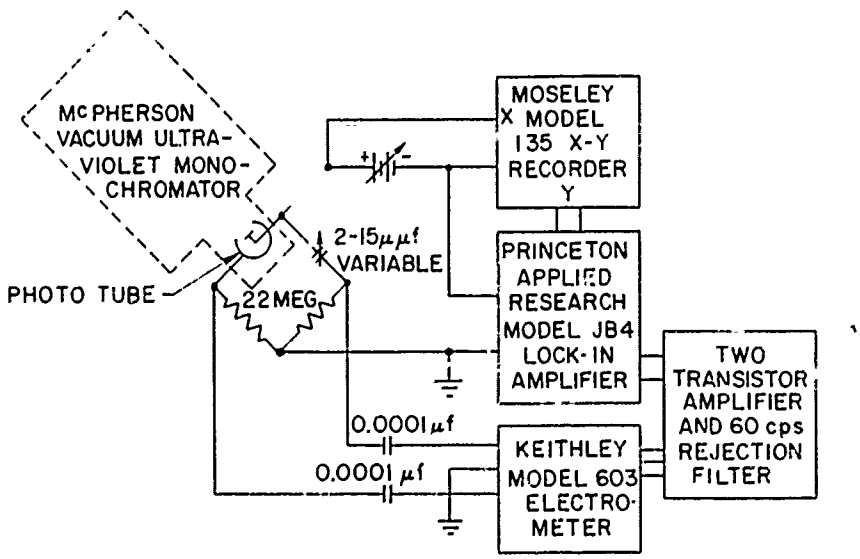

FIG. 11. CIRCUIT FOR MEASURING ELECTRON ENERGY DISTRIBUTIONS IN THE VACUUM ULTRAVIOLET.

The transistor amplifier shown in Figs. 10 and 11 is a low-gain differential amplifier with a single-ended output. It matches the double-ended output of the Keithley amplifier to the input of the PAR amplifier. Also included in the circuit is a 60-cps rejection filter. The circuit diagram is shown in Fig. 12.

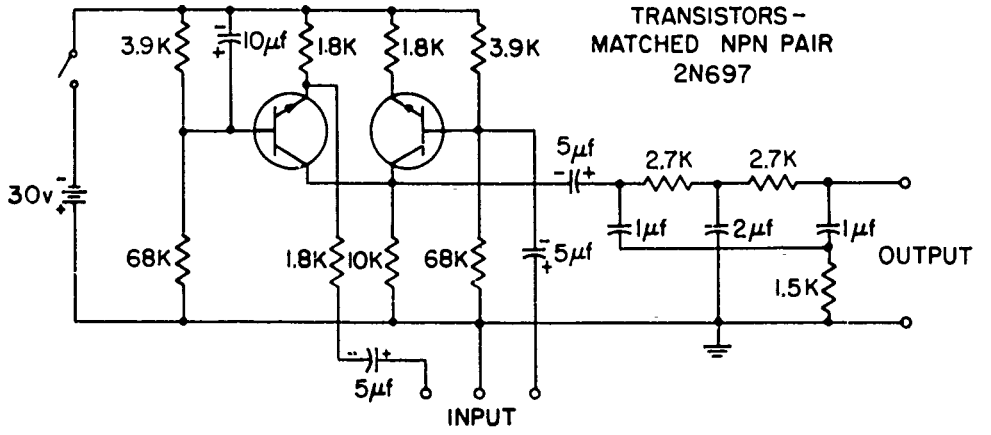

FIG. 12. TRANSISTORIZED AMPLIFIER AND 60-CPS REJECTION FILTER.

Since the small-signal conductances being measured are of the order of 10^{-11} mhos, 60-cps pick-up and ground-loop currents are the largest sources of noise. Careful wiring and shielding of all leads reduces the effects of these noise sources considerably. Figures 13 and 14 show typical energy-distribution measurements made using the circuits described. They also illustrate the amount of noise present in the measurements.

There are two fundamental sources of error possible in the described measurement of electron energy distributions. These are space-charge effect and transit-time distortion due to nonspherical geometry of the phototube. If there is significant space-charge effect, a potential minimum may exist in the region between the collector and the photo-emitter depending on the applied voltage. In Fig. 15, the potential in

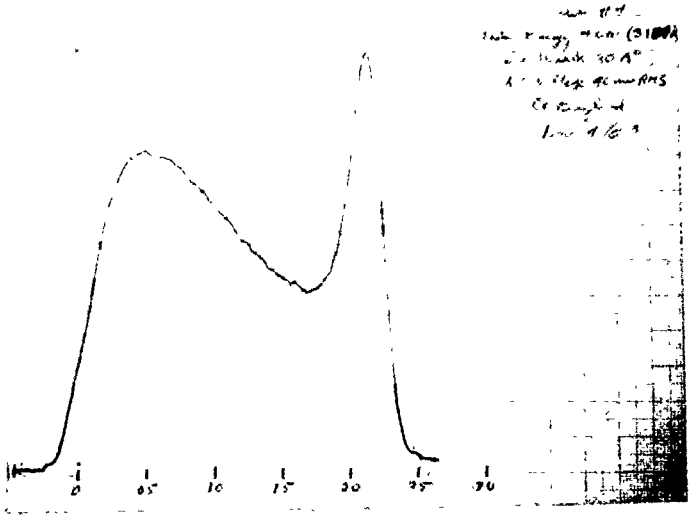

FIG. 13. PHOTOGRAPH OF TYPICAL ENERGY DISTRIBUTION MEASUREMENT IN COPPER.

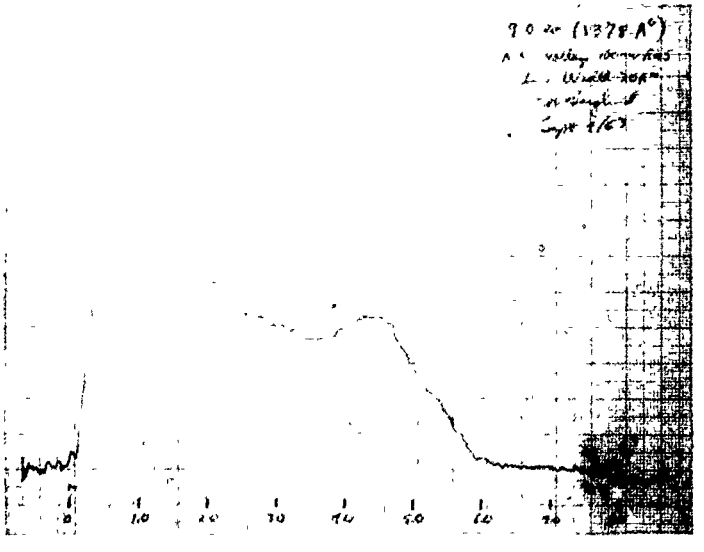

FIG. 14. PHOTOGRAPH OF TYPICAL ENERGY DISTRIBUTION MEASUREMENT IN SILVER.

the tube is plotted for several applied voltages to illustrate the space-charge effect. There is a voltage region near zero applied voltage where the potential minimum in the tube is in the region between the collector and the photoemitter. In this range Eq. (52) will not be valid and the tube small-signal conductance will not be proportional to

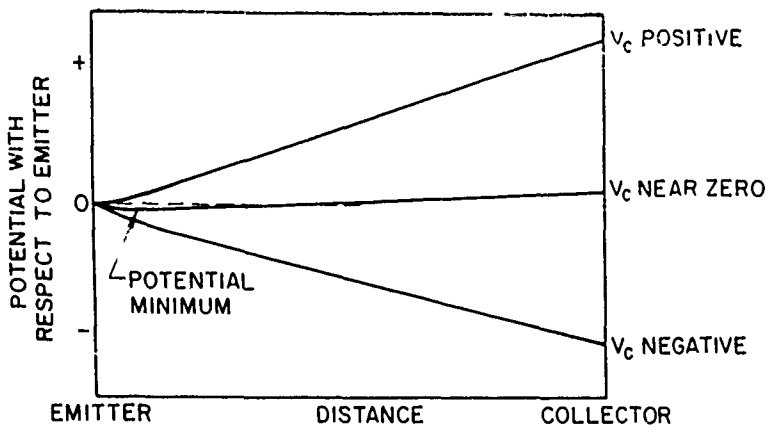

FIG. 15. ILLUSTRATION OF POTENTIAL IN PHOTOTUBE BETWEEN EMITTER AND COLLECTOR SHOWING POTENTIAL MINIMUM DUE TO SPACE CHARGE.

the energy distribution of the photoemitted electrons. Reducing the emission rate of electrons by decreasing the incident light intensity will limit the voltage range over which distortion occurs, and at sufficiently low light intensities the distortion will be negligible. Figure 16 shows energy-distribution measurements made on a phototube at various light intensities, and illustrates the distortion which can result due to space-charge effects. In all the measurements reported in this work, care has been taken to use light intensities low enough to keep distortion due to space charge negligible.

The second fundamental source of error in the measurement of $N_\omega(E)$ is the transit-time effect. If the tube geometry is nonspherical, there will be a spread in transit times for electrons emitted in different directions or from different areas of the cathode. If the difference in transit time is comparable to the period of the small ac voltage used in the measurements, the small-signal conductance of the phototube will not be proportional to $N_\omega(E)$. An estimate of the distortion due to this effect can be obtained by calculating the transit time of an electron for the longest trajectory in the tube as a function of emission energy, assuming that the electron just reaches the collector with zero velocity. In the phototubes used, the maximum distance from

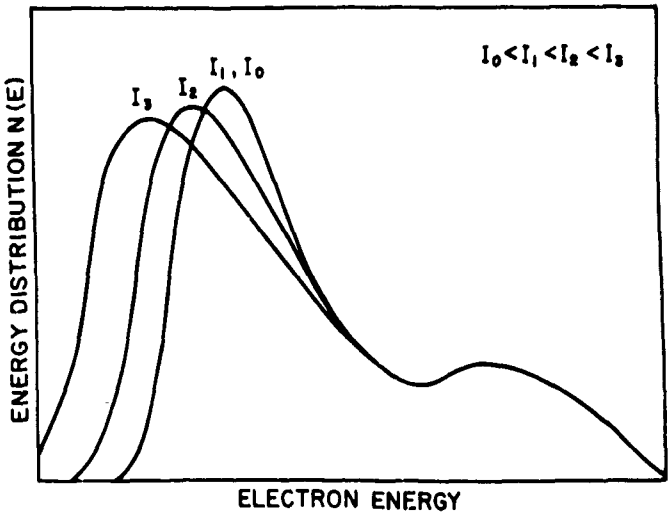

FIG. 16. ENERGY DISTRIBUTION CURVES MEASURED AT A SINGLE PHOTON ENERGY AT SEVERAL LIGHT INTENSITIES I.

emitter to collector is of the order of 3 cm, giving for a calculated transit time approximately

$$t = \frac{3 \times 10^{-4}}{\sqrt{E}} \quad \text{sec} \tag{54}$$

where E is in electron volts. Since the ac measurements are made at 20 cps, this time must be comparable to 1/20 sec for this effect to cause significant distortion. This only occurs for E within about 0.001 ev of zero, and for this reason the effect is neglected.

C. QUANTUM-YIELD MEASUREMENTS

The circuit for measuring relative quantum yield in the visible and near ultraviolet region of the spectrum is shown in Fig. 17. Chopped light at 20 cps is directed onto the phototube at the desired photon energy, and the resulting 20 cps photocurrent that flows is measured using the Keithley electrometer as a preamplifier and using the lock-in amplifier as an amplitude detector. The collector of the phototube during measurement is maintained at a sufficiently positive voltage so that all electrons emitted from the cathode are collected

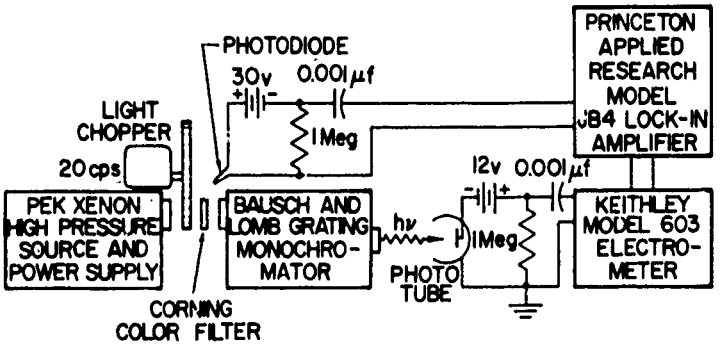

MEASUREMENT OF PHOTO TUBE RESPONSE

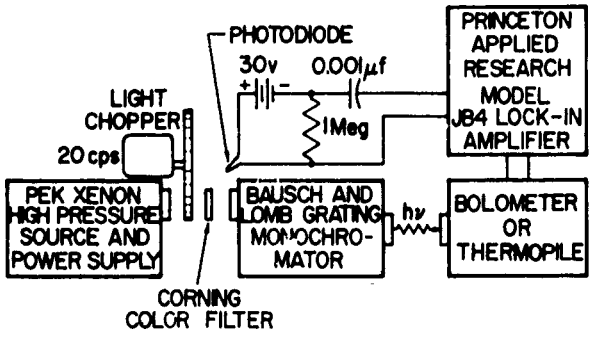

MEASUREMENT OF RESPONSE OF STANDARD

FIG. 17. CIRCUIT FOR MEASURING RELATIVE QUANTUM YIELD--$\hbar\omega < 6$ ev.

and no electrons emitted from the collector reach the cathode (about 12 v). The photodiode in the circuit provides a signal for the PAR amplifier that is at the same frequency as the chopping frequency.

The response of the phototube under study is compared to either a Reeder Model RHL-7 thermopile or to a Barnes thermistor bolometer type S 50-S. The response of both of these devices is proportional to the incident power of the radiation over a wide range of light frequency. Since at a given photon energy the photocurrent I_{ph} from the phototube is proportional to the rate of electron emission, and the response of the thermopile or bolometer S is proportional to the number of incident photons per second multiplied by the photon energy, the quantum yield in electrons per incident photon of the phototube is

$$Y = K_1 \frac{I_{ph} \hbar\omega}{S} \qquad (55)$$

where K_1 is a constant. Using Eq. (55), the relative yield at different photon energies can be determined by measuring S and I_{ph} at various incident light frequencies.

The constant K_1 in Eq. (55) is determined at a single photon energy by comparing the phototube under study to an RCA 934 phototube which had been calibrated for absolute yield at a photon energy of 3.0 ev by W. E. Spicer, and checked by H. R. Phillip at General Electric Research Laboratories [Ref. 34].

When the photon energy is only slightly greater than the work function of the photoemitter, the yield is many orders of magnitude smaller than at much higher photon energies. For this reason, care must be taken when making measurements near the photoemission threshold that no scattered light of higher photon energy gets into the phototube. Scattered light can be eliminated by placing Corning-glass color filters between the light source and the monochromator, as shown in Fig. 17. These filters are chosen to pass only the light with photon energy equal to or less than the photon energy of the measurement.

Under incident radiation with photon energies greater than 4 ev, it has been found that sodium salicylate fluoresces near 4200 Å, giving very nearly one photon at that wavelength per incident photon for incident photon energy greater than 4 ev. A phototube or photomultiplier coated with sodium salicylate will have a response nearly proportional to the number of incident photons per second for light with photon energy greater than 4 ev. This property has been used to measure the quantum yield of phototubes at photon energies greater than 4 ev, and is described in detail by Kindig [Ref. 35]. The relative quantum yield determined in this way is matched to the known absolute quantum yield measured using the bolometer or thermopile.

IV. PHOTOEMISSION FROM COPPER

A. THE CALCULATED BAND STRUCTURE OF COPPER

Calculations of the energy-band structure of copper have recently been made by Segall and Burdick [Refs. 2, 3]. It is of importance to describe the crystal potentials that were used in these calculations, since the extremely close agreement between the calculated band structure and the experimental results reported here indicates that the potential was very accurately approximated.

In Segall's work, the band structure was calculated twice by the Green's function method [Ref. 36] using two different potentials. One of the potentials used was that constructed by Chodorow [Ref. 37], and is the one which yields the 3d electron Hartree-Fock functions for the free Cu^+ ion. To this Segall added the contribution of a "metallic" s electron function (the s function for an electron of average energy). The use of this potential implies the Wigner-Seitz approximation that all conduction electrons, except those for the unit cell under consideration, are excluded from the cell by correlation and exchange interactions. The potential might be expected to be most accurate for the d electrons. Also, it includes the approximation that the same potential applies to all angular momentum components of the wave function.

The core and d-electron Hartree-Fock functions for neutral copper were renormalized in the Wigner-Seitz sphere and used for the second potential. The coulomb and exchange contributions to the potential for the various values of ℓ were computed for a configuration which included, in addition to the core and d electrons, a renormalized s function.

Segall found that the band structures calculated for the two different potentials were very similar. The positions of the bands were somewhat different, but the general features were the same.

Burdick calculated the band structure by the APW method [Ref. 38] using the Chodorow potential described above. His results agreed with those of Segall for the same potential to within 0.15 ev.

The band structure along the various symmetry axes in the reduced zone calculated by Segall using the ℓ-dependent potential is shown in

Fig. 18. This band structure will be used in discussing the photoemission data. (Detailed comparisons of the data to the calculations of both Segall and Burdick will be given in the text.) In Fig. 18 the points of symmetry are labeled according to the notation of Bouckaert, Smoluchowski, and Wigner [Ref. 39]. The relatively flat bands located approximately 2 to 6 ev below the Fermi level are the d-bands. Because of the flatness of the bands, they are characterized by a relatively high density of states. The difference in energy between the vacuum level marked on the figure and the Fermi level is the work function of copper with approximately a monolayer of cesium on the surface. This energy is determined by studying the quantum yield of a suitably treated copper photoemitter as a function of photon energy.

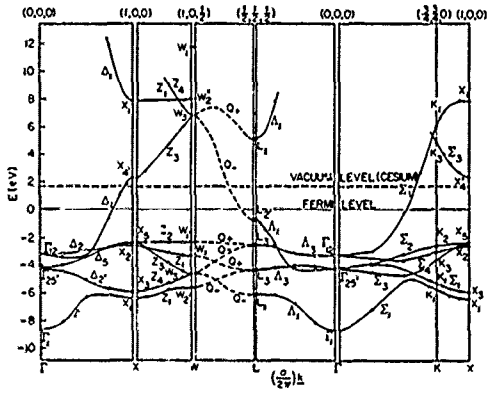

FIG. 18. CALCULATED BAND STRUCTURE OF COPPER.

B. THE QUANTUM YIELD

Figure 19 shows the quantum yield of a copper photoemitter with cesium on the surface. The solid curve is the measured yield per incident photon, corrected for the transmission of the LiF window of the phototube. The dashed curve is the yield per absorbed photon determined from the measured yield and the reflectivity of copper [Ref. 19].

In a theoretical treatment of photoemission from metals, Fowler [Ref. 40] has derived the following equation for the quantum yield near the threshold of photoemission:

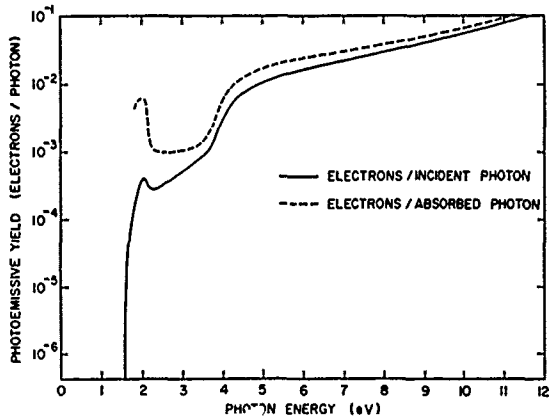

FIG. 19. QUANTUM YIELD OF COPPER.

$$Y \propto (\hbar\omega - E_W)^2 \qquad \hbar\omega \geq E_W$$
$$= 0 \qquad \hbar\omega < E_W \qquad (56)$$

where E_W is the work function of the metal. From Eq. (56) a plot of the square root of the yield as a function of photon energy should give a straight line extrapolating to the work function for zero yield. Such a plot for copper is shown in Fig. 20. The work function for copper determined from Fig. 20 is 1.55 ev.

The general features of the quantum-yield curve shown in Fig. 19 are due to the d-bands. This can most easily be demonstrated by the following argument. If scattering effects are negligible, the quantum yield can be written approximately as [Ref. 29]

$$Y \propto \frac{\alpha_a}{\alpha_a + \alpha_b} \qquad (57)$$

where α_a is that part of the absorption coefficient due to transitions to states above the vacuum level, and α_b is that part due to transitions to states between the Fermi level and the vacuum level. The decrease in yield in Fig. 19 at about 2.1 ev photon energy is due principally to an increase in α_b, since at this energy electrons from the d-bands are starting to be excited to states just above the Fermi level. At 3.7 ev photon energy, d-band electrons can be excited to states above the vacuum

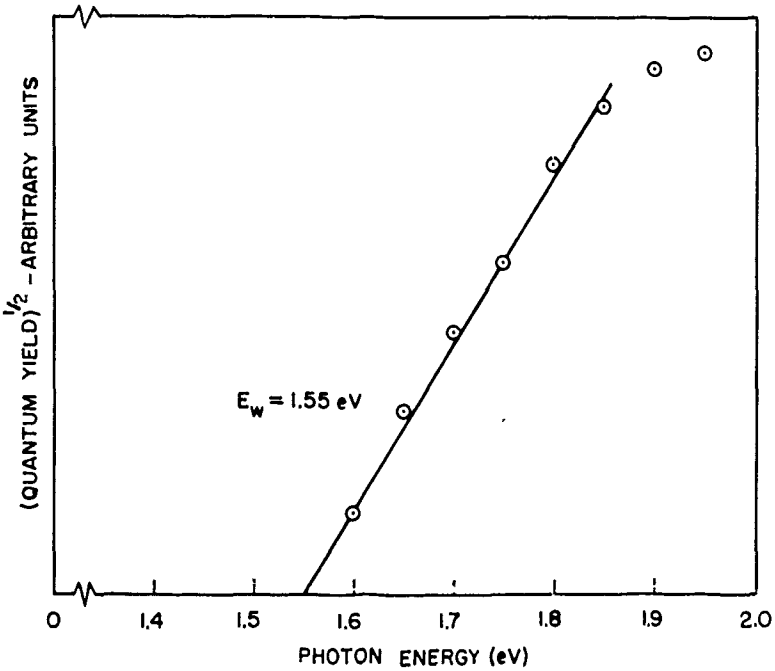

FIG. 20. EVALUATION OF WORK FUNCTION OF COPPER WITH CESIUM ON THE SURFACE.

level resulting in an increase in α_a and in the yield. The slow increase in yield at photon energies greater than 6 ev is due to scattering, and will be explained in detail in Sec. G.

C. ENERGY DISTRIBUTION OF PHOTOEMITTED ELECTRONS--$\hbar\omega \leq 3.7$ ev

At photon energies less than 3.7 ev, electrons excited from the d-bands do not gain enough energy to be able to escape, and structure in the energy distribution of photoemitted electrons is due almost entirely to transitions from the p-like states just below the Fermi level to s-like states just above the vacuum level. Details of the band structure in these energy regions can be determined by studying the energy distribution of photoemitted electrons.

Figure 21 shows the energy distributions which result for photon energies from 2.1 ev to 3.7 ev. Two peaks appear in the distribution, one fixed in energy independent of $\hbar\omega$ at about 0.25 ev above the vacuum level, and the other with energy E given by

$$E = \hbar\omega - 1.90 \text{ ev} \qquad (58)$$

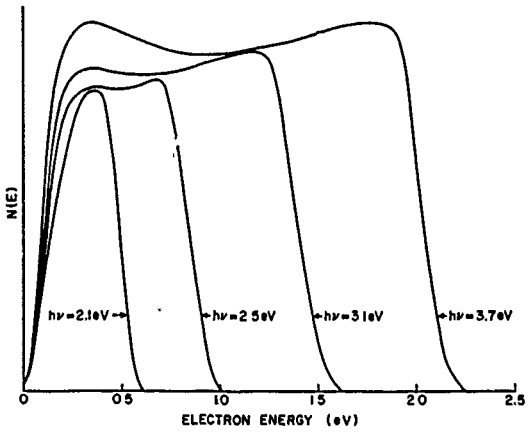

FIG. 21. ENERGY DISTRIBUTION OF PHOTOEMITTED ELECTRONS FROM COPPER--$\hbar\omega \leq 3.7$ ev.

The two peaks coincide at a photon energy of approximately 2.1 ev. The behavior shown in Fig. 21 is characteristic of indirect transitions and can be explained in terms of two peaks in the density of states. Assuming a work function of 1.55 ev, these peaks are located 0.35 ev below and 1.8 ev above the Fermi level. Figure 22 illustrates the transitions responsible for the observed energy distributions in more detail.

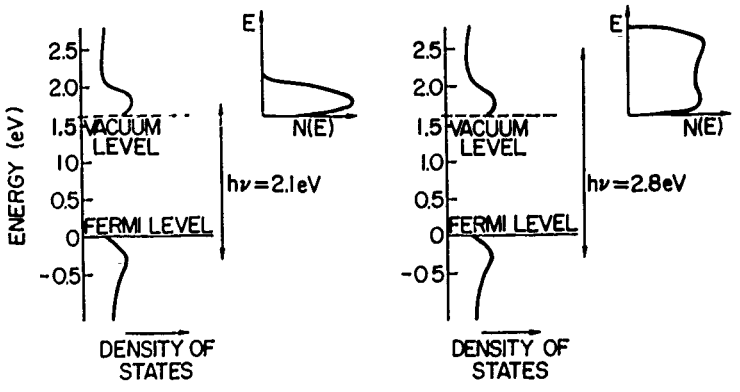

FIG. 22. INDIRECT TRANSITIONS IN COPPER.

Comparing this experimentally determined density of states to the calculated band structure in Fig. 18, it is evident that the peak 0.35 ev below the Fermi level is associated with symmetry point L_2' and that the peak 1.8 ev above the Fermi level is associated with symmetry point X_4', since high densities of states result at symmetry points in the band structure. Segall [Ref. 2] and Burdick [Ref. 3] indicate critical points at X_4' (2.3 or 2.0 ev, respectively, above the Fermi surface) and at L_2' (0.8 or 0.6 ev, respectively, below the Fermi surface). The energies at the symmetry points attributed to Segall are those calculated assuming the ℓ-dependent potential.

D. TRANSITIONS FROM THE d-BANDS

At photon energies greater than 3.7 ev, electrons can be optically excited from the d-bands to states above the vacuum level. These electrons will appear in the energy distribution of the photoemitted electrons at these photon energies. Figure 23 shows the energy distributions for photon energies of 3.7 and 3.9 ev. At 3.7 ev there is very little evidence of d-band electrons being excited to states above the vacuum level. At 3.9 ev, however, a large number of slow electrons

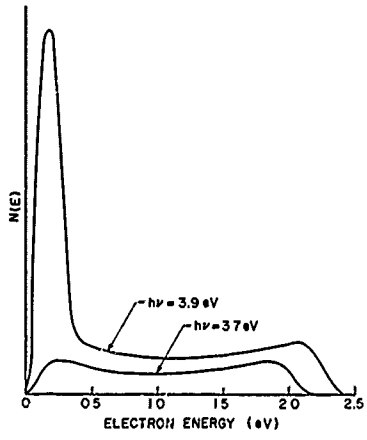

FIG. 23. ENERGY DISTRIBUTION OF PHOTOEMITTED ELECTRONS FROM COPPER--$\hbar\omega$ = 3.7 ev, 3.9 ev.

appear which can only be explained in terms of transitions from the d-bands. When the photon energy is further increased, as shown in Fig. 24, more of the d-bands become exposed.

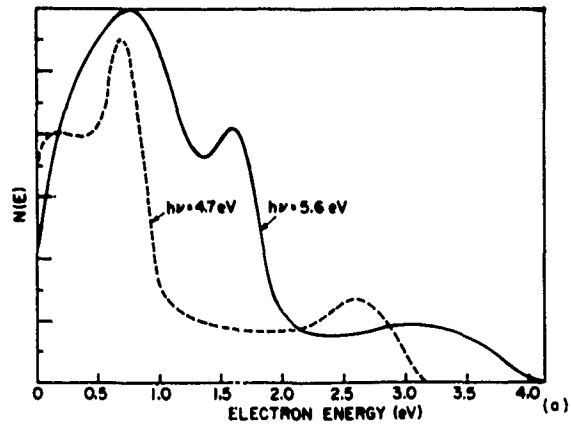

FIG. 24. ENERGY DISTRIBUTION OF PHOTOEMITTED ELECTRONS FROM COPPER--$\hbar\omega$ = 4.7 ev, 5.6 ev.

Two peaks in the d-band density of states are evident in Fig. 24. If the energy distribution of the photoemitted electrons from the d-bands is plotted vs $(E - \hbar\omega)$ rather than vs E, as shown in Fig. 25, the two peaks in the distributions always coincide. This coincidence shows that transitions from the d-bands are predominantly indirect [Ref. 23]. (The term indirect is used to describe all optical transitions in which k-vector conservation is not an important selection rule.) Using a work function of 1.55 ev, the two peaks in the d-band are located 2.4 ev and 3.3 ev below the Fermi level and are approximately 0.2 ev wide and 1.2 ev wide, respectively. A detailed description of the d-band density of states and a comparison with the calculated density of states is given in Sec. F. The distortion in the peaks in Fig. 25 that occurs as photon energy is increased is due primarily to strong inelastic scattering, and will be discussed in subsequent sections.

E. INDIRECT AND DIRECT TRANSITIONS IN COPPER

It has been shown in Secs. B and C that transitions to states above the vacuum level for $\hbar\omega < 3.7$ ev, and transitions from the d-bands

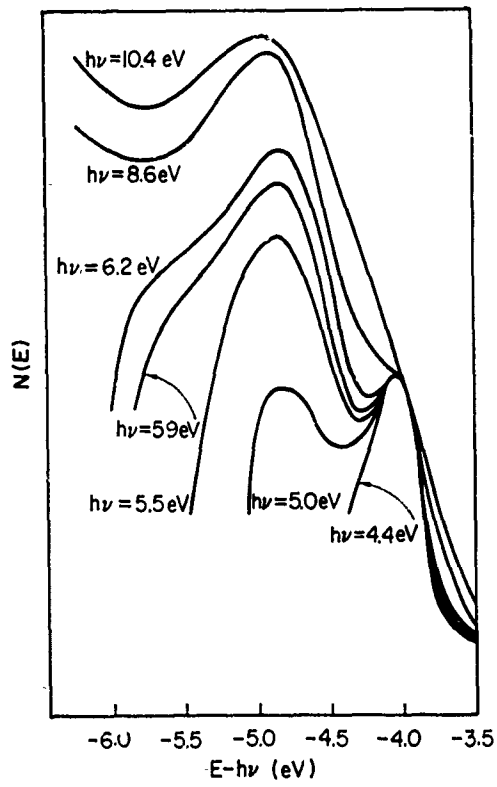

FIG. 25. ENERGY DISTRIBUTION OF PHOTOEMITTED ELECTRONS FROM COPPER PLOTTED VERSUS E-ħω.

to states above the vacuum level can be adequately explained in terms of indirect transitions. There is no evidence of direct transitions in these cases. However, for photon energies above 4.1 ev, direct transitions contribute to the observed results.

Referring to Figs. 21 and 24, the peak near the maximum electron energy attributed to transitions from states near L_2' in the calculated band structure grows in size at $\hbar\omega$ = 4.7 ev, and splits into two peaks as shown for $\hbar\omega$ = 5.6 ev. This behavior can be interpreted in terms of indirect and direct transitions, and is illustrated using the calculated band structure in Fig. 26. When the photon energy $\hbar\omega_1$ is just equal to the energy difference between L_1 and L_2', a strong peak in the energy distribution should occur near the maximum electron energy due to the sum of both indirect and direct transitions from L_2'. At a higher photon energy, $\hbar\omega_2$, two peaks in the energy distribution should appear, one due to direct transitions from states near L_2' to states

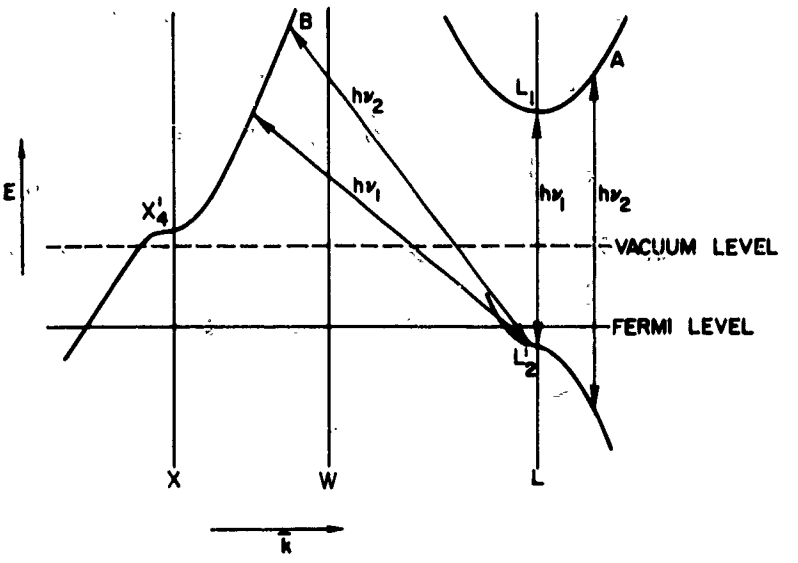

FIG. 26. PORTION OF BAND STRUCTURE OF COPPER SHOWING DIRECT AND INDIRECT TRANSITIONS.

near L_1 (labeled A in Fig. 26), and one due to indirect transitions from the high density of states near L_2' (labeled B). The peak due to direct transitions will not have an energy given by Eq. (58) since the energy of the initial states will depend on $\hbar\omega$ (see Fig. 26). In general, it will be found that the energy of the peak due to direct transitions will increase in energy with $\hbar\omega$ more slowly than that given by Eq. (58), but the peak due to indirect transitions will follow Eq. (58).

Figure 27 shows the portion of the energy distributions near the maximum electron energy for several values of $\hbar\omega$. The estimated fraction of electrons due to direct transitions is shown by the cross-hatched area. From this figure, it is apparent that the probability of electrons being involved in indirect transitions is somewhat stronger than that for direct transitions in the copper samples studied, a result which is the complete opposite of the behavior in the semiconductors Si and Ge [Ref. 14]. No other evidence of direct transitions in copper was found over the range of electron energy studied. In Fig. 28 the energy at the symmetry point L_1 is determined. The vertically plotted energy in the figure is the energy of the initial states

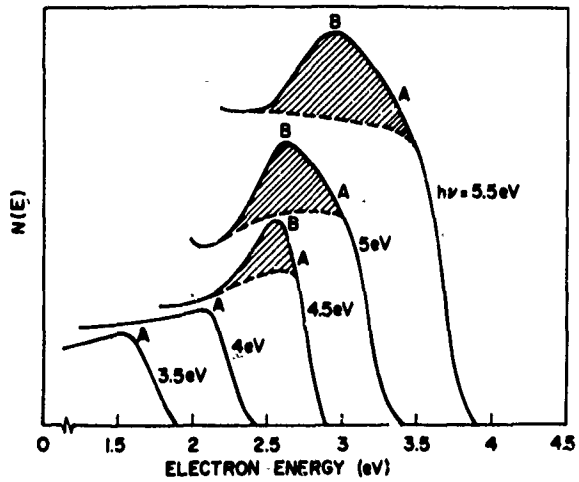

FIG. 27. EXPERIMENTAL EVIDENCE OF DIRECT AND INDIRECT TRANSITIONS IN COPPER.

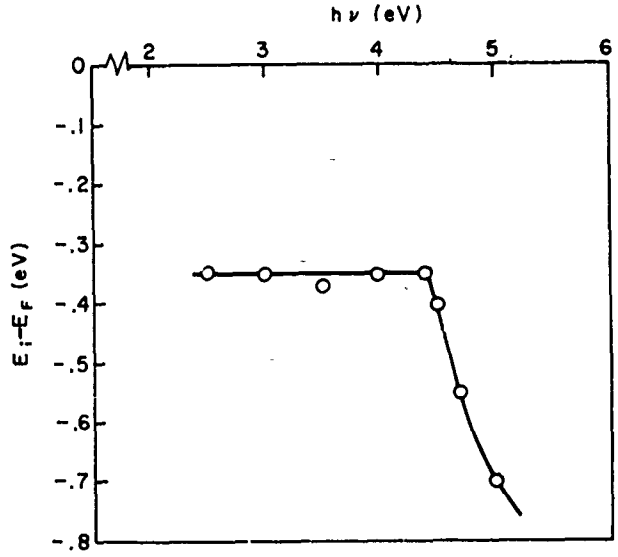

FIG. 28. ENERGY OF INITIAL STATES RESPONSIBLE FOR HIGH-ENERGY PEAK IN PHOTOEMISSION DATA.

responsible for the peak in the energy distributions of Fig. 27. This energy is given by

$$E_i = E_F + E - \hbar\omega + 1.55 \text{ ev} \qquad (59)$$

where E is the energy at the peak in Fig. 27. For $\hbar\omega$ less than 4.4 ev, the energy $E_i - E_F$ is constant at -0.35 ev. At $\hbar\omega$ = 4.4 ev, the energy breaks away from -0.35 ev and becomes rapidly more negative as $\hbar\omega$ increases. Assuming $\hbar\omega$ = 4.4 ev joins symmetry points L_2' and L_1 in energy, L_1 must be located 4.05 ev above the Fermi level. Segall and Burdick have located this point 5.1 ev and 4.2 ev above the Fermi surface respectively.

F. THE COPPER DENSITY OF STATES

It has been shown above that the energy distribution of photoemitted electrons from copper can be interpreted in terms of indirect transitions except for the small contribution of direct transitions from states near L_2' to states near L_1. Since the indirect-transition probability is proportional to the product of the initial and final densities of states, it is possible to determine very accurately the relative density of states from the photoemission data.

The procedure followed in determining the density of states of copper was one of trial and error. Many of the important features of the density of states can be determined without making a detailed analysis. The determination of the energy location and shape of the d-band, and of the peaks in the density of states 0.35 ev below and 1.8 ev above the Fermi level, has been described in Secs. C and D. From this information, an estimate of the density of states can be made as shown in Fig. 29. If the energy distributions of photoemitted electrons at several photon energies are calculated using this density of states and compared to the measured distributions, it is found that only small corrections to the density of states are required to bring the measured and predicted distributions into close agreement.

In order to predict the energy distribution of photoemitted electrons, information in addition to the density of states is required. The theoretical expression for the energy distribution is reproduced here for convenience:

$$N_\omega(E)\,dE = \frac{KC(E)\alpha'(\omega,E)\,dE}{\alpha(\omega) + \frac{1}{\ell(E)}}\left[1 + 2\int_E^{E_F+\hbar\omega} \frac{p_s(E',E)}{P_s(E')}\,\frac{\alpha'(\omega,E')}{\alpha'(\omega,E)}\,dE'\right] \quad (42)$$

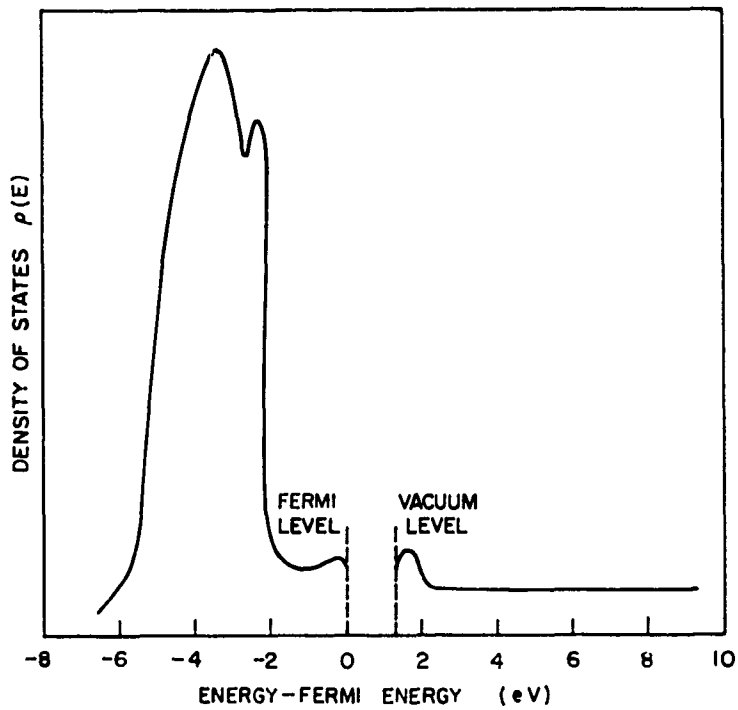

FIG. 29. ESTIMATED DENSITY OF STATES OF COPPER.

The threshold function $C(E)$ in copper is difficult to determine because of the peak in the density of states just above the vacuum level. However, $C(E)$ for silver is relatively easy to determine, and will be used here (see Fig. 63 in Chapter V). Since silver and copper are very similar metals, this assumption should result in only a small error. The absorption coefficient $\alpha(\omega)$ for copper is given in the literature [Ref. 19]. The scattering parameters $p_s(E',E)$, $P_s(E')$, and $\ell(E)$ can be estimated using the density of states. (A detailed description of these calculations is given in Sec. G.) The function $\alpha'(\omega,E)$ is given in Eq. (44), and for indirect transitions is proportional to the product of the initial and final densities of states if the squared momentum matrix element is assumed constant.

Figures 30 and 31 show the measured and predicted energy-distribution curves at two photon energies to illustrate the degree of accuracy obtained after corrections to the density of states had been made. These curves are indicative of the agreement obtained over the photon energy

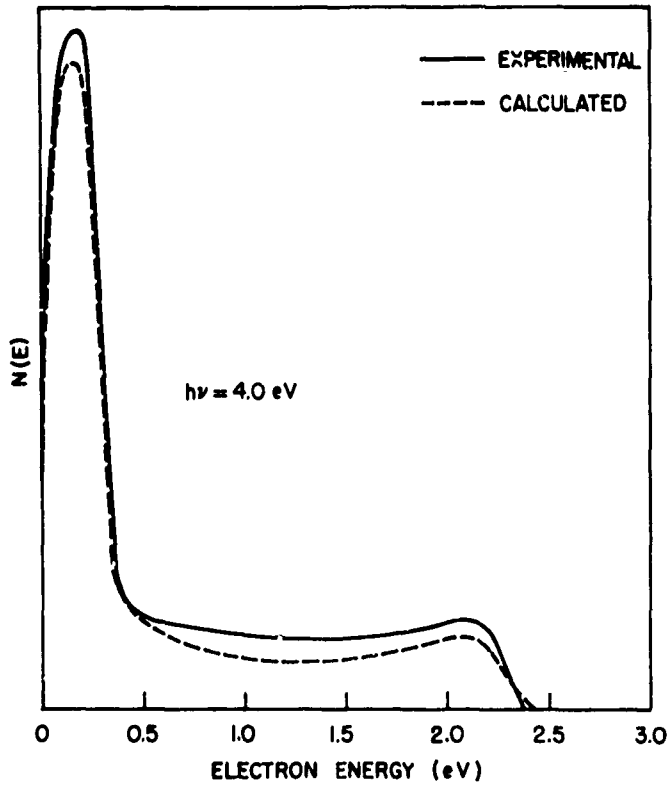

FIG. 30. CALCULATED AND MEASURED ENERGY DISTRIBUTION OF PHOTOEMITTED ELECTRONS--$\hbar\omega$ = 4.0 ev.

range from 2 ev to 11 ev. The excellent agreement indicates that the initial assumption of constant squared momentum matrix element was reasonable, and that the density of states and the threshold function have been accurately estimated.

Only the density of states above the vacuum level and below the Fermi level can be determined by comparing calculated and measured energy-distribution curves. However, the density of states between the Fermi level and the vacuum level can be estimated indirectly from the quantum-yield curve. At electron energies up to several electron volts above the vacuum level, scattering is nearly negligible in copper and Eq. (48) is an excellent approximation to the energy distribution. The quantum yield of copper at photon energies where Eq. (48) is accurate is then

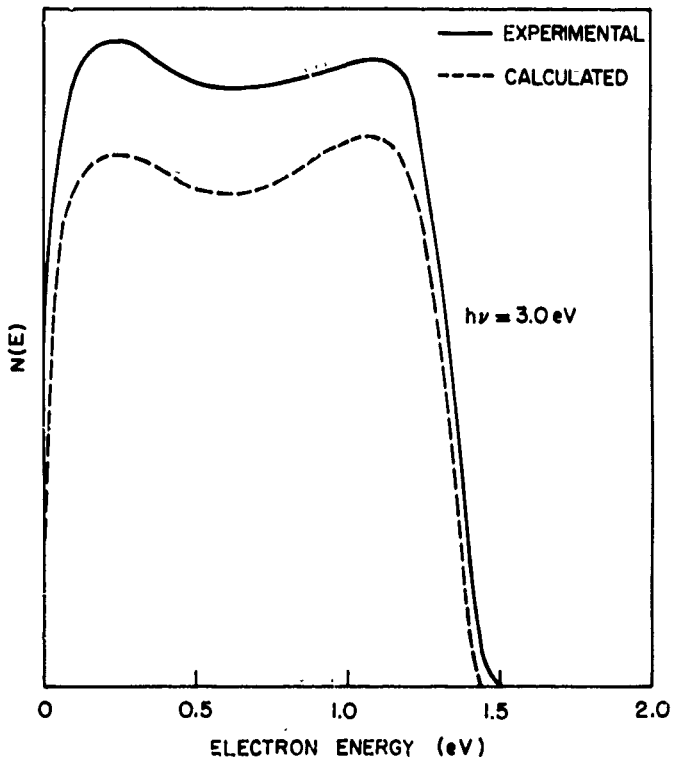

FIG. 31. CALCULATED AND MEASURED ENERGY DISTRIBUTION OF PHOTOEMITTED ELECTRONS--$\hbar\omega$ = 3.0 ev.

$$Y = \frac{\int_{E_F+E_W}^{E_F+\hbar\omega} C(E)\,\rho(E)\rho(E-\hbar\omega)\,dE}{\int_{E_F}^{E_F+\hbar\omega} \rho(E')\,\rho(E'-\hbar\omega)\,dE'} \qquad (60)$$

Since the denominator of Eq. (60) is highly dependent on the density of states between the Fermi level and the vacuum level, comparison of the yield calculated using Eq. (60) to the yield measured experimentally will give a measure of the density of states between the Fermi level and the vacuum level. The comparison of the measured yield and that calculated using Eq. (60) and the estimated density of states is shown in Fig. 32.

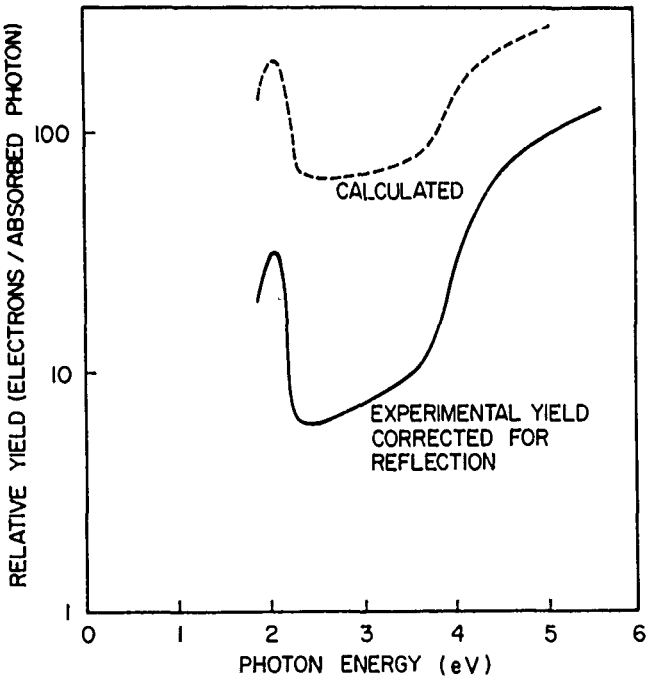

FIG. 32. MEASURED AND CALCULATED QUANTUM YIELD FOR COPPER.

The density of states derived from the trial and error methods described is shown in Fig. 33 and compared to the density of states calculated for copper by Burdick. The estimated accuracy in the experimentally determined density of states is ±15 percent. A more detailed comparison of the d-band density of states determined here with that calculated by Burdick is given in Fig. 34.

G. THE EFFECT OF ELECTRON-ELECTRON SCATTERING

1. Lifetime Broadening

Electron-electron scattering affects the photoemission data in two ways. From Eq. (1), it is evident that if the scattering frequency Λ of the states involved in optically excited transitions is large compared to the resolution of the measurements, a lifetime broadening will occur. From Eq. (42), it can be seen that a short electron-electron mean free path compared to $1/\alpha$ will result in distortion of the energy-distribution curves and will also result in an increased number of electrons which escape after scattering one or more times.

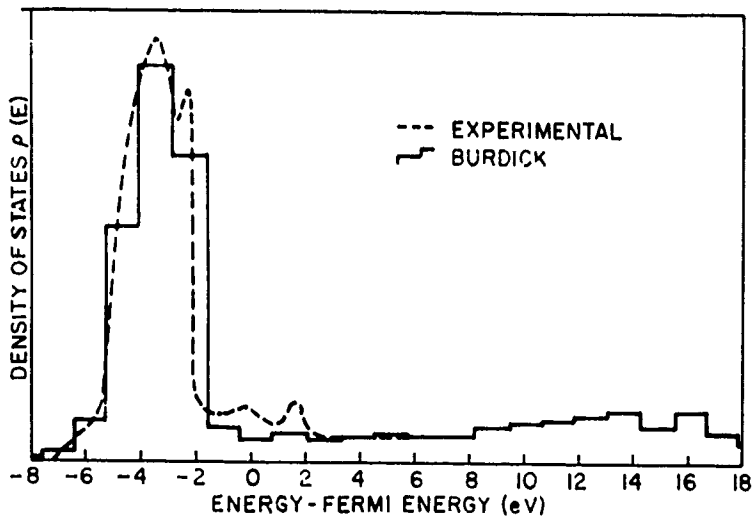

FIG. 33. DENSITY OF STATES OF COPPER.

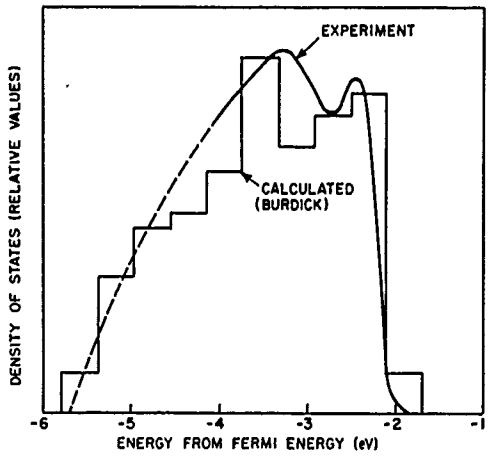

FIG. 34. DENSITY OF STATES OF
d-BAND OF COPPER.

Figures 25 and 35 illustrate the way in which the narrow peak near the top of the d-band is broadened due to lifetime broadening as the electrons are excited to higher energies. It is estimated that at approximately 6 ev above the Fermi surface the peak is broadened to a width of 0.3 ev from a width at low energies of 0.2 ev. Assuming at this energy that Λ in Eq. (1) corresponds to an energy of 0.1 ev

$$\hbar\Lambda = 0.1 \text{ ev} \qquad (61)$$

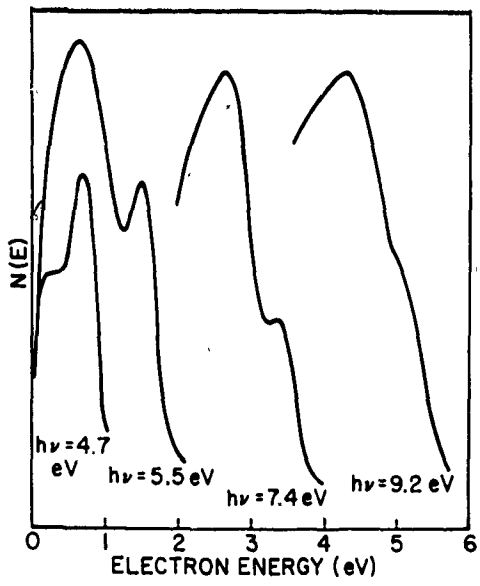

FIG. 35. ILLUSTRATION OF LIFETIME BROADENING IN COPPER.

and that Λ is $1/2\tau$ where τ is the final-state lifetime, the lifetime at 6 ev above the Fermi surface is 3×10^{-15} sec. The Fermi energy in copper is 7.0 ev [Ref. 41], so the group velocity of an electron 6 ev above the Fermi surface might be crudely estimated to be

$$E = e(6 + 7) = \frac{1}{2} m v_g^2 \qquad (62)$$

Assuming the free electron mass, the velocity v_g is 2.5×10^8 cm/sec. From the estimated lifetime and group velocity, the mean free path for electron-electron scattering in copper is 75 Å at 6 ev above the Fermi energy. This figure is in close agreement with measured mean free paths at similar energies [Ref. 42].

2. Contribution of Once-Scattered Electrons

At photon energies greater than 6 ev, a low-energy peak appears in the energy-distribution curves at a constant energy of about 0.5 ev above the vacuum level as shown in Figs. 36 and 37. This peak is due to those electrons which have been scattered before escaping. From the data it is possible to gain a great deal of information on the electron-electron scattering process in copper.

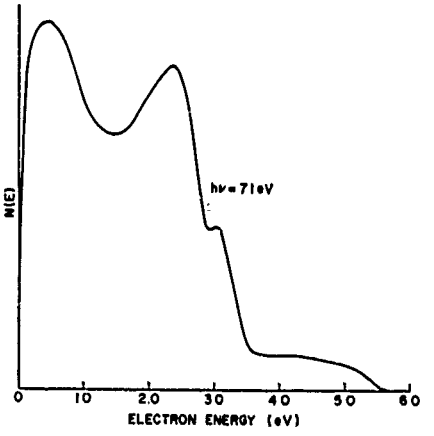

FIG. 36. ENERGY DISTRIBUTION OF PHOTOEMITTED ELECTRONS FROM COPPER--$\hbar\omega$ = 7.1 ev.

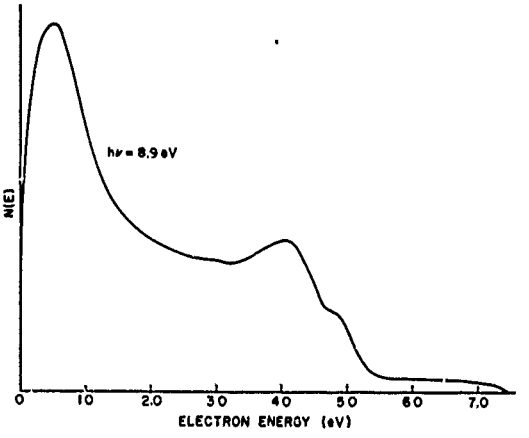

FIG. 37. ENERGY DISTRIBUTION OF PHOTOEMITTED ELECTRONS FROM COPPER--$\hbar\omega$ = 8.9 ev.

A theoretical expression for the energy distribution of photoemitted electrons including scattering is given approximately by Eq. (42) and more exactly in Appendix A. In order to use these expressions and the density of states to predict the energy distributions, it is necessary to know the matrix element M for the scattering probability in Eq. (23). Since the selection rules and wave functions involved in the scattering process are not well known, and since the Born approximation used in deriving Eq. (23) may not be valid in metals such as copper and silver [Ref. 5], it is not in general possible to

calculate the matrix element M. An approximation will be made which greatly simplifies the problem. This is that M is constant and energy independent, and that the only selection rule that applies to the scattering event is conservation of energy.

Using a constant M and the copper density of states determined in Sec. F, $g(E' - E)$ and $P_s(E')$ have been calculated according to Eqs. (24) and (26), and are shown in Figs. 38 and 39. The integrations required in the calculations were performed graphically using a compensating planimeter. Assuming a classical group velocity v_g given by

$$e(E + 7) = \frac{1}{2} m v_g^2 \qquad (63)$$

where E is the electron energy above the Fermi level in electron volts and the Fermi energy in copper is 7 ev, the relative mean free path for electron-electron scattering has been calculated using Eq. (29), and is shown in Fig. 40. The curve has been normalized to give a mean free path of 75 Å at 6 ev above the Fermi level as determined previously from the lifetime broadening.

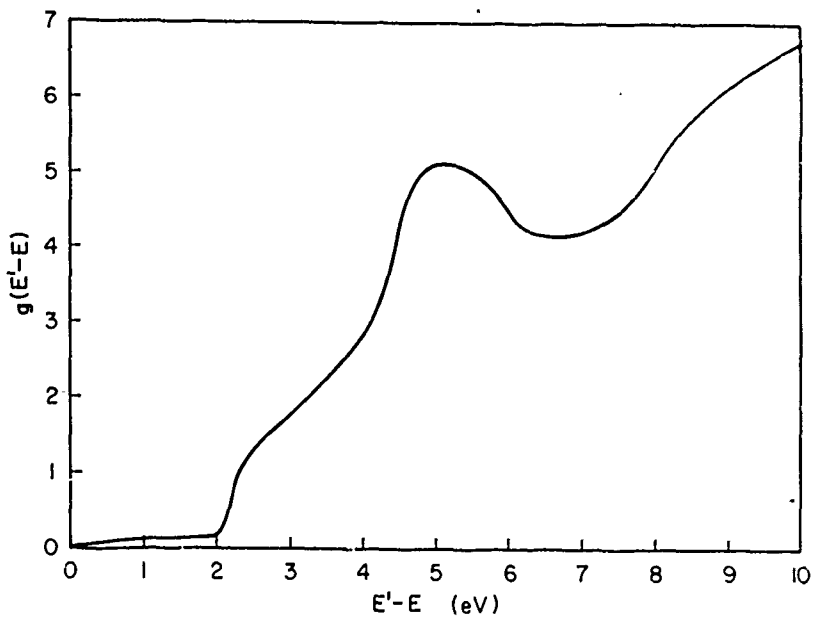

FIG. 38. FUNCTION $g(E' - E)$ FOR COPPER.

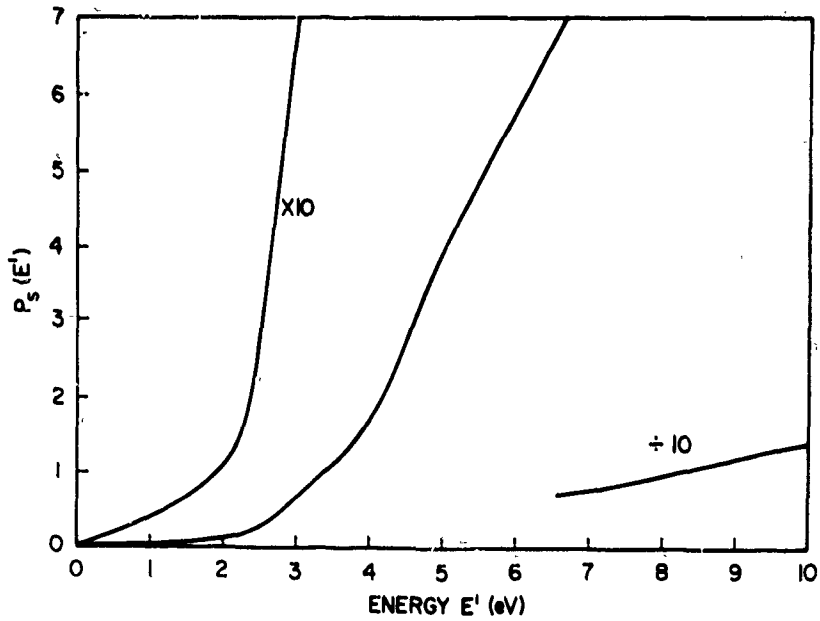

FIG. 39. CALCULATED $P_s(E')$ FOR COPPER.

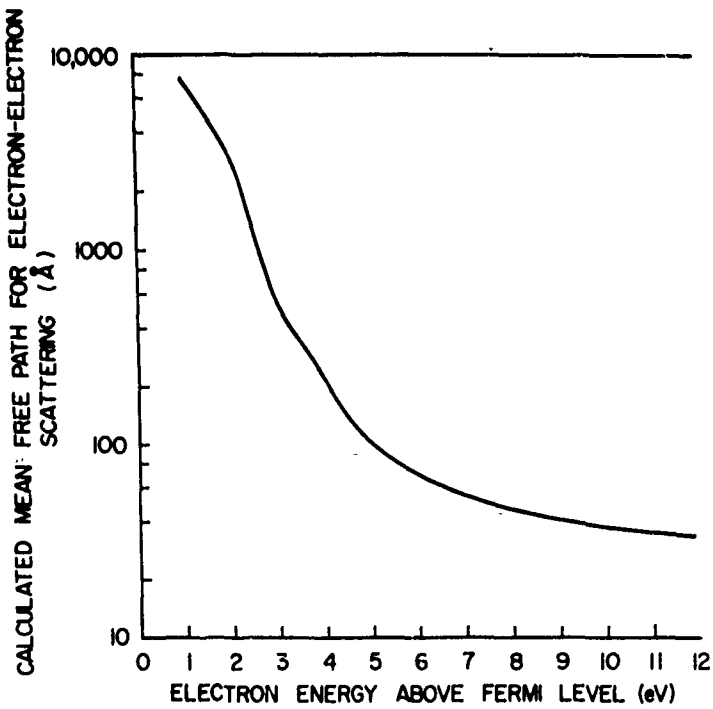

FIG. 40. CALCULATED MEAN FREE PATH FOR ELECTRON-ELECTRON SCATTERING FOR COPPER.

Using the values of $g(E' - E)$, $P_s(E')$ and $\ell(E)$ in Figs. 38, 39, and 40 respectively, and the copper density of states in Fig. 33, the energy distribution of photoemitted electrons was predicted according to Eq. (42) at photon energies of 7.5 ev and 11.0 ev. The comparisons between the predicted curves and the theoretical curves are shown in Figs. 41 and 42. The contribution of once-scattered electrons to the curves is shown shaded to illustrate the magnitude.

The surprisingly good agreement in Figs. 41 and 42 verifies that the low-energy peak is due to scattered electrons, and that the assumption of constant M is reasonable. The disappointing feature of the results is that the theory fails to predict the structure appearing at about 3 ev above the vacuum level in the curve of $\hbar\omega = 11.0$ ev. This failure is probably due to the fact that M is not a constant; however, the possibility that this structure is due to additional structure in the density of states cannot be presently ruled out.

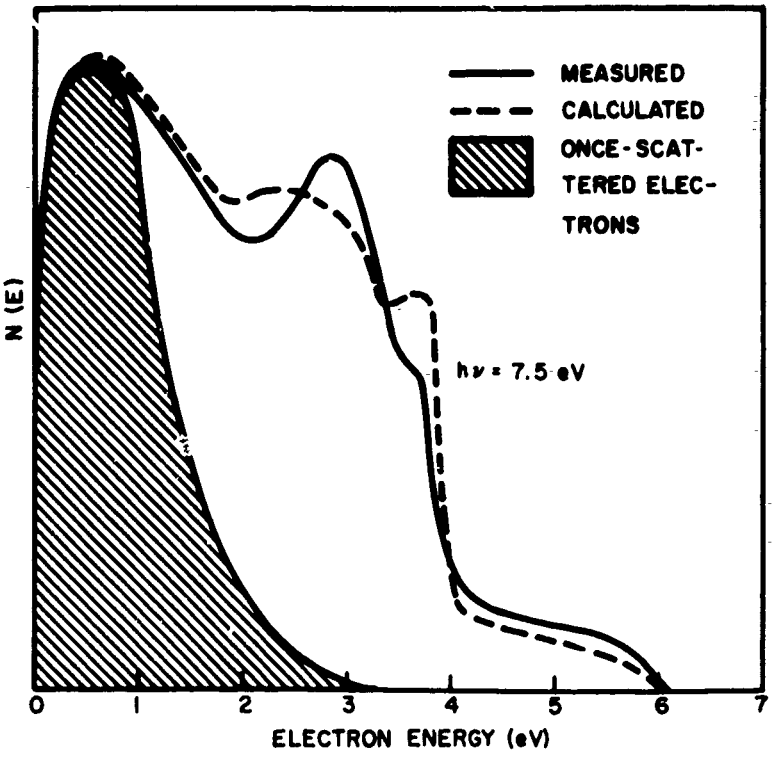

FIG. 41. CALCULATED AND MEASURED ENERGY DISTRIBUTION OF PHOTOEMITTED ELECTRONS--$\hbar\omega = 7.5$ ev.

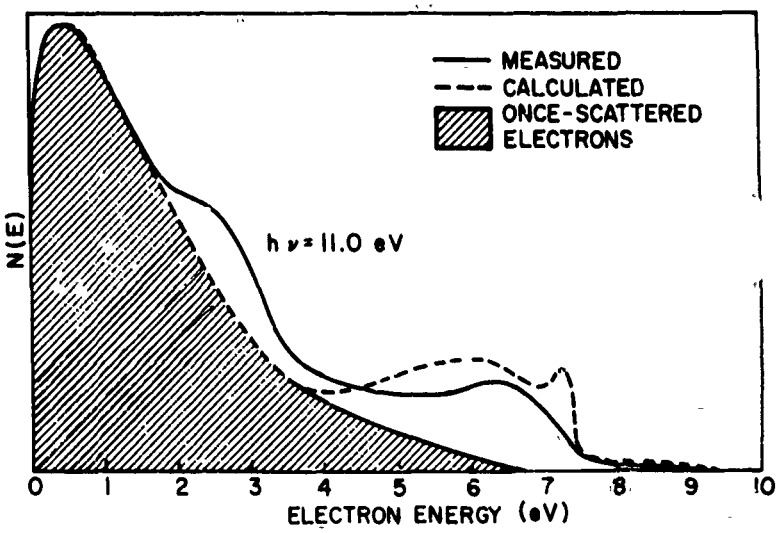

FIG. 42. CALCULATED AND MEASURED ENERGY DISTRIBUTION OF PHOTOEMITTED ELECTRONS--$\hbar\omega$ = 11.0 ev.

Figure 43 shows energy-distribution curves at photon energies where this peak occurs. It is evident that the peak moves to higher energies in increments equal to the increase in $\hbar\omega$, and appears to be about 4 ev lower in energy than that part of the distribution due to excitation of d-band electrons. Referring to the density of states of copper shown in Fig. 33, the peak appearing in Fig. 43 may be due to electrons initially excited from the d-bands which scatter before escaping by exciting the electrons at the top of the d-bands to the high density of states 1.8 ev above the Fermi level. The energy loss involved in this process is 4 ev, so a strong probability for this type of scattering would result in the observed behavior. The electron excited from the d-band by the scattering event may also escape, resulting in the increase in yield shown in Fig. 19 in this photon energy range.

H. THE OPTICAL CONSTANTS OF COPPER

The photoemission data have shown that conservation of k-vector in optically excited transitions is important for only a small fraction of the optical transitions in copper. Because of this, it has been possible to determine accurately the density of states from the bottom of the d-bands to more than 6 ev above the Fermi level. The information on

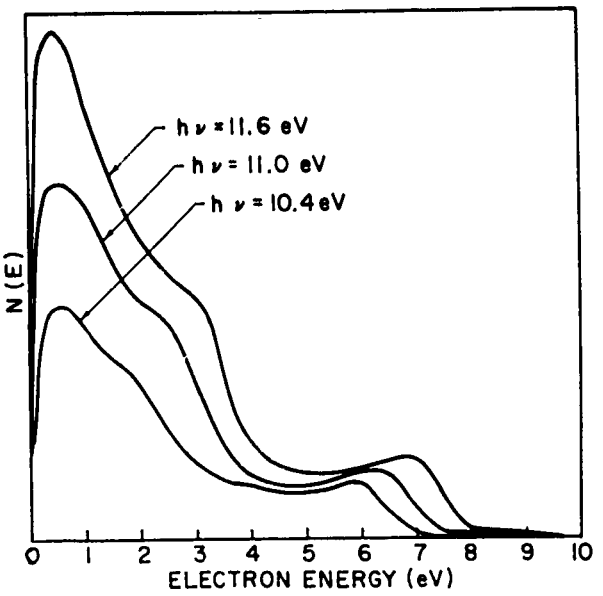

FIG. 43. ENERGY DISTRIBUTION OF PHOTOEMITTED ELECTRONS FROM COPPER--$\hbar\omega > 10$ ev.

density of states and selection rules can be used to predict one of the optical constants of copper.

The imaginary part of the dielectric constant, ϵ_2, at a frequency ω can be written in terms of the transition rate using Eqs. (11) and (13).

$$\epsilon_2(\omega) = \frac{2\hbar}{\epsilon_0 \mathcal{E}_o^2} \int_0^\infty N_T(E_1, E_0)\, dE_1 \qquad (64)$$

The transition rate is given in Eq. (8) for transitions where conservation of k-vector is not important and lifetime broadening is neglected.

$$\epsilon_2(\omega) = \frac{2Af_{10}}{\epsilon_0 \omega} \int_0^\infty \rho(E_0)F(E_o)\rho(E_1)[1 - F(E_1)]\delta(E_1 - E_0 - \hbar\omega)\, dE_1 \qquad (65)$$

This expression for $\epsilon_2(\omega)$ may be simplified further by assuming the Fermi function at absolute zero temperature and writing the oscillator strength f_{10} in terms of the squared momentum matrix element as given in Eq. (2)

$$\epsilon_2(\omega) = \frac{4|p_{10}|^2 A}{m\epsilon_0 \hbar\omega^2} \int_{E_F}^{E_F+\hbar\omega} \rho(E_1 - \hbar\omega)\rho(E_1)\, dE_1 \qquad (66)$$

The photoemission data have shown that the squared momentum matrix element $|p_{10}|^2$ does not depend strongly on the energies of the initial and final states involved in the optical transitions. It will be assumed here that $|p_{10}|^2$ is a constant. Although not correct in detail, such an assumption has been shown to be a good first approximation [Ref. 14].

Under the assumption of constant momentum matrix element, Eq. (66) can be written

$$\epsilon_2(\omega) = \frac{D}{(\hbar\omega)^2} \int_{E_F}^{E_F+\hbar\omega} \rho(E)\rho(E - \hbar\omega)\, dE \qquad (67)$$

where D is a constant. The imaginary part of the dielectric constant has been calculated from Eq. (67) using the experimentally determined density of states. The integration involved was performed graphically using a compensating planimeter. Curves of $\epsilon_2(\omega)$ calculated using the experimental data and using Burdick's density of states [Ref. 3] are shown in Fig. 44, and are compared to $\epsilon_2(\omega)$ obtained by Kramers-Kronig analysis of copper reflectance data [Ref. 19]. The calculated curves have been normalized for best fit.

The remarkably close agreement between the calculated curves in Fig. 44 and the curve obtained from the reflectance data indicates that the assumption of constant momentum matrix element is a very good approximation. It also gives further proof of the conclusion reached directly from the photoemission data that conservation of k-vector is not important in optically excited transitions in copper.

I. REPRODUCIBILITY OF RESULTS

Data were taken from four copper phototubes. Except for minor differences in the sizes of peaks in the density of states, the results from all the tubes were the same.

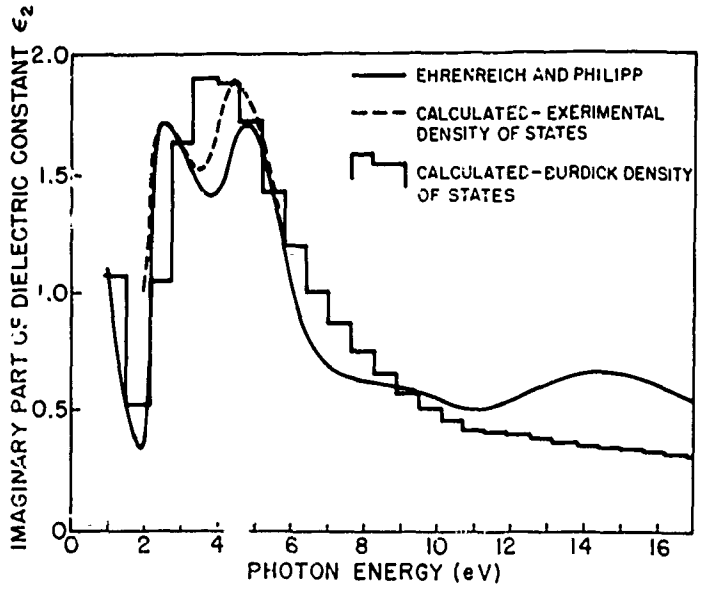

FIG. 44. IMAGINARY PART OF THE DIELECTRIC CONSTANT ϵ_2 FOR COPPER.

Figures 45 and 46 show energy-distribution curves for the four tubes at photon energies of 3.9 and 5.7 ev to illustrate the differences that did occur. At 3.9 ev, the small differences between the tubes can be attributed to a slight difference in the threshold function C(E). At 5.7 ev, the peaks in the d-band density of states occur at the same energies, but the relative sizes of the peaks vary slightly from tube to tube.

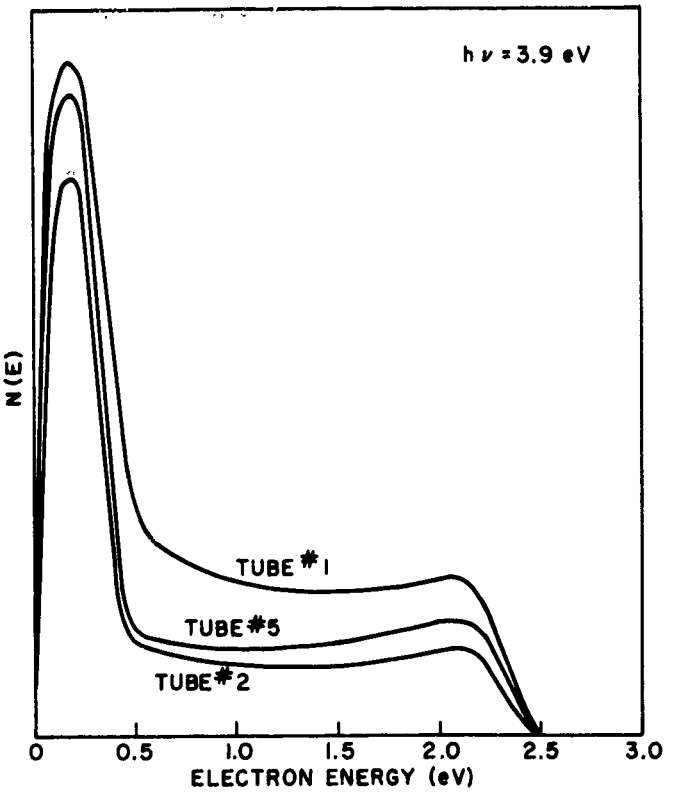

FIG. 45. ENERGY DISTRIBUTIONS OF PHOTOEMITTED ELECTRONS FOR SEVERAL COPPER PHOTOTUBES-- $\hbar\omega$ = 3.9 ev.

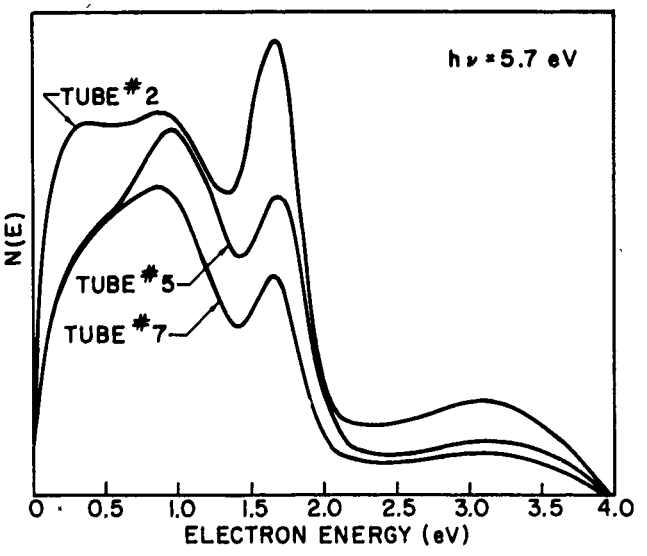

FIG. 46. ENERGY DISTRIBUTIONS OF PHOTOEMITTED ELECTRONS FOR SEVERAL COPPER PHOTOTUBES-- $\hbar\omega$ = 5.7 ev.

V. PHOTOEMISSION FROM SILVER

A. THE CALCULATED BAND STRUCTURE OF SILVER

The band structure of silver is somewhat more difficult to calculate accurately than that of copper. Because of the fact that silver is a moderately heavy atom, the use of nonrelativistic atomic-wave functions and the potential based on them will lead to more error.

Segall [Ref. 43] has calculated the band structure of silver, ignoring relativistic effects, using two different potentials. The first was determined from the free ion Ag^+ Hartree functions in the same manner as that for copper, and the second used the Hartree-Fock free-ion function. The results for the two fairly different potentials were not too dissimilar, their main difference being that the d-bands were located in different positions--2.2 ev and 5.2 ev below the Fermi level for the Hartree and Hartree-Fock methods respectively. This result is to be expected, since it is well known that the Hartree-Fock orbitals are more tightly bound than the Hartree functions. The band structure above and just below the Fermi level was very similar for the two calculations.

From the calculations, Segall concluded that the band structure of silver was relatively insensitive to the details of the potential used for the calculation. Knowing that the d-bands are located in silver about 4 ev below the Fermi level, he simply shifted the d-bands in an ad hoc way to their proper location, and assumed that all other features of the band structure were correct. The resulting band structure is shown in Fig. 47.

B. THE QUANTUM YIELD

Comparing the band structure of silver in Fig. 47 to that of copper in Fig. 18, the only major difference appears to be in the location of the d-bands. For this reason, very similar results in the quantum-yield measurement might be expected. Referring to Fig. 48, there is no strong similarity between the silver and copper quantum yield. The silver yield increases from threshold to a peak at $\hbar\omega \approx 3.5$ ev, then has a

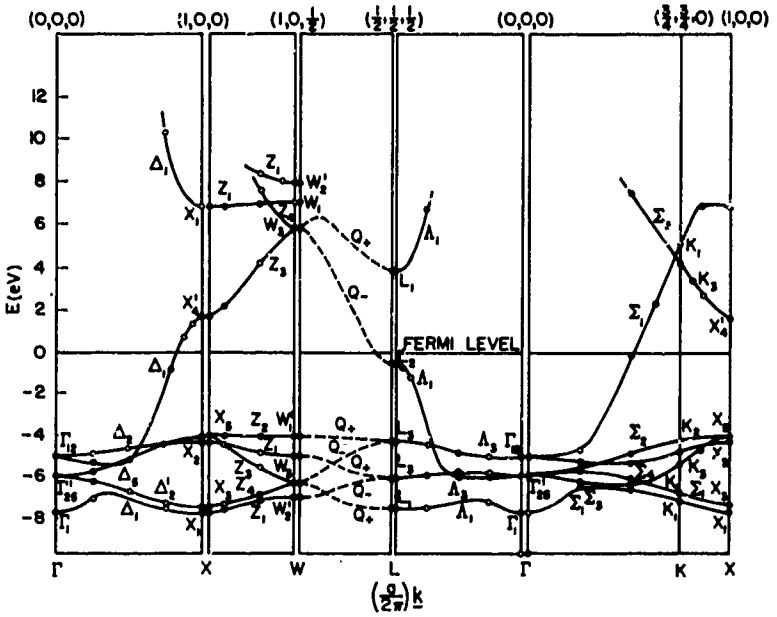

FIG. 47. CALCULATED BAND STRUCTURE OF SILVER

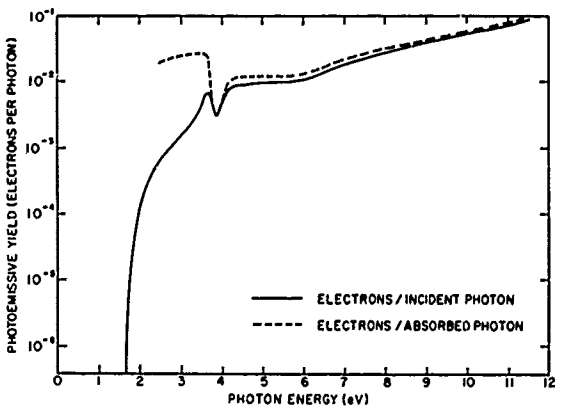

FIG. 48. QUANTUM YIELD OF SILVER.

very sharp minimum in yield at $\hbar\omega$ = 3.85 ev. At $\hbar\omega$ = 5.6 ev, the yield begins to increase slowly as a result of the d-band electrons which are beginning to be excited to states above the vacuum level. However, the increase in yield is not as great as it was in copper.

The quantum yield near threshold can be used to determine the work function of silver (with a monatomic layer of cesium on the surface) in a manner similar to that used for copper. Figure 49 shows the square

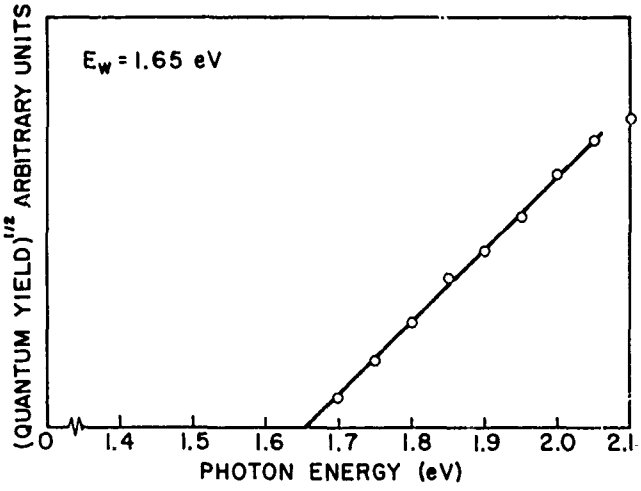

FIG. 49. EVALUATION OF WORK FUNCTION OF SILVER WITH CESIUM ON THE SURFACE.

root of the yield vs photon energy. The figure gives a work function for silver of 1.65 ev.

The sharp minimum in the yield curve in Fig. 48 occurs at $\hbar\omega = 3.85$ ev, the same energy as the strong plasma resonance in silver [Ref. 19]. One effect of this resonance is shown in Fig. 50, where the silver absorption coefficient is plotted. It was first thought that the minimum in the yield curve was due to the fact that at the plasma frequency the absorption coefficient becomes very small. Referring to Eq. (42), if the absorption coefficient becomes smaller than $1/\ell$, the yield will decrease since the electrons are excited deeper in the metal and they must travel further to reach the surface and escape. This effect is probably responsible in part for the minimum in yield. However, the observed yield curve including the minimum can be explained qualitatively in another way, and the interpretation is verified by the electron energy-distribution measurements. As a result, it is not certain how much the minimum in the absorption coefficient contributes to the minimum in yield.

The explanation of the yield curve which is consistent with the energy-distribution measurements is as follows: Since silver is similar to copper (except for the fact that the d-bands are approximately 4 ev below the Fermi level), the yield is expected to rise to a maximum at

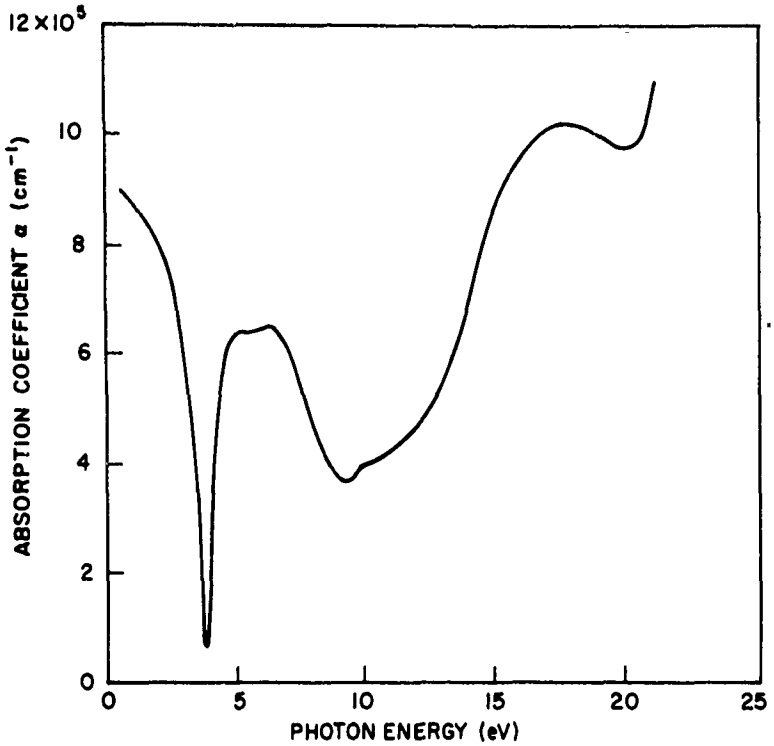

FIG. 50. ABSORPTION COEFFICIENT α FOR SILVER.

$\hbar\omega \approx 4$ ev, then decrease as d-band electrons begin to be excited to states above the Fermi level. At $\hbar\omega \approx 5.6$ ev, d-band electrons can be excited to states above the vacuum level and the yield should increase. This behavior is noted in Fig. 48. Another contribution to the yield occurs for $h\omega > 4$ ev. At these photon energies, electrons are being excited from d-band states. The holes left behind may take part in an Auger process [Ref. 44] resulting in electrons being excited to states above the vacuum level. Hence, at $\hbar\omega \approx 4$ ev, the yield should rise due to the increase of Auger-excited electrons with enough energy to escape. The decrease in yield when d-band electrons begin to be excited to states above the Fermi level followed by the increase in yield due to the Auger process can combine to form the yield minimum noted in Fig. 48. The Auger process in silver is described in Sec. D of this chapter.

C. ENERGY DISTRIBUTION OF PHOTOEMITTED ELECTRONS--$\hbar\omega \leq 3.5$ ev

It has been pointed out in a previous section, and described in detail by Ehrenrich and Phillip [Ref. 19], that interband transitions do not

become dominant in silver until $\hbar\omega \geq 3.5$ ev. The energy distribution of photoemitted electrons from silver for $\hbar\omega \leq 3.5$ ev shown in Fig. 51 demonstrates this. A peak near the maximum electron energy becomes more apparent as $\hbar\omega$ increases, but does not dominate the distribution. This peak is due to indirect transitions from the peak in the density of states at L_2' in the calculated band structure (Fig. 47). The remainder of the distribution curves is due to the characteristic "free" electron contribution.

The peak near the maximum electron energy for $\hbar\omega \leq 4.0$ ev follows the relation

$$E = \hbar\omega - 1.95 \text{ ev} \qquad (68)$$

where E is the energy of the peak with respect to the vacuum level. Since the work function of silver is 1.65 ev, the peak in the energy distributions is due to a peak in the density of states at L_2' located 0.3 ev below the Fermi level. Figure 51 indicates that a larger peak in the density of states is associated with symmetry point L_2' in silver than in copper.

In the photoemission data of silver, there is no evidence of a peak in the density of states at X_4', 1.8 ev above the Fermi level, as has

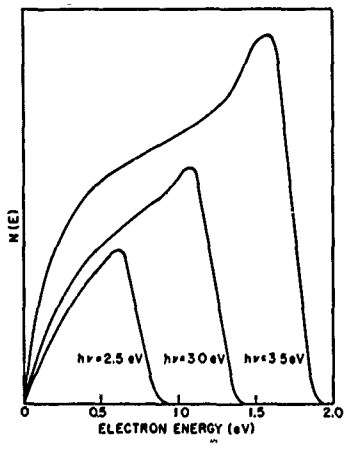

FIG. 51. ENERGY DISTRIBUTION OF PHOTOEMITTED ELECTRONS FROM SILVER--$\hbar\omega \leq 3.5$ ev.

been found in copper. No peak would result if a smaller density of states were associated with X_4' in silver, or if the symmetry point were located at a slightly lower energy so that the peak was masked by the threshold function. It is most likely that the former is true. In Sec. G of this chapter, ϵ_2 for silver is calculated based on the assumption that there is no strong peak in the density of states above the Fermi level. The calculated ϵ_2 agrees very closely with the measured values.

D. EVIDENCE OF THE AUGER PROCESS

The Auger process has been considered theoretically by several authors [Ref. 45]. However, detailed treatments of the process are of little value in interpreting the photoemission data since the wave functions and selection rules are not known accurately. A simple model is sufficient to explain the experimental results.

The Auger process in a metal is illustrated in Fig. 52. An electron is excited from a state with energy E_0, leaving an empty state at this energy. Another electron with higher energy E_1 may recombine with this hole. To conserve energy this electron gives up energy to a neighboring electron of energy E_2, exciting it to an empty state at energy E. The probability of the described process depends on the wave functions of the electrons taking part and the selection rules governing the transitions.

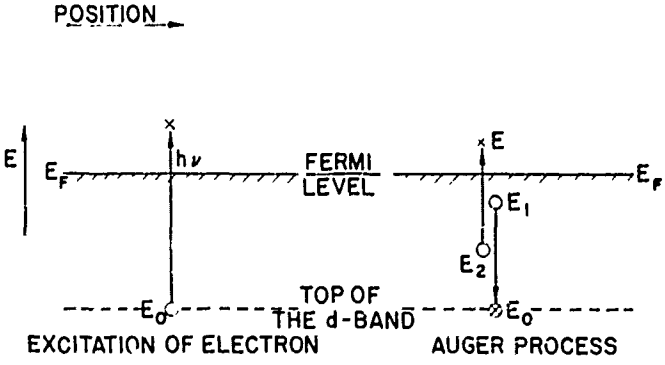

FIG. 52. THE AUGER PROCESS IN SILVER.

In silver, the d-bands produce a very high density of states which extends from approximately 4 ev to 7 ev below the Fermi level (see Fig. 47). As a first approximation, it will be assumed that the only holes that take part in the Auger process are those located at the top of the d-bands. (Reasons why this is a good approximation will be given in Sec. D of this chapter.) Under this assumption, there will be no evidence of an Auger effect in the photoemission data until the photon energy is large enough to excite d-band electrons ($\hbar\omega \approx 4$ ev). In addition, for photon energies greater than 4 ev, the effect of the Auger process on the energy distribution of the photoemitted electrons will be independent of photon energy since the holes involved will always lie at the top of the d-band.

A similar analysis to that given for electron-electron scattering can be given for the Auger process. Assuming that the probability of a state at a given energy taking part in the Auger process is proportional only to the density of states at that energy, and that there are N_0 holes located at E_0 4 ev below the Fermi level, the probability of an electron being excited by the Auger process to an energy E as shown in Fig. 52 is

$$P_A(E,E_0,E_1,E_2) = C_0 N_0 \rho(E_1)F(E_1)\rho(E)[1 - F(E)]\rho(E_2)F(E_2)$$
$$\delta[(E_1 - E_0) - (E - E_2)] \qquad (69)$$

where C_0 is some constant. The total number of electrons $N_A(E)$ excited to energy E by the process is given by Eq. (69) integrated over all E_1 and E_2 (E_1 and E_2 are defined in Fig. 52). Assuming the Fermi function at absolute zero, and eliminating E_2 in Eq. (69) using the delta function, the integral is

$$N_A(E) = C_0 N_0 \rho(E) \int_{E_0+(E-E_F)}^{E_F} \rho(E_1)\rho(E - E_1 + E_0)\, dE_1$$
$$0 \leq (E - E_F) \leq 4 \text{ ev} \qquad (70)$$

Except for the peak in the density of states 0.3 ev below the Fermi level in silver, the density of states above the d-bands is approximately constant. If the density of states is assumed to be constant ρ_0, Eq. (70) becomes

$$N_A(E) = \rho_0^3 C_0 N_0 [4 - (E - E_F)] \qquad 0 \leq (E - E_F) \leq 4 \text{ ev} \quad (71)$$

The energy distribution of photoemitted electrons due to the Auger process, if electron-electron scattering is negligible, is Eq. (71) modified by a threshold function as shown in Fig. 53.

Holes located at other energies than the top of the d-bands should have negligible effect on the distribution shown in Fig. 53. Holes between the d-bands and the Fermi level can be neglected because the density of states is smaller and because fewer electrons can achieve energy greater than threshold. Holes produced deeper in the d-bands will likely relax through the Auger process to the top of the d-bands, the energy exchange involved generally being too small to excite any electrons to states above the vacuum level.

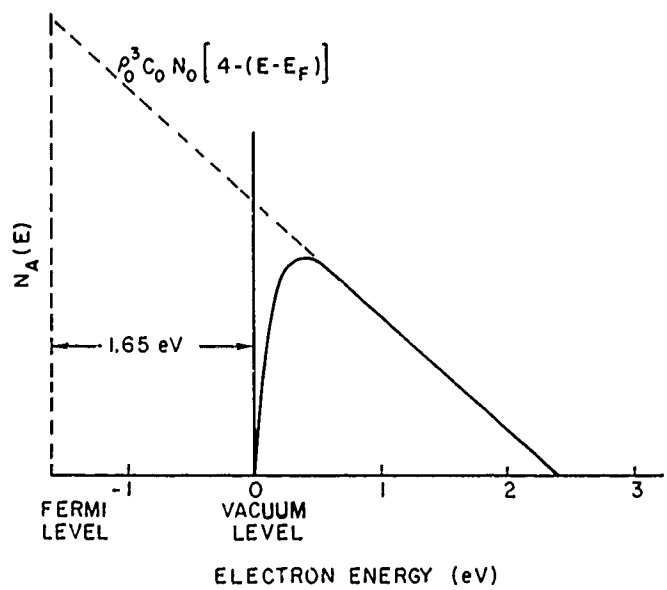

FIG. 53. ENERGY DISTRIBUTION OF PHOTOEMITTED ELECTRONS TO BE EXPECTED DUE TO AUGER PROCESS.

Figure 53 indicates that the Auger process will result in an energy distribution of electrons decreasing with energy to a maximum energy of approximately 2.4 ev above the vacuum level. Figure 54 shows the experimentally determined energy distribution curves for silver for photon energies of 4.1, 4.3, 4.8, and 5.4 ev. The distributions have been normalized to coincide at low energies. Figure 55 shows the energy distributions at photon energies of 3.6, 3.8, and 4.0 ev. Except for the high-energy peak associated previously with a peak in the density of states 0.3 ev below the Fermi level, the energy distributions shown in Figs. 54 and 55 are very similar to the distributions predicted on

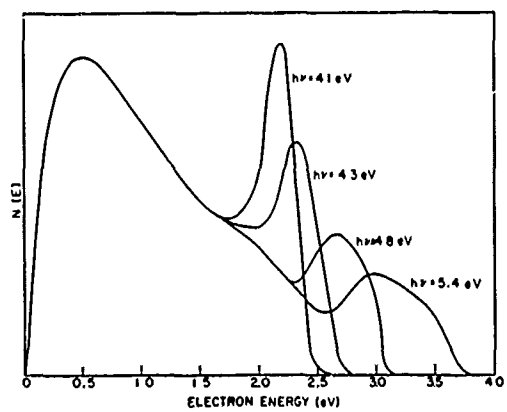

FIG. 54. ENERGY DISTRIBUTION OF PHOTOEMITTED ELECTRONS FROM SILVER--$\hbar\omega$ = 4.1 ev to 5.4 ev.

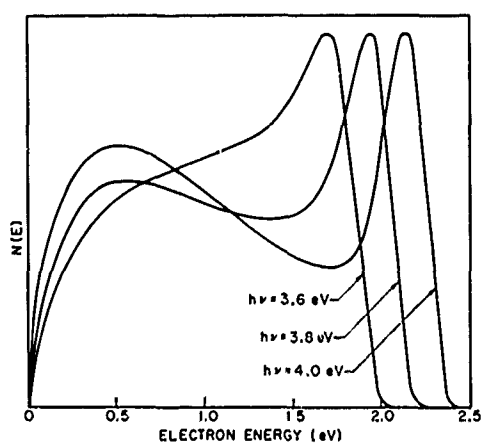

FIG. 55. ENERGY DISTRIBUTION OF PHOTOEMITTED ELECTRONS FROM SILVER--ω NEAR THE PLASMA FREQUENCY.

the simple model of the Auger process. A low-energy peak due to the Auger process begins to appear when the photon energy is approximately 4 ev, and the distribution at higher photon energies is essentially independent of photon energy, extrapolating to an energy of 2.5 ev as shown in Fig. 54.

The broad peak in Fig. 54 located between 1.5 ev and 2.5 ev can be explained in terms of the peak in the density of states at L_2'. A very probable event is for electrons near L_2' to recombine with holes at the top of the d-band, energy being given up to neighboring electrons also near L_2'. The energies are such that this process will result in a peak approximately 1.8 ev above the vacuum level.

The simple model for the Auger process that has been used also explains why the process is negligible in copper. Since the d-bands in copper are only 2 ev below the Fermi level, a negligible fraction of the Auger-excited electrons is excited to energies above the vacuum level.

E. INDIRECT AND DIRECT TRANSITIONS IN SILVER

The high-energy peak in the electron energy distributions in Fig. 54 exhibits the same behavior as that noted for the similar peak in copper. At a photon energy of approximately 4.1 ev, the peak is a maximum, and at higher photon energies it splits into two peaks. One of the peaks moves to higher energy in increments equal to the change in photon energy, while the other moves to higher energy at a somewhat slower rate. The amplitudes of the peaks get smaller as the peaks are excited to high energies because of strong energy-dependent scattering.

The peaks in the energy distributions can be explained in terms of direct and indirect transitions in the same way as the similar peaks were explained in copper. Figure 56 shows the energy of the initial states responsible for the largest peak in the distributions of Fig. 54 plotted vs $\hbar\omega$. The peak is due to indirect transitions from the peak in the density of states at L_2' for photon energies less than 3.5 ev. From the figure, it is evident that L_2' is located 0.3 ev below the Fermi level. At $\hbar\omega = 3.5$ ev, the direct transition is beginning to contribute. The initial states involved in the direct transition lie

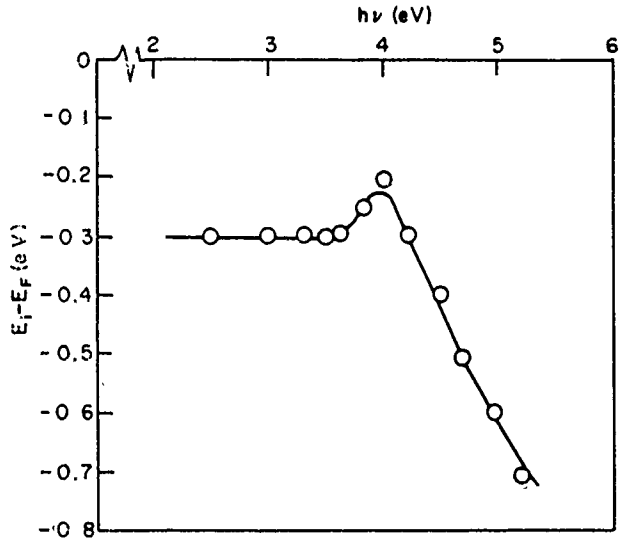

FIG. 56. ENERGY OF INITIAL STATES RESPONSIBLE FOR HIGH-ENERGY PEAK IN PHOTOEMISSION DATA.

above L_2' for $3.5 < \hbar\omega < 4.2$ ev. As a result, the curve in Fig. 56 goes through a maximum at $\hbar\omega = 4.0$ ev. At $\hbar\omega = 4.2$ ev, the transition is occurring again from initial states at L_2', 0.3 ev below the Fermi level. Since the peak at $\hbar\omega = 4.2$ ev is due to direct transitions from L_2' to L_1, L_1 is located 3.9 ev above the Fermi level.

F. TRANSITIONS FROM THE d-BANDS

Since the d-bands in silver are located approximately 4 ev below the Fermi level, at photon energies greater than 5.7 ev, d-band electrons should be excited to states above the vacuum level. Figure 57 shows the electron energy distributions from silver for photon energies of 5.7 ev and 6.3 ev. At 5.7 ev there is no evidence of d-band electrons in the distribution, but at 6.3 ev a low-energy peak appears which is due to transitions from the d-bands. The energy distributions at $\hbar\omega = 7.8$ ev and 8.4 ev are shown in Figs. 58 and 59. The narrow peak in the distributions is due to a peak in the d-band density of states, and the peak following the first peak at approximately 1 ev lower energy is also due to the d-bands. The low-energy peak appearing in the curve at $\hbar\omega = 7.8$ ev, and more strongly in the curve at $\hbar\omega = 8.4$ ev, is due to scattering.

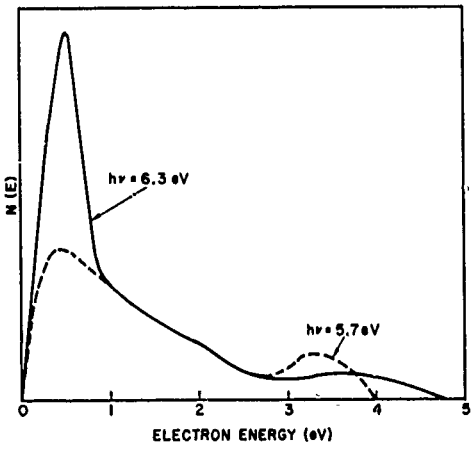

FIG. 57. ENERGY DISTRIBUTION OF PHOTOEMITTED ELECTRONS FROM SILVER--$\hbar\omega$ = 5.7 ev, 6.3 ev.

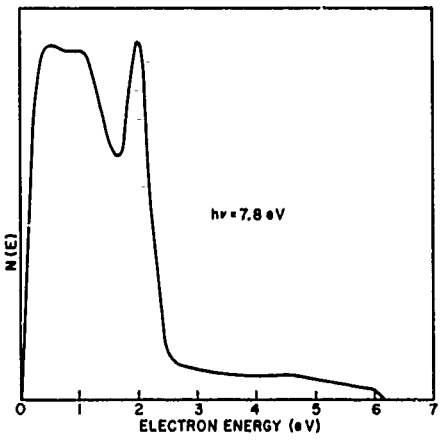

FIG. 58. ENERGY DISTRIBUTION OF PHOTOEMITTED ELECTRONS FROM SILVER--$\hbar\omega$ = 7.8 ev.

In a similar manner to that used for copper, it can be shown that optical transitions from the d-bands in silver are not constrained by conservation of k. For this reason, features of the d-band density of states can be determined from Figs. 57, 58, and 59. It is found that the d-bands in silver are located 3.75 ev below the Fermi level. There are at least two peaks in the density of states, one 0.3 ev wide located 4.1 ev below the Fermi level, and the other about 1.2 ev wide located approximately 5.3 ev below the Fermi level. The location and width of the second peak cannot be determined exactly because of the

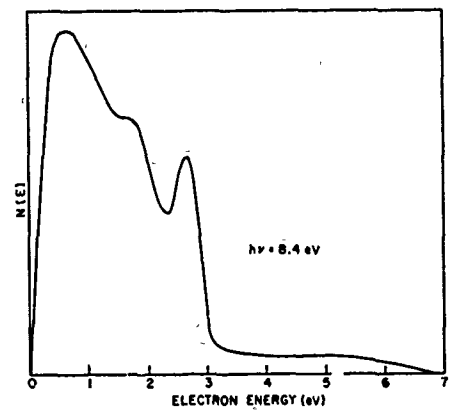

FIG. 59. ENERGY DISTRIBUTION OF PHOTOEMITTED ELECTRONS FROM SILVER--$\hbar\omega$ = 8.4 ev.

masking due to scattered electrons. When the magnitude of the scattered peak is estimated using Eq. (42) and subtracted from the distributions shown in Figs. 58 and 59, there is no evidence of further structure in the d-bands. Because of this, it is likely that the silver d-band density of states consists of only the two peaks mentioned above.

G. THE SILVER DENSITY OF STATES

The density of states of silver is considerably more difficult to determine exactly from the photoemission data than that of copper. At photon energies less than 3.5 ev, the electron energy distributions are dominated by the free electron effects: at photon energies between 3.8 ev and 6.5 ev, the distributions are dominated by the Auger effect; and at photon energies above 7.0 ev, the distributions are distorted badly due to scattering. However, several important features of the density of states can be determined. The location and density of states of part of the d-band can be estimated, and two peaks in the density of states identified. The only other evidence of structure in the density of states is the peak at L_2', 0.3 ev below the Fermi level. From these considerations, a silver density of states has been estimated and is shown in Fig. 60. The accuracy of the density of states in Fig. 60 is not as good as that for copper. However, the general features are correct as indicated in Fig. 61 where the imaginary part of the dielectric

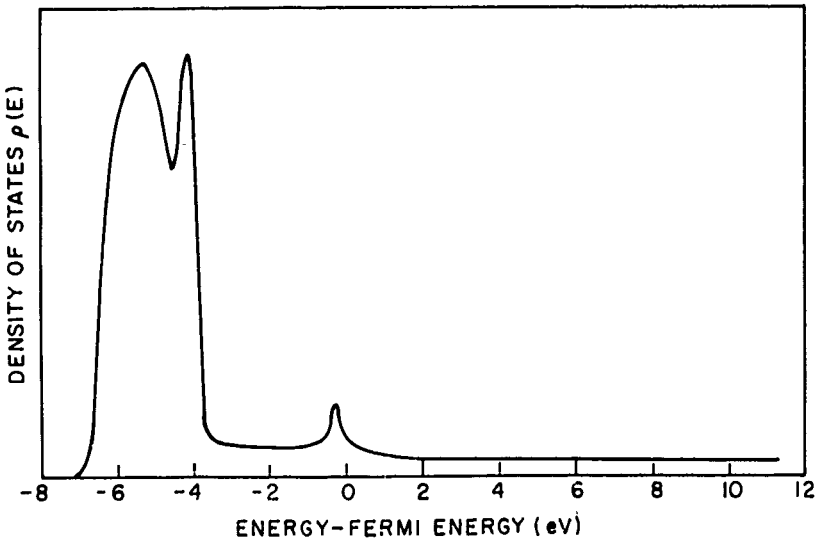

FIG. 60. ESTIMATED DENSITY OF STATES FOR SILVER.

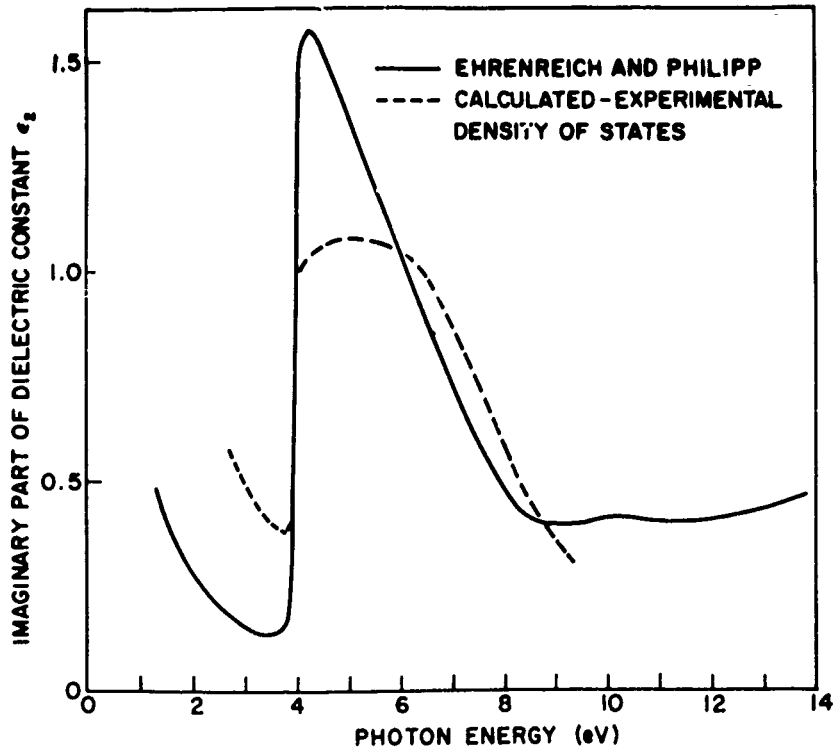

FIG. 61. IMAGINARY PART OF THE DIELECTRIC CONSTANT ϵ_2 FOR SILVER.

constant has been calculated and compared to the measured values in the same way as was done for copper.

H. THE THRESHOLD FUNCTION C(E) FOR SILVER

Because of the relatively constant density of states in silver above the Fermi level and the accuracy with which it was possible to predict the electron energy distributions due to the Auger process, the threshold function C(E) can be determined very accurately. Figure 62 shows the measured energy distribution of photoemitted electrons at a photon energy of 4.8 ev. If the threshold function is essentially constant at energies more than 1 ev above the vacuum level, the threshold function C(E) must be proportional to the ratio between the measured energy-distribution curve and the straight-line extrapolation of the Auger distribution to lower energies shown dotted in Fig. 62. The threshold function determined in this way is shown in Fig. 63. It is this threshold function that has been used with the copper data.

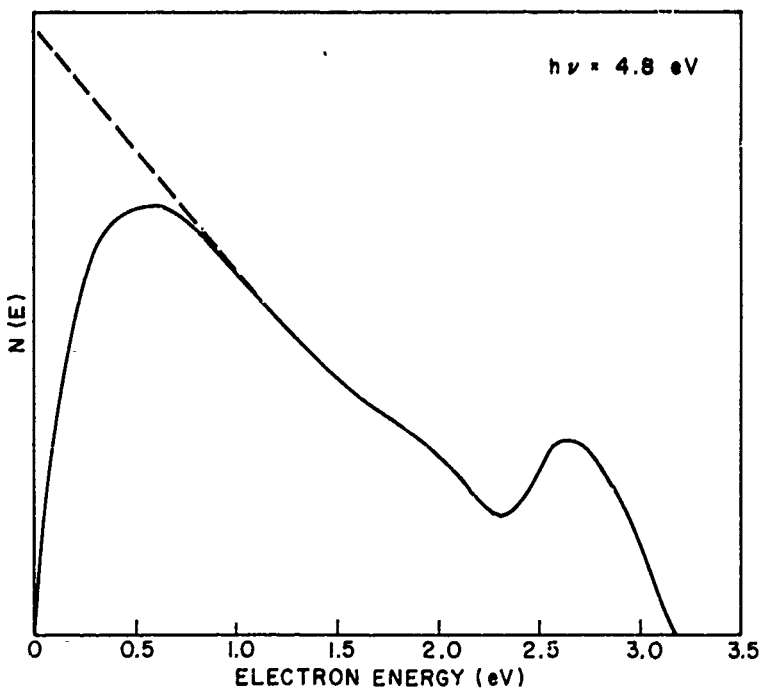

FIG. 62 EVALUATION OF THRESHOLD FUNCTION C(E) FOR SILVER.

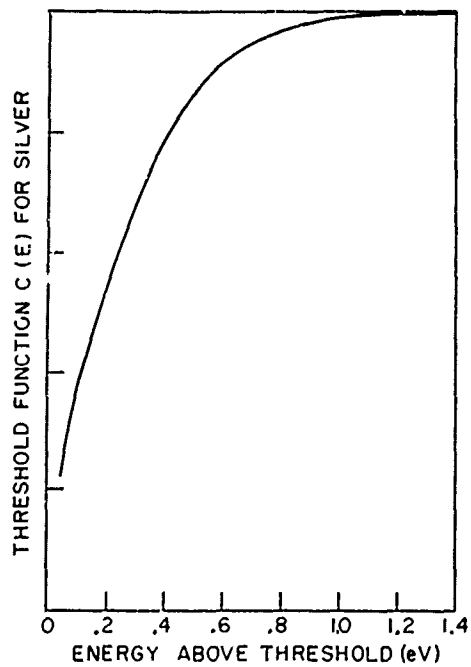

FIG. 63. THRESHOLD FUNCTION C(E) FOR SILVER.

I. EFFECT OF ELECTRON-ELECTRON SCATTERING

Electron-electron scattering in silver affects the photoemission data in a similar way to that in copper. Figure 54 shows the high-energy peak in the energy distribution being reduced in size as the peak is excited to higher energy, but the quantum yield in this photon-energy range is relatively constant. One would expect that, since direct transitions are beginning to occur, the height of the peak should increase rather than decrease. The observed behavior is due to the fact that the mean free path is a decreasing function of energy, and the probability of escape without scattering of a high-energy electron is correspondingly smaller than that of a lower energy electron. Figures 58 and 59 show the low-energy peak in the energy distribution which is due to the scattering of high-energy electrons. Figures 64 and 65 are the energy distributions of photoemitted electrons from silver at photon energies of 9.3, 10.5, and 11.4 ev, and show the lifetime broadening of the high-energy d-band peak (labeled C).

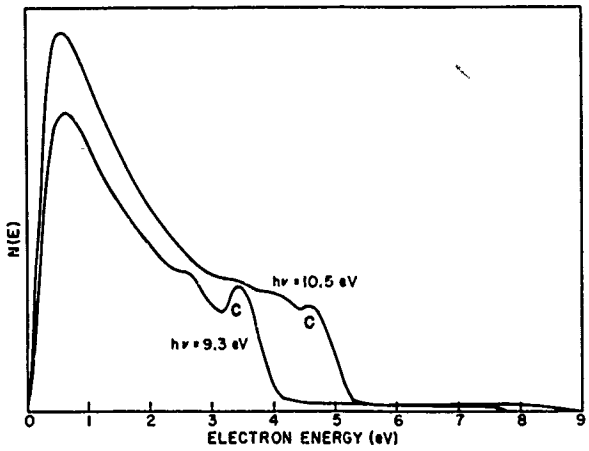

FIG. 64. ENERGY DISTRIBUTION OF PHOTOEMITTED ELECTRONS FROM SILVER--$\hbar\omega > 9$ ev.

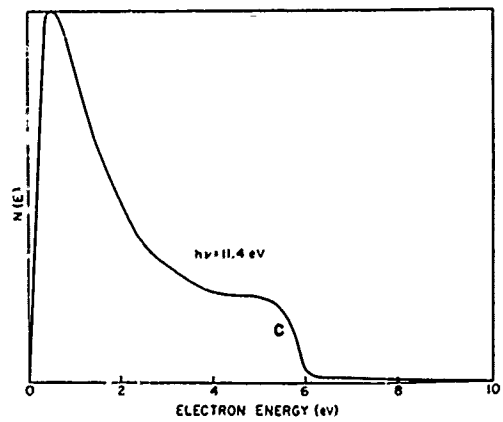

FIG. 65. ENERGY DISTRIBUTION OF PHOTOEMITTED ELECTRONS FROM SILVER--$\hbar\omega = 11.4$ ev.

The mean free path at one energy can be estimated from the lifetime broadening of the sharp d-band peak in silver. This has been done in the same way as was done for copper in Sec. G1 of Chapter IV, but using a Fermi energy of 5.5 ev [Ref. 41]. The estimated mean free path for electron-electron scattering at 5.5 ev above the Fermi level is 70 Å.

Since it was not possible to determine the density of states in silver with the accuracy achieved with copper, no detailed calculations of $\ell(E)$, $p_s(E',E)$, and $P_s(E')$ were carried out. However, several of the important features of the scattering and their effect on the

energy distribution of photoemitted electrons can be described without detailed calculations.

There is a high density of states in silver in the d-band approximately 4 ev below the Fermi level. When electrons have enough energy to scatter with these d-electrons and excite them to states above the Fermi level, there will be a large probability for scattering (short electron-electron mean free path). Referring to Fig. 54, it can be seen that strong scattering begins to reduce the size of the high-energy peak in the energy-distribution curves when the peak corresponds to electron energies more than 2.3 ev above the vacuum level, or 3.95 ev above the Fermi level, in close agreement with the intuitive argument. In addition, since the density of states in silver is relatively constant above the Fermi level, no structure in the scattering peak similar to that appearing in Fig. 43 for copper is to be expected, and none is observed (see Fig. 65).

J. EFFECT OF THE PLASMA RESONANCE AT $\hbar\omega = 3.85$ ev

The plasma frequency at $h\omega = 3.85$ ev in silver may affect the photoemission data in several ways. The decrease in yield at incident light frequencies near the plasma frequency which can be brought about by a decrease in the absorption coefficient has already been described. It might be expected that a further decrease in yield should result because photons absorbed in producing plasma oscillations do not directly produce photoelectrons. However, if photoelectrons are produced by the relaxation of these plasma oscillations, this effect will not occur.

A further effect of the plasma resonance in silver has been mentioned briefly in Chapter IIB. Energetic electrons may lose energy in traveling through the metal by exciting plasma oscillations. In this scattering mechanism, the energy loss per scattering event is approximately equal to the energy corresponding to the plasma frequency. Hence, if this scattering process were strong in silver, there would be a large probability of a scattering event with an energy loss of 3.85 ev. In the photoemission data, this would result, for instance, in a strong scattered peak in the energy-distribution curves following by 3.85 ev the sharp peak in the distributions due to optical excitation of electrons

from the top of the d-band. Since no such structure is observed in the energy-distribution curves of silver, it is concluded that scattering of energetic electrons by the creation of plasma oscillations is a weak scattering process compared to electron-electron scattering over the range of electron energy studied. This conclusion is in agreement with the theoretical results of Quinn [Ref. 6].

VI. DISCUSSION AND CONCLUSIONS

One of the most significant features of the experimental results is the evidence that conservation of k-vector in most optically excited transitions is not important in copper and silver. For transitions from the s- and p-like bands just below the Fermi level, this behavior is not unexpected since the same mechanism that conserves k-vector in the "free carrier" absorption referred to in the literature [Ref. 19] may be expected to do so for these transitions. However, when the photon energy is such that a strong direct transition should occur, direct transitions are observed, but it is found that the direct transitions are not as strong as the indirect transitions. In addition, no evidence is found for direct transitions from the d-bands.

There are several possible explanations for the observed behavior. The second-order transition probability involving phonons [Eq. (9)] may be large enough in the metals to result in indirect transitions being stronger than direct transitions. This behavior may occur even if the second-order matrix element is smaller than the first-order matrix element because of the larger number of electrons available to take part in phonon-assisted transitions. However, measurements of the quantum yield per incident photon of a copper phototube from threshold to $\hbar\omega = 3.5$ ev, at room temperature and at 77° K, showed no noticeable difference in yield. If phonons were strongly involved in the transitions, a change in yield would have occurred.

Another possible explanation for the observations is that a large probability exists for some other mechanism such as defects [Ref. 46] to conserve k-vector. This mechanism would not be expected to have a strong temperature dependence in agreement with the yield measurements at room temperature and at 77° K.

There is the additional possibility that the Bloch-wave representation of some of the electronic states in copper and silver may not be adequate [Refs. 22, 23]. In particular, this may be true for the d-band states because of the fact that no evidence of direct transitions from the d-bands was found. This possibility cannot be ruled out on the basis of the close agreement between the measured density of states and that

calculated assuming Bloch-wave solutions for the wave equation [Ref. 3]. The density of states if the Bloch-wave representation is not correct will be very similar to that calculated using the Bloch-wave representation because the density of states is much more dependent on the crystal potential than on the representation of the wave function.

The experimental results of the photoemission study can be used to compare the metals copper and silver. It has already been mentioned that k-vector conservation is not a strong selection rule in either of the metals for many optical transitions. The band structure and density of states of both are very similar, the major difference being that the d-bands are located 4 ev below the Fermi level in silver and 2 ev below the Fermi level in copper. Both have two peaks in the d-band density of states, a sharp peak near the top of the band and a broader peak deeper in the band, and both d-bands are approximately 3.5 ev wide. The p- and s-like bands above and just below the Fermi level appear to be similar. The symmetry points L_2' and L_1 differ in energy by less than 0.2 ev. However, the difference between copper and silver in the density of states at L_2', and the difference in the way in which the effect of the direct transition from L_2' to L_1 varies with photon energy (Figs. 28 and 56), in addition to the lack of evidence of a peak in the silver density of states at X_4, indicate that the shape of the bands in the two metals is somewhat different. These results bear out Segall's conclusion [Ref. 44] that the band structure of silver is very similar to that of copper, the only major difference being that the d-bands are moved to a lower energy 4 ev below the Fermi level.

Electron-electron scattering is the strongest inelastic-scattering mechanism in both silver and copper for electrons with energies from 1.5 ev to 11.5 ev above the Fermi level. There is no evidence of scattering due to plasmon creation. The mean free path for electron-electron scattering for copper is a decreasing function of electron energy. From lifetime-broadening considerations a value of approximately 75 Å is found for the mean free path against this scattering for electrons 6 ev above the Fermi surface. The mean free path for silver appears to be a more sharply decreasing function of electron energy, and is slightly shorter than that for copper at energies more than 5 ev above the Fermi level.

The close agreement between the calculated imaginary part of the dielectric constant ϵ_2 (based on the experimental observation) and the measured ϵ_2 indicates that the observations are not peculiar to the photoemission process, but are characteristic of the metals studied.

It was possible to explain the photoemission data from both copper and silver in detail. In particular, it was possible to predict with considerable accuracy the energy distribution of photoemitted electrons to be expected at any photon energy from 1.5 to 11.5 ev. It should be pointed out, however, that total agreement between the predicted and the measured distributions could have been achieved by slight changes in the densities of states and matrix elements involved in the transitions. Such adjustments in the data were not made in order to illustrate the ease and accuracy with which photoemission results can be interpreted, and to indicate the vast amount of information that can be gained without a detailed analysis.

APPENDIX A. PROBABILITY OF ELECTRON ESCAPE AFTER ONE SCATTERING EVENT

The probability of an electron with energy E a distance x from a photoemitting surface escaping into vacuum without suffering an inelastic collision has been derived in Sec. C1 of Chapter II. The probability of this electron escaping after scattering once is also of interest.

Consider an electron excited to energy E' a distance x from the photoemitting surface, as shown in Fig. 66. The probability of this electron escaping with energy between E and $(E + dE)$ is the product of three probabilities:

1. The probability that it will scatter after moving a distance r in the solid at an angle θ with respect to the normal to the photoemitting surface.
2. The probability that it will be scattered to an energy between E and $(E + dE)$.
3. The probability that it will escape after this scattering event without further scattering.

Referring to Fig. 66, the first probability, assuming random electron velocity direction, is

$$p_1 = \frac{1}{2} e^{-r/\ell'} \sin\theta \, d\theta \, \frac{dr}{\ell'} \tag{72}$$

where ℓ' is the mean free path for inelastic scattering for electrons with energy E'. The probability of producing an electron with energy between E and $(E + dE)$ in the scattering event was derived in Chapter IID.

$$p_2 = \frac{2p_s(E',E)\, dE}{P_s(E')} \tag{73}$$

The third probability is given by Eq. (31), where the distance of the electron from the photoemitting surface is $(x - r \cos\theta)$.

$$p_3 = \frac{1}{2} \int_{p_c/p}^{1} \exp\left(\frac{-x + r\cos\theta}{\ell z} \right) dz \tag{74}$$

Changing variables so that $y = \cos\theta$, and integrating Eq. (75) over r gives

$$p'_{esc}(E',E,x)\,dE = \frac{p_s(E',E)\,dE}{2\ell' P_s(E')}\left\{\int_{-1}^{0} dy \int_{p_c'/p}^{1} dz\ \frac{\exp\left(-\frac{x}{\ell z}\right)}{\frac{1}{\ell'} - \frac{y}{\ell z}}\right.$$

$$\left. + \int_{0}^{1} dy \int_{p_c/p}^{1} dz\ \frac{\left[1 - \exp\left(-\frac{x}{\ell' y} + \frac{x}{\ell z}\right)\right]\exp\left(-\frac{x}{\ell z}\right)}{\frac{1}{\ell'} - \frac{y}{\ell z}}\right\} \tag{76}$$

Electrons are optically excited to energy E' according to Eq. (32), so the rate of escape of electrons with energy between E and (E + dE) is

$$R'(E',E)\,dE = \int_{0}^{\infty} [G_0(E')e^{-\alpha x} p'_{esc}(E',E)\,dE]\,dx \tag{77}$$

Substituting Eq. (76) in Eq. (77) and carrying out the integration over x gives

$$R'(E',E)\,dE = \frac{G_0(E')p_s(E',E)\,dE}{2\ell' P_s(E')}\left[\int_{-1}^{0} dy \int_{p_c/p}^{1} dz\ \frac{1}{\left(\frac{1}{\ell'} - \frac{y}{\ell z}\right)\left(\alpha + \frac{1}{\ell z}\right)}\right.$$

$$\left. + \int_{0}^{1} dy \int_{p_c/p}^{1} dz\ \frac{1/y}{\left(\alpha + \frac{1}{\ell z}\right)\left(\alpha + \frac{1}{\ell' y}\right)}\right] \tag{78}$$

Simplifying Eq. (78) and performing the y integration, one obtains

Changing variables so that $y = \cos\theta$, and integrating Eq. (75) over r gives

$$p'_{esc}(E',E,x)\,dE = \frac{p_s(E',E)\,dE}{2\ell' P_s(E')}\left\{\int_{-1}^{0} dy \int_{p_c/p}^{1} dz\ \frac{\exp\left(-\frac{x}{\ell z}\right)}{\frac{1}{\ell'} - \frac{y}{\ell z}}\right.$$

$$\left. + \int_{0}^{1} dy \int_{p_c/p}^{1} dz\ \frac{\left[1 - \exp\left(-\frac{x}{\ell' y} + \frac{x}{\ell z}\right)\right]\exp\left(-\frac{x}{\ell z}\right)}{\frac{1}{\ell'} - \frac{y}{\ell z}}\right\} \tag{76}$$

Electrons are optically excited to energy E' according to Eq. (32), so the rate of escape of electrons with energy between E and (E + dE) is

$$R'(E',E)\,dE = \int_{0}^{\infty} [G_0(E')e^{-\alpha x} p'_{esc}(E',E)\,dE]\,dx \tag{77}$$

Substituting Eq. (76) in Eq. (77) and carrying out the integration over x gives

$$R'(E',E)\,dE = \frac{G_0(E')p_s(E',E)\,dE}{2\ell' P_s(E')}\left[\int_{-1}^{0} dy \int_{p_c/p}^{1} dz\ \frac{1}{\left(\frac{1}{\ell'} - \frac{y}{\ell z}\right)\left(\alpha + \frac{1}{\ell z}\right)}\right.$$

$$\left. + \int_{0}^{1} dy \int_{p_c/p}^{1} dz\ \frac{1/y}{\left(\alpha + \frac{1}{\ell z}\right)\left(\alpha + \frac{1}{\ell' y}\right)}\right] \tag{78}$$

Simplifying Eq. (78) and performing the y integration, one obtains

$$R'(E',E)\,dE = \frac{G_0(E')p_s(E',E)\,dE}{2P_s(E')} \int_{p_c/p}^{1} \left[\frac{1}{\alpha\ell'}\,\ell n\,(1+\alpha\ell') + \frac{\ell z}{\ell'}\,\ell n\left(1+\frac{\ell'}{\ell z}\right)\right]\frac{dz}{\alpha+\frac{1}{\ell z}} \tag{79}$$

This integration may be carried out exactly, but the result is rather difficult to interpret. A considerable simplification can be made with very little loss in accuracy as follows: The major contribution to the integral occurs for z near unity. Since in metals ℓ' is generally shorter than ℓ, and $x\,\ell n\,[1+(1/x)]$ is a very slowly varying function of x for x large, very little error is introduced by inserting $z = 1$ in the $\ell z/\ell'\,\ell n\,[1+(\ell'/\ell z)]$ term of Eq. (79). Under this approximation, Eq. (79) becomes, from Eq. (35),

$$R'(E',E)\,dE = \frac{KG_0(E')p_s(E',E)C(E)\,dE}{P_s(E')(\alpha+\frac{1}{\ell})}\left[\frac{1}{\alpha\ell'}\,\ell n\,(1+\alpha\ell') + \frac{\ell}{\ell'}\,\ell n\left(1+\frac{\ell'}{\ell}\right)\right] \tag{80}$$

For $\alpha\ell'$ and ℓ'/ℓ much less than unity, $[1/\alpha\ell']\,\ell n\,(1+\alpha\ell') \approx 1 \approx [\ell/\ell']\,\ell n\,[1+(\ell'/\ell)]$ and Eq. (80) gives the same result as derived in Eq. (42) using the very simple model.

The expression given in Eq. (80) for the rate of escape of electrons after scattering once is easily interpreted. The $[\ell/\ell']\,\ell n\,[1+\ell'/\ell]$ term represents those electrons initially excited to energy E' which are moving away from the photoemitting surface. These electrons eventually will be scattered regardless of the value of the mean free path for scattering, and their probability of escaping after scattering once will depend on the ratio of the mean free paths ℓ/ℓ'. This interpretation suggests that inelastic scattering will always affect photoemission data irrespective of the mean free paths. The $(1/\alpha\ell')\,\ell n\,(1+\alpha\ell')$ term represents those electrons initially excited to energy E' which are moving toward the photoemitting surface. The probability of these electrons escaping after scattering once will depend on the probability of their scattering once before reaching the surface. If $\ell' \gg 1/\alpha$, most of these electrons will escape without scattering. If $\ell' \ll 1/\alpha$, few will escape without scattering.

23. W. E. Spicer, Phys. Rev. Lett., 11, 1963, p. 1-3.

24. W. E. Spicer and N. B. Kindig, Solid State Communications, 2, 1964, p. 13.

25. L. H. Hall, J. Bardeen, and F. J. Blatt, Phys. Rev., 95, 1954, p. 559.

26. K. Sawada, et al, Phys. Rev., 108, 1957, p. 507.

27. E. O. Kane, Phys. Rev., 127, 1962, p. 131.

28. C. Kittel, Introduction to Solid State Physics, John Wiley and Sons, Inc., New York, 1960.

29. W. E. Spicer, J. Appl. Phys., 31, 1960, p. 2077.

30. R. N. Stuart, F. Wooten, and W. E. Spicer, Phys. Rev. Lett., 10, 1963, p. 1-3.

31. C. Kittel, Elementary Solid State Physics, John Wiley and Sons, Inc., New York, 1962, p. 112.

32. F. I. Vilesov, Soviet Physics, 6, 1962, p. 1078.

33. W. E. Spicer, J. Phys. Chem. Solids, 22, 1961, p. 365.

34. W. E. Spicer, personal communication.

35. B. Kindig, "Photoemission Studies of CdS," to be published.

36. ohn and N. Rostoker, Phys. Rev., 94, 1954, p. 1111.

37. M. Ch. ow, Phys. Rev., 55, 1939, p. 675; Ph.D. Thesis, M.I.T., 1939, (unpublished).

38. J. C. Slater, Phys. Rev., 51, 1937, p. 846; Phys. Rev., 92, 1953, p. 603.

39. L. P. Bouckaert, R. Smoluchowski, and E. Wigner, Phys. Rev., 50, 1936, p. 58.

40. R. H. Fowler, Phys. Rev., 38, 1931, p. 45.

41. A. J. Dekker, Solid State Physics, Prentice-Hall, Inc., N. J., 1957, p. 215.

42. C. A. Mead, personal communication.

43. B. Segall, "Theoretical Energy Band Structures for the Noble Metals," Report No. 61-RL-(2785G), General Electric Research Laboratory, Schenectady, N. Y., Jul 1961.

44. J. Blakemore, Semiconductor Statistics, Pergamon Press, New York, 1962, p. 214.

45. H. D. Hagstrum, Phys. Rev., 96, 1954, p. 336.

46. D. L. Dexter, Photoconductivity Conference, edited by R. G. Breckenridge and B. R. Russel, John Wiley and Sons, Inc., New York, 1956, p. 155.

SOLID STATE DISTRIBUTION LIST

February 1964

GOVERNMENT

USAELRDL
Ft. Monmouth, New Jersey
1 Attn: SIGRA/SL-PF
Dr. Harold Jacobs

Commanding General
USAELRDL, Bldg. 42
Ft. Monmouth, New Jersey
5 Attn: SIGRA/SL-SC

Commanding Officer
USAELRDL
Ft. Monmouth, New Jersey
1 Attn: SIGRA/TNR
1 Attn: Data Equipment Branch

Commanding Officer
U.S. Army Electronics Research
Dev't. Lab.
Ft. Monmouth, New Jersey
1 Attn: SIGFM/EL/PEP
R. A. Gerhold
1 Attn: SIGRA/SL-PRT, M. Zinn
1 Attn: SIGRA/SL-PRT, L.N.
Heynick

Engineering Procedures Br.
U.S. Army Signal Materiel
Support Agency
Ft. Monmouth, N.J.
1 Attn: Millard Rosenfeld

Commanding Officer
Frankford Arsenal
Library Branch 0270, Bldg. 40
Bridge and Tacony Streets
1 Philadelphia 37, Pa.

Ballistics Research Lab.
Aberdeen Proving Ground, Md.
2 Attn: V.W. Richard, BML
1 Attn: Ballistics Res. Lab.
K.A. Pullen
1 Attn: Chief, Computer Res. Br.

Chief of Naval Research
Dept. of the Navy
Washington 25, D.C.
2 Attn: Code 427
2 Attn: Code 437, Inf. Syst. Br.

Commanding Officer
Office of Naval Research
Branch Office
1000 Geary St.
1 San Francisco 9, Calif.

Chief Scientist
Office of Naval Research
Branch Office
1030 E. Green St.
1 Pasadena, Calif.

San Francisco Ordnance Dist.
Basic Research and Special
Projects Br.
P.O. Box 1829, 1515 Clay St.
Oakland 12, Calif.
1 Attn: Mr. M.B. Sundstrom, Chief

ONR
Branch Office Chicago
230 N. Michigan Ave.
1 Chicago 1, Ill.

Commanding Officer
ONR Branch Office
495 Summer Street
1 Boston 10, Mass.

Commanding Officer
U.S. Army Electronics Res. Unit
P.O. Box 205
1 Mountain View, Calif.

Commanding Officer
ONR Branch Office
207 West 24th St.
New York 11, N.Y.
1 Attn: Dr. I. Rowe

U.S. Naval Applied Science Lab.
Tech. Library
Bldg. 291, Code 9832
Naval Base
1 Brooklyn, N.Y. 11251

Officer-in-Charge
Office of Naval Research
Navy No. 100, Box 39
Fleet Post Office
16 New York, N.Y.

U.S. Naval Research Lab.
2 Washington 25, D.C.
6 Attn: Code 2000
1 Attn: Code 5240
1 Attn: Code 5430
1 Attn: Code 5200
1 Attn: Code 5300
1 Attn: Code 5400
1 Attn: Code 5266, G. Abraham
1 Attn: Code 5260
1 Attn: Code 6430

Chief, Bureau of Ships
Navy Dept.
2 Washington 25, D.C.
1 Attn: Code 732, Mr. A. E. Smith
1 Attn: Code 335
1 Attn: Code 684A, R. Jones
1 Attn: Code 686
1 Attn: Code 687E
1 Attn: Code 687D
3 Attn: Code 670B
1 Attn: Code 681A1D
1 Attn: Code 691A1
1 Attn: Code 670 NTDS
1 Attn: Code 607A LCDR
E.B. Mashinke
1 Attn: Code 681A

Chief, Bureau of Naval Weapons
Navy Dept.
Washington 25, D.C.
1 Attn: RAAV 6

Chief, Bur. of Naval Weapons
Navy Dept.
Washington 25, D.C.
2 Attn: RREN-3
1 Attn: RAAV-44
1 Attn: ASW Detection and Control Div.
1 Attn: RMWC, Missile Weapons Control Div.
1 Attn: DIS-31
1 Attn: RAAV, Avionics Div.

Chief of Naval Operations
Navy Dept.-Pentagon 4C717
Washington 25, D.C.
1 Attn: Op 94T
1 Attn: Op 07T 12

Commanding Officer & Dir.
U.S. Navy Electronics Lab.
San Diego 52, Calif.
1 Attn: Tech. Library

U.S. Naval Post Grad. Sch.
Monterey, Calif.
1 Attn: Tech. Reports Library

Weapons Systems
Test Div., Naval Air Test Center
Patuxent River, Md.
1 Attn: Library

U.S. Naval Weapons Lab.
Dahlgren, Va.
1 Attn: Technical Library
1 Attn: G.H. Gleissner,
Computation Div.

U.S. Naval ORD Test Station
Pasadena Annex
3202 E. Foothill Blvd.
Pasadena, Calif.
1 Attn: Tech. Library (Code P80962)

U.S. Army R and D Lab.
Ft. Belvoir, Va.
1 Attn: Tech. Doc. Ctr.

U.S. Naval Weapons Lab.
Dahlgren, Va.
1 Attn: Computation and Analysis
Lab.

U.S. Naval Ordance Lab.
Corona, Calif.
1 Attn: Robert Conger, 423
1 Attn: H. H. Wieder 423

Commander
U.S. Naval Air Devel. Center
Johnsville, Pa.
1 Attn: NADC Library

U.S. Naval Avionics Facility
Indianapolis 18, Ind.
1 Attn: Station Library

Naval Ordance Lab.
White Oaks
Silver Spring 19, Md.
1 Attn: Tech. Library

Commanding Officer
U.S. Army Materiel Command
Washington 25, D.C.
1 Attn: AMCRD-DE-E
1 Attn: AMCRD-RS-PE-E

Commanding Officer
U.S. Army Research Office
(Durham)
Box CM, Duke Station
Durham, N.C.
3 Attn: CRD-AAIP

Dept. of the Army
Office, Chief, Research and Dev't.
Room 3D442, Pentagon
Washington 25, D.C.
1 Attn: Research Support Div.

Commanding General
USAELRDL
1 Attn: Technical Documents Ctr.
Evans Signal Lab. Area,
Bldg. 27
Ft. Monmouth, N.J.

Commander
Army Ballistic Missile Agency
1 Attn: ORDAB-DGC
Redstone Arsenal, Ala.

Advisory Group on Reliability of
Electronic Equipment
Office, Ass't Sect. of Defense
The Pentagon
1 Washington 25, D.C.

Commanding General
U.S. Army Electronics Comm.
Attn: AMSEL-AD
1 Ft. Monmouth, N.J.

Office, Chief of Res. and Dev't
Dept. of the Army
3045 Columbia Pike
Arlington 4, Va.
1 Attn: L.H. Geiger, Res. Planning Div.

Office of the Chief of Engineers
Chief, Library Branch
Dept. of the Army
1 Washington 25, D.C.

Office of the Ass't Sec'y of
Defense (AE)
Pentagon, Room 3D-984
1 Washington 25, D.C.

Chief of Staff
U.S. Air Force
Washington 25, D.C.
2 Attn: AFDRT-ER

U.S. Army Signal Liaison Office
ASD
Wright-Patterson AFB, Ohio
1 Attn: AS:DL - 9

Commander
Aeronautical Systems Div.
Wright-Patterson AFB, Ohio
1 Attn: ASRNE-2, Mr. D. R. Moore
1 Attn: ASRNRS-2
2 Attn: ASRNEM
1 Attn: ASRNE -32
1 Attn: ASAPT
1 Attn: ASAPR
1 Attn: WWKSC-M. Mergulis
1 Attn: ASNXRR

Commandant
AF Institute of Technology
Wright-Patterson AFB, Ohio
1 Attn: AFIT-Library

DFEE, Lib. Officer
USAF Academy
1 USAF Academy, Colorado

Executive Director
Air Force Office of
Scientific Research
Washington 25, D.C.
1 Attn: Code SRPP
1 Attn: Code SREE

Office of Scientific Res.
Dept. of the Air Force
Washington 25, D.C.
1 Attn: SRGL

AFWL (WLL)
2 Kirtland AFB, N.M.

Director, Air Univ. Library
Maxwell AFB, Alabama
1 Attn: CR 4582

AFSC Liaison Office
Los Angeles Area
1 Attn: Lt. Col. A.A. Konkel
6331 Hollywood Blvd.
Hollywood 28, Calif.

Hq. USAF (AFRDR-NO-3)
The Pentagon
1 Attn: Harry Mulkey
Rm 4D 335
Washington 25, D.C.

Air Force Systems Command
Scientific and Tech. Liaison
Office
111 E. 16th St.
1 New York 23, N.Y.

School of Aerospace Medicine
USAF Aerospace Medical Div.
(AFSC)
1 Attn: SMAP, Brooks AFB, Texas

Commanding General
Rome Air Dev't. Center
Griffiss AFB, Rome, N.Y.
1 Attn: RCWID, Maj. B.J. Long
1 Attn: RCIMA, J. Dove

Commanding General
Air Force Cambridge Res. Labs.
Air Res. and Dev't. Command
L. G. Hanscom Field
Bedford, Mass.
1 Attn: CRTOTT-2, Electronics
1 Attn: Elec. Res. Lab. (CRR)
1 Attn: Chief, CRRB
1 Attn: Dr. H.H. Zschirnt
Computer and Mathematical
Sciences Lab.

Headquarters, AFSC
Attn: SCTAE
Andrews AFB,
1 Washington 25, D.C.

Ass't Sect. of Defense (Research
and Dev't)
Dept. of Defense
Washington 25, D.C.
1 Attn: Technical Library

Office of Director of Defense
Research and Engineering
Dept. of Defense
1 Washington 25, D.C.

Nat'l Aeronautics and Space
Admin.
Goddard Space Flight Center
Greenbelt, Md.
1 Attn: Chief, Data Systems Div.

Nat'l Aeronautics and Space
Admin.
George C. Marshall Space
Flight Center
Huntsville, Alabama
1 Attn: M-G and C-R

Federal Aviation Agency
Bureau of Res. and Dev't
Washington 25, D.C.
1 Attn: RD-40651, Mr. Harry
Hayman

Ass't of Sect. of Defense for
Res. and Engineering
Information Office, Library Br.
Pentagon Bldg.
2 Washington 25, D.C.

Dept. of Defense
Defense Communications Agency
Washington 25, D.C.
1 Attn: 121A, Tech. Lib.

Institute for Defense Analyses
1666 Connecticut
Washington 9, D.C.
1 Attn: W.E. Bradley

David Taylor Model Basin
Washington 7, D.C.
1 Attn: Tech. Lib., Code 142

U.S. Coast Guard
1300 E. Street, N.W.
Washington 25, D.C.
1 Attn: EEE

Advisory Group on Electron
Devices
346 Broadway, 8th Floor East
New York 13, N.Y.
2 Attn: Harry Sullivan

DDC (TISIA)
Cameron Station
20 Alexandria, Va.

Census Bureau
Washington 25, D.C.
1 Attn: Office of Ass't. Dir.
for Statistical Services
J. L. McPherson

Program Director
Engineering Section
Nat'l Science Foundation
1 Washington 25, D.C.

Commanding Officer
Diamond Ordnance Fuze Labs.
Washington 25, D.C.
2 Attn: ORDTL 930, Dr. R.T. Young
1 Attn: Library
1 Attn: ORDTL-450-638, Mr. R. H.
Comyn

Nat'l Bureau of Standards
Washington 25, D.C.
1 Attn: R.D. Elbourn
1 Attn: Mr. S.N. Alexander
1 Attn: Librarian

U.S. Dept. of Commerce
Nat'l Bureau of Standards
Boulder Labs.
Central Radio Propagation Lab.
1 Boulder, Colorado

U.S. Dept. of Commerce
Nat'l Bureau of Standards
Boulder Labs.
Boulder, Colorado
1 Attn: Miss J. Lincoln, Chief
Radio Warning Services
Section

Director, Nat'l Security Agency
1 Ft. George G. Meade, Md.
1 Attn: R31
1 Attn: R42
1 Attn: Howard Campaigne
1 Attn: C3/TDL, Rm. 2C087, Tech. Doc.

Chief, U.S. Army Security Agency
Arlington Hall Station
2 Arlington 12, Va.

Central Intelligence Agency
2430 E. St., NW
Washington, D.C.
1 Attn: A. Borel

UNIVERSITIES

School of Engineering
Sciences
Arizona State University
1 Tempe, Arizona

University of Arizona
Elec. Engr. Dept.
Tucson 25, Arizona
1 Attn: Robert L. Walker
1 Attn: Dr. Douglas J. Hamilton

Jet Propulsion Lab.
Calif. Inst. of Technology
4800 Oak Grove St.
Pasadena 3, Calif.
1 Attn: Library

Univ. of Calif.
Elec. Engineering Dept.
Berkeley 4, Calif.
1 Attn: Prof. R.M. Saunders, Chm.

Univ. of Calif.
Radiation Lab.
Information Div., Bldg. 30,
Room 101
Berkeley, Calif.
1 Attn: Dr. R.K. Wakerling

Univ. of Calif.
Lawrence Radiation Lab.
P.O. Box 808
Livermore, Calif.
1 Attn: Tech. Info. Div.

Univ. of Calif. at Los Angeles
Los Angeles 24, Calif.
1 Attn: Dept of Engineering
Prof. Gerald Estrin
1 Attn: Electromagnetics Div.,
R.S. Elliott
1 Attn: C.R. Viswanathan,
SS Electr. Lab.

Univ. of Chicago
Institute for Computer Research
Chicago 37, Illinois
1 Attn: Nicholas C. Metropolis

Columbia University
New York 27, N.Y.
1 Attn: Dept. of Physics
Prof. L. Brillouin
1 Attn: Columbia Radiation Lib.

Cornell University
Cognitive Systems Res. Program
Hollister Hall
Ithaca, N.Y.
1 Attn: F. Rosenblatt

Univ. of Florida
Dept. of Elect. Engr.
Rm. 336, Engineering Bldg.
Gainesville, Florida
1 Attn: M.J. Wiggins

George Washington Univ.
Washington, D.C.
1 Attn: Prof. N. Grisamore

Drexel Inst. of Tech.
Dept. of Elect. Engr.
Philadelphia 4, Pa.
1 Attn: F.B. Haynes

Georgia Inst. of Tech.
Atlanta, Ga.
1 Attn: Mrs. J.H. Crosland
Librarian

Harvard University
Technical Reports Collection
Rm. 303A, Pierce Hall
Cambridge 38, Mass.
2 Attn: Mrs. Elizabeth Farkas,
Librarian

Harvard University
Pierce Hall 217
Cambridge 38, Mass.
1 Attn: Div. of Engineering and
Applied Physics
Dean Harvey Brooks

Univ. of Ill.
Elect. Engineering Res. Lab.
Urbana, Ill.
1 Paul D. Coleman, Rm. 218
1 Attn: William Perkins

University of Ill.
Digital Computer Lab.
Urbana, Ill.
1 Attn: Dr. J. E. Robertson

Univ. of Ill.
Coordinated Science Lab.
Urbana, Ill.
1 Attn: Prof. Daniel Alpert

Univ. of Ill.
Library Serials Dept.
1 Urbana, Ill.

Univ. of Ill.
Dept. of Physics
Urbana, Ill.
1 Attn: Dr. John Bardeen

Johns Hopkins Univ.
Applied Physics Lab.
8621 Georgia Ave.
Silver Spring, Md.
1 Attn: A.W. Nagy
1 Attn: N.H. Choksy
1 Attn: Document Library
1 Attn: Supervisor of Tech.
Reports

Carlyle Barton Labs.
Johns Hopkins Univ.
Charles and 34th Sts.
Baltimore 18, Md.
1 Attn: Librarian

Linfield Research Inst.
McMinnville, Oregon
1 Attn: Guy N. Hickok, Dir.

Marquette Univ.
Dept. of Elect. Engr.
1515 W. Wisconsin Ave.
Milwaukee 3, Wis.
1 Attn: Arthur C. Moeller

State Univ. of Iowa
Dept. of Electrical Engineering
Iowa City, Iowa
1 Attn: Prof. Donald L. Epley

M.I.T.
Cambridge 39, Mass.
1 Research Lab. of Electronics
(Document Rm. 26-327)
1 Lab. of Insulation Research
Miss Sils, Librarian, Rm 4-244

Lincoln Lab.
M.I.T.
P.O. Box 73
Lexington 73, Mass.
1 Attn: Dr. Walter I. Wells
1 Attn: Library
1 Attn: Navy Representative
1 Attn: Kenneth L. Jordan, Jr.

Dynamic Analysis and Control Lab.
M.I.T.
Rm. 3-457
Cambridge, Mass.
1 Attn: D. M. Baumann

Director, Cooley Electronics
Lab., N. Campus
Univ. of Mich.
1 Ann Arbor, Mich.

Univ. of Mich.
Dept. of Elect. Engr.
3503 E. Engineering Bldg.
Ann Arbor, Mich.
1 Attn. Prof. Joseph E. Rowe

Univ. of Mich.
180 Frieze Bldg.
Ann Arbor, Mich.
1 Attn: Dr. Gordon E. Peterson,
Dir. of Communication
Science Lab.

Univ. of Mich.
Inst. of Science and Tech.
Ann Arbor, Mich.
1 Attn: Tech. Documents Service

Univ. of Minn.
Dept. of Elect. Engr.
Inst. of Tech.
Minneapolis 14, Minn.
1 Attn: Prof. A. Van der Ziel

Univ. of Nevada
College of Engineering
Reno, Nev.
1 Attn: Dr. Robert A. Manhart,
Chm. Elect. Engr. Dept.

New York University
University Heights
New York 53, N.Y.
1 Attn: Dr. J. H. Mulligan, Jr.
Chm. of EE Dept.

New York University
Solid State Lab.
4 Washington Pl.
New York 3, N.Y.
1 Attn: Dr. H. Kallmann

Northwestern Univ.
Aerial Measurements Lab.
2422 Oakton St.
Evanston, Ill.
1 Attn: Walter S. Toth

North Carolina State College
Dept. of E.E.
Raleigh, N.C.
1 Attn: Prof. Robert W. Lade

Univ. of Notre Dame
Elect. Engr. Dept.
South Bend, Indiana
1 Attn: Eugene Henry

Ohio State University
Dept. of Elect. Engr.
Columbus 10, Ohio
1 Attn: Prof. E.M. Boone

Oregon State Univ.
Dept. of Elect. Engr.
Corvallis, Oregon
1 Attn: H.J. Oorthuys

Univ. of Pennsylvania
Moore School of E.E.
200 S. 34th St.
Philadelphia 4, Pa.
1 Attn: Miss . , Campion

Polytechnic Institute
Elect. Engr. Dept.
333 Jay St.
1 Attn: Leonard Shaw

Polytechnic Inst. of Brooklyn
Graduate Center
Rt. 110
Farmingdale, N.Y.
1 Attn: Librarian

Princeton Univ.
Elect. Engr. Dept.
Princeton, N.J.
1 Attn: Prof. F.S. Acton

Research Inst. of Advanced Studies
7212 Bellona Ave.
Baltimore, Md.
1 Attn: Dr. R.E. Kalman

Purdue Univ.
Elect. Engr. Dept.
Lafayette, Ind.
1 Attn: Library

Rensselaer Polytechnic Institute
Library---Serials Dept.
1 Troy, N.Y.

Univ. of Rochester
Gavett Hall
River Campus Station
Rochester 20, N.Y.
1 Attn: Dr. Gerald H. Cohen

VARSI Library
Univ. of Santa Clara
1 Santa Clara, Calif.

Stanford Research Inst.
Menlo Park, Calif.
1 Attn: External Reports G-037

Stanford Research Inst.
Computer Lab.
Menlo Park, Calif.
1 Attn: H.D. Crane

Syracuse University
Dept. of Elect. Engr.
Syracuse 10, N.Y.
1 Attn: Dr. Stanford Goldman

Univ. of Tennessee
Dept. of E.E.
Ferris Hall
1 Knoxville, Tenn.

Texas Technological College
Lubbock, Texas
1 Attn: Dir. Inst. of Science Engineering, Office of Dean of Engr.

Univ. of Utah
Electrical Engineering Dept.
Salt Lake City, Utah
1 Attn: Richard W. Grow

Villanova Univ.
Dept. of Elect. Engr.
Villanova, Pa.
1 Attn: Thomas C. Gallagiele, Asst. Prof.

Univ. of Virginia
Charlottesville, Va.
1 Attn: J.C. Wyllie, Alderman Library

Wayne State University
Detroit, Mich.
1 Attn: Prof. Harry Josselson
Dept. of Slavic Languages

Engineering Library
Yale University
New Haven, Conn.
1 Sloane Physics Lab.
1 Dept. of Elect. Engr.
1 Dunham Lab.

INDUSTRY

Admiral Corporation
3800 Cortland St.
Chicago 47, Ill.
1 Attn: E.N. Roberson, Librarian

Airborne Instruments Lab.
Comac Road
Deer Park, L.I., New York
1 Attn: John Dyer, Vice Pres. and Tech. Director

Amperex Corporation
230 Duffy Ave.
Hicksville, L.I., New York
1 Attn: S. Barbasso, Proj. Eng.

Auerbach Corp.
1634 Arch St.
1 Philadelphia 3, Pa.

Autonetics
Div. of N. American Aviation
9150 E. Imperial Highway
Downey, Calif.
1 Attn: Tech. Library 3040-3

Bell Telephone Laboratories
Murray Hill Labs.
Murray Hill, N.J.
1 Attn: Dr. J.K. Galt
1 Attn: Dr. J. R. Pierce
1 Attn: Dr. S. Darlington
1 Attn: A.J. Grossmann
1 Attn: Dr. M. Sparks
1 Attn: A. J. Morton
1 Attn: Dr. R. M. Ryder

Bendix Corp.
Research Labs. Division
Southfield (Detroit), Mich.
1 Attn: A.G. Peifer

Benson-Lehner Corp.
14761 California St.
Van Nuys, Calif.
1 Attn: George Ryan

Boeing Scientific Res. Labs.
P.O. Box 3981
Seattle 24, Wash.
1 Attn: Dr. D.J. Nalos

Bomac Laboratories, Inc.
Beverly, Mass.
1 Attn: Research Library

Columbia Radiation Lab.
538 W. 120th St.
1 New York, N.Y.

Convair-San Diego
A Div. of Gen. Dynamics Corp.
San Diego 12, Calif.
1 Attn: Engr. Library
Mail Zone 6-157

Cook Research Labs.
6401 W. Oakton St.
1 Morton Grove, Ill.

Cornell Aeronautical Lab.
4455 Genesee St.
Buffalo 21, N.Y.
1 Attn: D.K. Plummer
2 Attn: Library

Eitel-McCullough, Inc.
301 Industrial Way
San Carlos, Calif.
1 Attn: Research Librarian
1 Attn: W.R. Luebke

Electro-Optical Instruments, Inc.
125 N. Vinedo
Pasadena, Calif.
1 Attn: I. Weiman

Fairchild Semiconductor Corp.
4001 Junipero Serra Blvd.
Palo Alto, Calif.
1 Attn: Dr. V.H. Grinich

General Electric Co.
Defense Electronics Div., LMED
Cornell Univ.
Ithaca, N.Y.
1 Attn: Library
VIA: Commander
Aeronautical Systems Div.
Wright-Patterson AFB, Ohio
Attn: ASRNC-5
Donald E. Lewis

General Electric TWT Product Sect.
601 Calif. Ave.
Palo Alto, Calif.
1 Attn: C.G. Kob
1 Attn: Tech. Library

General Electric Co.
Research Lab.
P.O. Box 1088
Schenectady, N.Y.
1 Attn: Dr. Philip M. Lewis
1 Attn: V.L. Newhouse
Applied Physics

General Electric Co.
Electronics Park-Bldg. 3
Room 143-1
Syracuse, N.Y.
1 Attn: Documents Librarian
(Yolanda Burke)

General Electric Co.
Schenectady 5, N.Y.
1 Attn: Library, LME Dept.
Bldg. 28-501

General Telephone and Electronics Labs., Inc.
Bayside 60, N.Y.
1 Attn: Louis R. Bloom

Gilfillan Brothers
1815 Venice Blvd.
Los Angeles, Calif.
1 Attn: Engineering Library

Goddard Space Flight Center
Code 611
1 Greenbelt, Md.

The Hallicrafters Co.
5th and Kostner Ave.
1 Chicago 24, Ill.

Hewlett-Packard Co.
1501 Page Mill Rd.
1 Palo Alto, Calif.

Hoffman Electronics Corp.
Semiconductor Div.
1001 Arden Dr.
El Monte, Calif.
1 Attn: P.N. Russel, Tech. Dir.

Hughes Aircraft Co.
Florence at Teale St.
Culver City, Calif.
1 Attn: Tech. Library
Bldg. 6, Rm. C2048
1 Attn: Solid-State Group-M 107
1 Attn: Tech. Doc. Ctr., Bldg. 6,
Mail Station E-110
1 Attn: B.J. Forman
Antenna Dept., Res. and
Dev. Labs.

HRB Singer
Science Park
P.O. Box 60
State College, Pa.
1 Attn: Tech. Info. Center

Hughes Aircraft Co.
Bldg. 6, Mail Station E-150
Culver City, Calif.
1 Attn: A.S. Jerrems,
Aerospace Group

Hughes Aircraft Co.
Semiconductor Div.
P.O. Box 278
Newport Beach, Calif.
1 Attn: Library

Hughes Aircraft Co.
Bldg. 604, Mail Station C-213
Fullerton, Calif.
1 Attn: A. Eschner, Jr.
Ground Systems Group

Hughes Aircraft Co.
3011 Malibu Canyon Rd.
Malibu, Calif.
1 Attn: H.A. Iams, Res. Lab.

International Business Machines
Product Development Lab.
Poughkeepsie, N.Y.
1 Attn: E.M. Davis - (Dept. 362)

International Business Machines
Data Systems Div.
Box 390, Boardman Rd.
Poughkeepsie, N.Y.
1 Attn: J.C. Logue

IBM Research Library
Box 218
1 Yorktown Heights, N.Y.

International Business Machines
San Jose, California
1 Attn: Majorie Griffin

ITT Federal Labs.
500 Washington Ave.
Nutley, N.J.
1 Attn: Librarian, Ellis Mount

Lab. for Electronics, Inc.
1079 Commonwealth Ave.
Boston 15, Mass.
1 Attn: Dr. H. Fuller
1 Attn: Library

LEL, Inc.
75 Akron St.
Copiague, L.I., N.Y.
1 Attn: Robert S. Mautner

Lenkurt Electric Co.
San Carlos, Calif.
1 Attn: M.L. Waller, Librarian

Librascope, Div. of General
Precision, Inc.
808 Western Ave.
Glendale 1, Calif.
1 Attn: Engineering Library

Lockheed Missile and Space Co.
Dept. 67-33, Bldg. 324
P.O. Box 504
Sunnyvale, Calif.
1 Attn: G.W. Price

Lockheed Missile and Space Co.
Dept. 67-34, Bldg. 520
P.O. Box 504
Sunnyvale, Calif.
1 Attn: Dr. W.M. Harris, Dev't.
Planning Staff

Lockheed Missiles & Space Co.
Rm. 59-34, Bldg. 102
P.O. Box 504
Sunnyvale, Calif.
1 Attn: Stephent Paine

Lockheed Missile Systems Co.
Sunnyvale, Calif.
1 Attn: Tech. Info. Ctr. 50-14

Lockheed Missile and Space Co.
Palo Alto, Calif.
1 Attn: M.E. Browne-Dept. 52-40
Bldg. 202

The Martin Co.
P.O. Box 5837
Orlando, Florida
1 Attn: Engr. Library M.P. 30

Marquardt Aircraft Corp.
16555 Saticoy St.
P.O. Box 2013, -South Annex
Van Nuys, Calif.
1 Attn: Dr. Basun Chenge
Research Scientist

Mauchley Associates
50 E. Butler
1 Amplar, Pennsylvania

Melpar, Incorporated
Applied Science Div.
3000 Arlington Blvd.
Falls Church, Va.
1 Attn: Librarian

Micro State Electronics Corp.
1 Attn: A.L. Kestenbaum
152 Floral Ave.
Murray Hill, N.J.

Microwave Assoc., Inc.
North West Industrial Park
Burlington, Mass.
1 Attn: Dr. Kenneth Mortenson
1 Attn: Librarian

Microwave Electronics Corp.
3165 Porter Drive
Palo Alto, Calif.
1 Attn: Stanley F. Kaisel
1 Attn: M.C. Long

Minneapolis-Honeywell Regulator
Company
Semiconductor Library
1177 Blue Heron Blvd.
Riviera Beach, Florida

The Mitre Corporation
Bedford, Mass.
1 Attn: Library

Monsanto Chemical Co.
800 N. Lindbergh Blvd.
St. Louis 66, Mo.
1 Attn: Edward Orban, Mgr.
Inorganic Development

Motorola, Semiconductor Prod. Div.
5005 E. McDowell Rd.
Phoenix, Ariz.
1 Attn: Dr. A. Lesk
1 Attn: Peter B. Myers

Motorola, Inc.
8330 Indiana Ave.
Riverside, Calif.
1 Attn: R.E. Freese
Tech. Info. Analyst

Nat'l Biomedical Inst.
8600 16th St.
Silver Spring, Md.
1 Attn: Dr. R.S. Ledley

Nortronics
Palos Verdes Research Park
6101 Crest Rd.
Palos Verdes Estates, Calif.
1 Attn: Technical Info. Agency

Pacific Semiconductors, Inc.
14520 S. Aviation Blvd.
Lawndale, Calif.
1 Attn: H.Q. North

Dr. Alex Mayer, Ass't Dir.
Applied Res. Lab.
Philco WDL
3875 Fabian Way
1 Palo Alto, Calif.

Philco Corp.
Tech. Rep. Div.
P.O. Box 4730
Philadelphia 34, Pa.
1 Attn: F.R. Sherman, Mgr. Editor
Philco Tech. Rep. Div.
BULLETIN

Philco Corp.
Lansdale Div.
Church Rd.
Lansdale, Pa.
1 Attn: John R. Gordon

Philco Scientific Lab.
Blue Bell, Pa.
1 Attn: Dr. J.R. Feldmeier,
Assoc. Dir. of Research
1 Attn: C.V. Bocciarelli
1 Attn: C.T. McCoy, Res. Advisor

Polarad Electronics Corp.
43-20 Thirty-Fourth St.
Long Island City 1, N.Y.
1 Attn: A.H. Sonnenschein
Ass't to the President

RCA, Surf. Comm. Div.
Front and Market Streets
Bldg. 17-C-6
Camden, N.J.
1 Attn: K.K. Miller, Mgr.
Minuteman Project Of.

RCA Labs.
Princeton, N.J.
1 Attn: Harwick Johnson
1 Attn: Dr. W.M. Webster

RCA
Bldg., 108-134
Moorestown, N.J.
1 Attn: H.J. Schrader

The Rand Corp.
1700 Main St.
Santa Monica, Calif.
1 Attn: Lib., Helen J. Waldron
1 Attn: Computer Science Dept.
Willis H. Ware

Raytheon Co.
Microwave and Power Tube Div.
Spencer Lab.
Burlington, Mass.
1 Attn: Librarian

Raytheon Manufacturing Co.
28 Seyon St.
Research Div.
Waltham, Mass.
1 Attn: Dr. Herman Statz
1 Attn: Librarian

Raytheon Corp.
Waltham, Mass.
1 Attn: Dr. H. Scharfman

Roger White Electron Devices, Inc.
Tall Oaks Rd, Laurel Ledges
1 Stamford, Conn.

Space Technology Labs, Inc.
One Space Park
Redondo Beach, Calif.
2 Attn: Tech. Library
Doc. Acquisitions

Space Tech. Labs., Inc.
Physical Research Lab.
P.O. Box 95002
Los Angeles 45, Calif.
1 Attn: D. Fladlein

Sperry Gyroscope Company
Div. of Sperry Rand Corp.
Great Neck, N.Y.
1 Attn: Leonard Swern (M.S.3T103)

Sperry Microwave Electronics Co.
Clearwater, Florida
1 Attn: John E. Pippin,
Res. Section Head

Sperry Electron Tube Div.
Sperry Rand Corp.
1 Gainesville, Florida

Sylvania Electronic Defense Lab.
P.O. Box 205
1 Mountain View, Calif.

Sylvania Electric Products, Inc.
500 Evelyn Ave.
1 Mt. View, Calif.

Sylvania Electronics System
Waltham Labs.
100 First Ave.
Waltham 54, Mass.
1 Attn: Librarian
1 Attn: Ernest E. Hollis

Technical Research Group
1 Syosset, Long Island, N.Y.

Texas Instruments Incorporated
Apparatus Div.
P.O. Box 6015
Dallas 22, Texas
1 Attn: M.E. Chun

Texas Instruments, Inc.
Semiconductor-Components Div.
P.O. Box 5012
Dallas 22, Texas
1 Attn: Semiconductor Components Library
1 Attn: Dr. Willis A. Adcock, Mgr. Integrated Circuits Components Div.

Texas Instruments Inc.
Corporate Res. and Engr.
Technical Reports Service
P.O. Box 5474
1 Dallas 22, Texas

Tektronix, Inc.
P.O. Box 500
Beaverton, Oregon
4 Attn: Dr. Jean F. Delord
Dir. of Research

Transitron Electronic Corp.
144 Addison St.
East Boston, Mass.
1 Attn: Dr. H.G. Rudenberg, Dir. R and D

Varian Associates
611 Hansen Way
Palo Alto, Calif.
1 Attn: Tech. Library

Westinghouse Electric Corp.
Friendship Internat'l Airport
Box 746, Baltimore 3, Md.
1 Attn: G. Ross Kilgore, Mgr.
Applied Research Dept.
Baltimore Laboratory

Westinghouse Electric Corp.
Beulah Rd.
Pittsburgh 35, Pa.
1 Attn: Dr. G.C. Sziklai

Melbourne J. Hellstrom, Supv. Engr.
Westinghouse Electronics Corp.
Molecular Electronics Div.
Box 1836
1 Baltimore, Md. 21203

Westinghouse Electric Corp.
Research Laboratories
Beulah Rd., Churchill Boro
Pittsburg 35, Pa.
1 Attn: J.G. Castle, Jr.-401-1B5
1 Attn: Solid State Dept.
1 Attn: R.E. Davis

Zenith Radio Corporation
6001 Dickens Ave.
Chicago 39, Ill.
1 Attn: Joseph Markin

FOREIGN RECIPENTS

Northern Electric Co., Ltd.
Res. and Dev't Labs.
**P.O. Box 3511, Station "C"
1 Ottawa, CANADA

University of Ottawa
Dept. of Electrical Engr.
**Ottawa 2, CANADA
1 Attn: G. S. Glinsky
Via: ASD, Foreign Release of. (ASYF)
Wright-Patterson AFB, Ohio
Attn: J. Troyan

Dr. Sidney V. Soanes
Research Dept.
Ferranti-Packard Elect. Ltd.
**Industry St.
1 Toronto 15. Ontario, CANADA

Central Electronics Engr. Research Institute
* Pilani, Rajasthan, INDIA
1 Attn: Omp. Gandhi

Prof. Sanai Mito
Dept. of Applied Physics
Faculty of Engineering
Osaka City University
* 12 Nishi-Ogimachi, Kitaku
1 Osaka, JAPAN

Prof. Jose M. Borrego
Centro de Investigacion Y de Estudios
Avazados Del Instituto Politecnico Nacional
**Apartado Postal 26740
1 Mexico 14, D.E.

Prof. E.H. Rhoderick
**Manchester College of Science and Tech.
1 Manchester 1, ENGLAND

Mr. Heikki Ihantola
**Fiskars Electronics Lab.
1 Elimaenkatu 17, Helsinki, FINLAND

Prof. Takuo Sugano
Faculty of Engineering
University of Tokyo
Bunkyo-ku, Tokyo
1 JAPAN

Dr. Niels I. Meyer
Physics Dept.
The Technical University of Denmark
Lundtoftevej 100, Lyngby
1 DENMARK

Prof. G. Bruun
Royal Technical University of Denmark
Ostervolgade 10, G.
1 Copenhagen K, DENMARK

Dr. Georges Alon
E.N.S. Laboratoire des Hautes Energies
Orsay/Seine et Oise
1 B.P. No. 2, FRANCE

Dr. P. A. Tove
Fysiska Institutionen
Uppsala University
1 Uppsala, SWEDEN

Prof. W. E. Dahlke
Telefunken, GmbH
Soflinger Strasse 100
Postfach 627
Ulm/Donau
1 GERMANY

Dr. G. B. B. Chaplin
The Plessey Company (U.K.) Ltd.
Caswell, Towcester
1 Northants, ENGLAND

Dr. D. H. Roberts
The Plessey Company (U.K.) Ltd.
Caswell, Towcester
1 Northants, ENGLAND

Royal Radar Establishment
Physics Dept.
St. Andrews Rd.
Great Malvern, Worcs.
ENGLAND
1 Attn: Dr. P. N. Butcher

National Physical Lab.
Teddington, Middlesex
ENGLAND
1 Attn: Dr. A. M. Uttley

Swiss Federal Institute of Technology
Gloriastrasse 35
Zurich, SWITZERLAND
1 Attn: Prof. M.J.O. Strutt

Prof. A. Bebock
University of Louvain
Institute of Physique
61 Rue de Namur
Louvain, Belgium

Dr. Maurice Bernard
Dept. PCM
CNET
Issy-Les-Moulineaux
Seine, FRANCE
1 Attn: Solid-State and Electron Devices

Prof. Karl Steinbuch
Institute für Nachrichtenverarbeitung und Nachrichtenubertragung
Technische Hochschule Karlsruhe
1 Karlsruhe, GERMANY

* ONR 44 Reports ONLY
** AF 26 Reports ONLY
VIA: ASD, Foreign Release Office (ASYF)
Wright-Patterson AFB
Ohio
Attn: J. Troyan